PROBING THE BINDING PROPERTIES OF POLYELECTROLYTES AS SUPRAMOLECULAR HOSTS

by

ASHLEY M. JOLLY

MARCO BONIZZONI, COMMITTEE CHAIR
STEPHEN A. WOSKI
MICHAEL P. JENNINGS
GREGORY SZULCZEWSKI
CAROL DUFFY

A DISSERTATION

Submitted in partial fulfillment of the requirements
for the degree of Doctor of Philosophy
in the Department of Chemistry
in the Graduate School of
The University of Alabama

TUSCALOOSA, ALABAMA

2015

ABSTRACT

The use of polyelectrolytes in the field of supramolecular chemistry has flourished in recent years. Specifically, commercially available PAMAM dendrimers have attracted attention due to their large globular structures and high loading capacities. In this dissertation, we focus on using optical spectroscopy to study the intermolecular interactions responsible when these charged polyelectrolytes, mainly PAMAM dendrimers, act as encapsulating agents for guest molecules in aqueous solutions. We found electrostatics, hydrogen bonding, and interactions mediated by aromatic moieties in the guest molecules to be the main drivers to complex formation in these systems. Chapter 2 and Chapter 3 details original research directed toward gaining insight about the intermolecular interactions and properties of these systems.

Upon the discovery that aromatic moieties in guest molecules play a role in increased binding affinity to the dendritic scaffold, we conducted experiments, presented in Chapter 4, examining the ability of these polyelectrolytes to act as solubilizing agents for hydrophobic molecules. Through extensive dissolution studies using aromatic hydrocarbon probes we propose that cationic polyelectrolytes increase solubilization of the aromatic hydrocarbons by interactions with the ammonium cations located on their surface. These studies afforded a more complete understanding of the fundamental intermolecular interactions involved when cationic polyelectrolytes function as supramolecular hosts, a role they commonly assume in many of their applications e.g. as drug delivery vectors.

Macrocycles have also attracted attention due to their symmetrical architecture and high count of functional sites. Chapter 5 introduces the preliminary studies on the preparation of

amine macrocycles that are important for studying dicarboxylate recognition in aqueous solvent using optical techniques. These studies provide the synthesis of a series of the desired amine macrocycles and their stoichiometry upon binding copper(II).

LIST OF ABBREVIATIONS AND SYMBOLS

1,5-NaphDiCarb	1,5-naphthalenedicarboxylate
9,10-AnDiCarb	9,10-anthracenedicarboxylate
9,10-AnDiCarbH2	9,10-anthracenedicarboxylic acid
9-AnCarb	9-anthracenecarboxylate
A	Anionic probe
ANS	8-anilino-1-naphthalenesulfonic acid
CF	5(6)-carboxyfluorescein
D	Dendrimer
D•CF_n	Dendrimer-dye complex
DNA	Deoxyribonucleic acid
ESP	Electrostatic potential maps
F	Fluorescein
FRET	Fluorescence resonance energy transfer
G	Generation
HEPES	4-(2-hydroxyethyl)-1-piperazineethanesulfonic acid, free acid
I	Integrated fluorescence
M_r	relative molecular mass
MS	Mass spectroscopy
n	refractive index

NMR	Nuclear magnetic resonance
OD	Optical density
PA	poly(allylamine)
PAMAM	polyamidoamine
PEI	poly(ethyleneimine)
PET	Photoinduced electron transfer
polyDADMAC	Poly(diallyldimethylammonium chloride)
Φ	Quantum yield
r	Measured anisotropy
r_0	Anisotropy of free dye
Ref	Reference
r_{max}	Limiting anisotropy upon complete binding
Xanth	Aromatic moiety of fluorescein

ACKNOWLEDGMENTS

This dissertation would not have been possible without the instruction and guidance of my research advisor, Prof. Marco Bonizzoni. I appreciate his support and encouragement throughout my studies.

I would also like to thank my committee members, Prof. Stephen A. Woski, Prof. Michael P. Jennings, Prof. Gregory Szulczewski, and Prof. Carol Duffy for their advice and support throughout my graduate studies. I am also grateful for my fellow coworkers and especially lab mates for staying encouraging and being there for practices, inspiration and advice.

I would also like to thank The University of Alabama for providing funding that supported my research. I sincerely want to thank the GAANN fellowship for financially supporting me and my research for two years, while also creating a program which helped to shape me into the inspiring instructor I aspire to be. I am grateful to the GAANN fellowship advisors, Dr. Silas Blackstock and Dr. Stephen A. Woski, for helping me to succeed as a graduate student at The University of Alabama.

Finally, I would like to thank my family and friends for their patience, love, and support.

CONTENTS

LIST OF TABLES

LIST OF FIGURES

LIST OF SCHEMES

CHAPTER 1

INTRODUCTION

1.1 INTRODUCTION AND SCOPE

Since the synthesis of dendrimers in the late 1970's a surge of research has occurred, with applications spanning areas from molecular sensing,[1] to nanoreactor systems,[2] to drug delivery.[3,4] During the first five years of the 1990's publications on dendrimers increased from the dozens to thousands and has continued to climb at a remarkable pace ever since.[5] The fascination with dendrimers in research stems from the lack of extensive knowledge available about them.

The immense collection of literature concerning the preparation and applications of dendrimers has inspired the work presented in the following chapters on discovering the fundamental properties of how these molecules behave in aqueous solutions. A small portion is dedicated to other linear and hyperbranched polyelectrolytes that, due to their wide size distribution, are harder to study but in most cases cheaper than the dendrimers used in these studies and therefore more immediately relevant to large scale applications. A thorough review of this work requires a discussion on polyelectrolytes, the molecules of interest, and on the molecular recognition properties used to study these systems. Molecular recognition events are paramount in understanding these systems and are essential to the field of supramolecular chemistry.

1.2 SUPRAMOLECULAR CHEMISTRY

It took more than 40 years from the introduction of the term "Übermolekül", the German word for supramolecule, until a definition of supramolecular chemistry was announced.[6] One of its advocates, Jean-Marie Lehn, the 1987 Nobel Prize winner for his work in the area, defined supramolecular chemistry as the "chemistry of molecular assemblies and of the intermolecular bond."[7] Since those times intermolecular interactions became the focus of a great deal of research and a new field of chemistry was born.

The systems studied in this field often self-assemble thanks to a variety of molecular recognition events. The driving forces for assembly include not only non-covalent interactions such as electrostatic interactions, hydrogen bonding, and cation–π interactions but also interactions that possess a significant covalent nature such as metal-ligand interactions. Compared to covalent bonds these non-covalent interactions are relatively weak, which often allows them to break and reform repeatedly under mild conditions until the lowest energy structure is formed.[8] One common goal of supramolecular chemistry is to design molecular components in a way that directs the assembly of a complex system into a well-defined structure. When using molecular recognition events to assemble supramolecular systems, it is important to consider that it is often not one non-covalent interaction alone which provides host-guest binding, but the cooperation of all the interactions relating both to the host and guest as well as their surroundings.

Providing a means for directing the spontaneous formation of supramolecular systems can be done through molecular recognition events.[9] Emil Fischer provided a classical example of this concept with his description of the interaction between an enzyme and its substrate as a "lock and key" process. He hinted at the perceived need for perfect complementarity between the

structure of the enzyme's binding cavity and its substrate.[10] Molecular recognition has since expanded to describe the specific interactions of organization between two or more chemical species based on their electronic and geometric complementarity. This section provides a brief summary of the non-covalent interactions that are particularly relevant to the work described in this dissertation.

1.2.1 Electrostatic Interactions

Based on Coulombic forces, an electrostatic interaction is an attractive force observed between two chemical species of opposite charge or a repulsive force observed between species with the same charge. These interactions include ion-ion, ion-dipole, and dipole-dipole interactions. Electrostatic interactions range in strength from 5 kJ mol^{-1} (weak dipole-dipole interactions) to 250 kJ mol^{-1} (ion-ion interactions).[8]

1.2.2 Hydrogen Bonding

A hydrogen bond is the interaction between the hydrogen attached to an electronegative atom of one molecule (donor) and an electronegative atom with available lone pair electrons of a different molecule (acceptor). Usually the electronegative atom is oxygen, nitrogen, or fluorine, which bear a partial negative charge giving the hydrogen a partial positive charge. Hydrogen bonds come in a wide range of strengths and can be classified as strong, moderate, or weak, which range from 60-120 kJ mol^{-1}, 16-60 kJ mol^{-1}, 16 or less kJ mol^{-1}, respectively.[8] Being ubiquitous in supramolecular chemistry, hydrogen bonds are responsible for the overall shape of proteins and in large part for the double helix structure of DNA.

Hamilton and coworkers[11] show the utility of hydrogen bonding interactions in the design of a receptor for neutral molecules depicted in Figure 1.1. The neutral target molecules consist of barbiturate derivatives which are well known sedatives. Substrates like **1.2** were found to bind to the receptor **1.1** through multiple hydrogen bonds, shown as **1.3**.[11] The synthesis of the

macrocyclic receptor **1.1** demonstrates that careful positioning of inwardly facing hydrogen-bonding groups can lead to a strong and selective complexation of substrates with complimentary attributes.

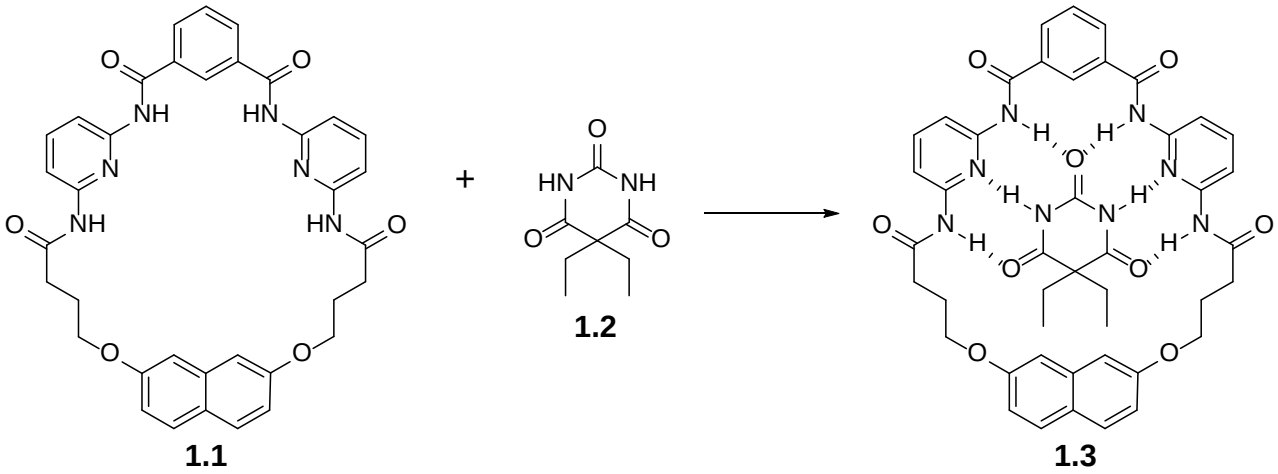

Figure 1.1. Receptor **1.1** binds the barbituric acid core **1.2** in chloroform through several hydrogen bonds, as shown in **1.3**.

1.2.3 Cation-π Interactions

A cation-π interaction is that of a cation with the face of an electron rich π-system (Figure 1.2). Aromatic rings, such as benzene, are characterized by a partially positive σ scaffold and a region of negative electrostatic potential above and below the ring plane. When cations are located above the center of the negatively charged portion of the aromatic ring they can form an attractive interaction. The strength of this type of interaction is approximately 5-80 kJ mol^{-1}.[12]

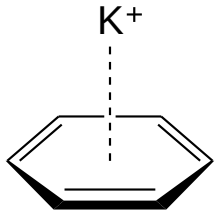

Figure 1.2 Stabilizing interaction between a cation (potassium) and the face of a simple aromatic (benzene).

Some of the beginning studies of cation-π interactions were reported in the early 1980's by gas phase studies. Deakyne and Meot-Ner[13] referred to these interactions as unconventional "ionic" bonds when they found that substituted ammonium ligands and π-donors bind to one another, as seen in the clustering reactions of NH_4^+ and Me_4N^+ (alkylammoniums) with benzene derivatives in the gas phase.

Diederich and Dougherty established that cation-π interactions can be established in water as well using water soluble cyclophane **1.4** (Figure 1.3).[14,15] Specifically, a surprising discovery from Dougherty and coworkers[16] arose when studying the ability of cyclophane **1.4** to bind molecules in its hydrophobic cavity (Figure 1.3). They found that **1.4** strongly favored N-methylquinolinium over 4-methylquinoline. These two guests are almost identical in size, shape, and hydrophobic area, but 4-methylquinoline is neutral where N-methylquinolinium is cationic. They realized that the positive charge was playing an important role in recognition and soon after, in 1990, Dougherty coined the term "cation-π interaction".[15,17]

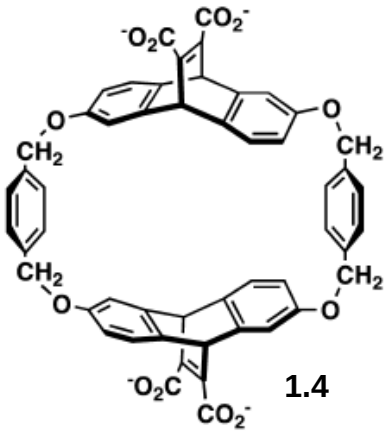

1.4

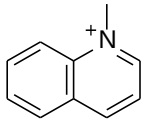

N-methylquinolinium

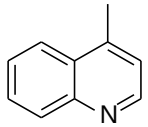

4-methylquinoline

Figure 1.3. Structures of the cyclophane receptor (**1.4**), N-methylquinolinium and 4-methylquinoline.[16]

1.2.4 Hydrophobic Effects

The hydrophobic effect relates to the exclusion of hydrophobic molecules from polar solvents. Essentially, hydrophobic species are squeezed out of the way of the strong inter-solvent

interactions and tend to aggregate (Figure 1.4). The combination of two or more hydrophobic organic molecules in aqueous solution causes less disruption in the hydrophilic phase, requires fewer solvent molecules to solvate the hydrophobic compounds, and causes a net entropic gain, thus lowering the overall free energy of the system.

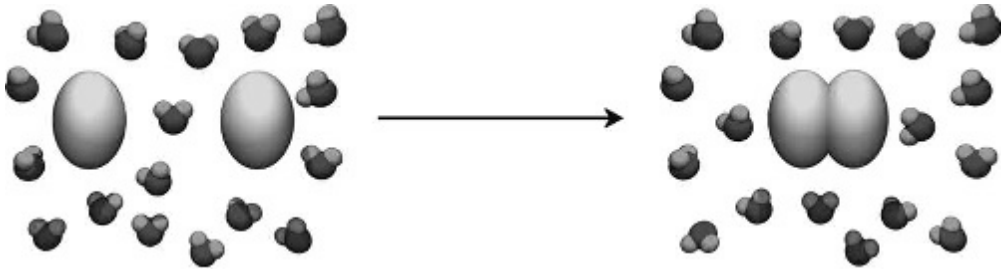

Figure 1.4. Solvent molecules are freed up when the two hydrophobic molecules interact in water, causing an entropic gain and lowering the overall energy of the system.[18]

1.3 MOLECULAR SENSING

Compounds that can carry out the tasks of molecular recognition and sensing concurrently are termed molecular sensors. A sensor in the simplest means includes a receptor that interacts with an analyte and generates a detectable change in signal.[19] The modulation can be optical or electrochemical in nature. Using molecular sensors to construct supramolecular devices has proven very successful, although the design of a successful sensor can be challenging. First, the molecular recognition phenomena must provide sufficient discrimination between structurally similar analytes (selectivity); secondly, the requisite change in physical properties must be observable at the desired concentration (sensitivity).

This section will focus on signal transduction methods generally exploited in optical molecular sensors. There are several ways a recognition event can be transduced into a measureable output, such as a change in color (absorbance), a change in the intensity or wavelength of emitted light, or a change in redox potential. Two of the important mechanisms of signal transduction presented in this work are described below.

1.3.1 Fluorescence Resonance Energy Transfer

Fluorescence resonance energy transfer (FRET or RET) is a distance dependent energy transfer that occurs between two chromophores, one of which is in its excited state. A donor molecule (D) absorbs a photon and can transfer this energy non-radiatively to the acceptor molecule (A) if they are within a characteristic distance of one another (Scheme 1.1). This parameter, called the Förster distance, is the distance at which the efficiency of the FRET process is 50%. This type of energy transfer is a through space interaction; Förster distances range from 15-60 Å for typical organic chromophores in solution.[20]

$$D + h\nu \longrightarrow D^*$$

$$D^* + A \longrightarrow D + A^*$$

$$A^* \longrightarrow A + h\nu'$$

Scheme 1.1. Equations describing resonance energy transfer between a donor (D) molecule to an acceptor (A) molecule. * denotes an excited state.

The energy transfer leads to a reduction in the donor's fluorescence intensity while increasing the acceptors. The pair of molecules that interact in such a manner are referred to as a FRET donor/acceptor pair. The well characterized and steep distance-dependence of FRET has made it widely utilized in studying conformation changes and as a powerful indicator of biochemical events.[21,22]

1.3.2 Photo-Induced Electron Transfer

Photo-induced electron transfer (PET) is the transfer of an electron from the excited state of a donor to an acceptor molecule. When a photon excites a molecule, an electron in a ground state orbital is excited to a higher energy orbital, thus leaving a vacancy in a ground state orbital that can be filled by an electron donor. The 'crown-anthracene' system, shown in Figure 1.5, is

an example of the use of PET in a fluorescent sensor.[23] Using anthracene as the signaling unit, its fluorescence intensity is quenched entirely as a result of electron transfer from the reducing nitrogen lone pair. The addition of potassium, however, ties up the lone pair in interactions with the metal center allowing anthracene's fluorescence to be switched on. The resulting signal was shown to respond linearly to very low concentrations of potassium cation providing a very sensitive "turn-on" molecular sensor for this ion in solution.

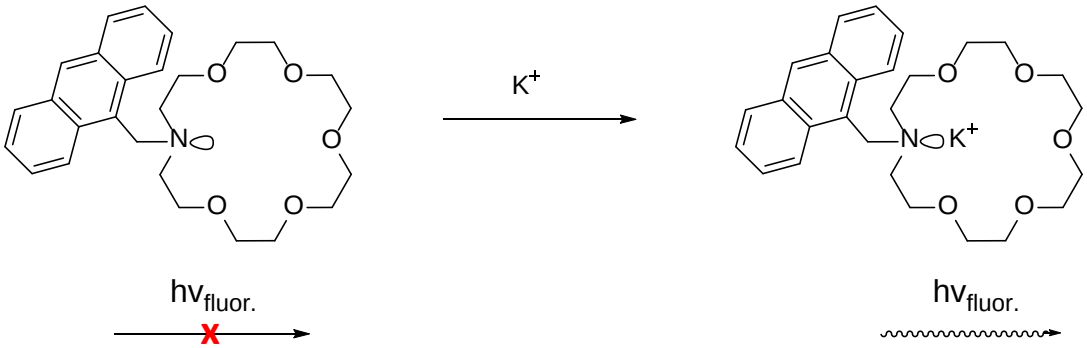

Figure 1.5. PET sensor detecting cations by anthracene-substituted aza[18]crown-6 moiety.[23]

The work described in this dissertation is centered on the study of the supramolecular chemistry of hyperbranched polyelectrolytes. It is only fitting to introduce this fascinating group of compounds directing the remainder of this chapter towards their use in molecular sensing. The role of various intermolecular interactions and the modulation of the optical signal remain at play in polyelectrolyte molecular recognition.

1.4 POLYELECTROLYTES

Polyelectrolytes include any polymer containing charged functional groups attached along their chain or surface. These charged molecules are usually termed polyanions if they bear negative charges or polycations if they bear positive charges. A distinction is typically made between polyelectrolytes where all charges have the same sign, and polyampholytes that include positively as well as negatively charged monomers.

Polyelectrolytes have drawn a great deal of attention due to their wide range of industrial applications being used in water treatment,[24] as degradable capsules which can carry emulsions,[25] and in drug delivery.[26] The applications of these compounds have been recently reviewed by Farinato.[27] One example is that of hyaluronic acid, an anionic polyelectrolyte that is naturally occurring in the body in fluids in the eyes and joints. It can be used as a lubricant to alleviate the pain caused by osteoarthritis by injecting it into joints. Attention has also been brought to polyelectrolytes because of their resemblance to water soluble bio-polymers such as DNA. All nucleic acids are highly charged anionic polyelectrolytes due to their negatively charged phosphate groups located on their phosphate-sugar backbone.

There have been extensive investigations on polyelectrolytes including the pioneering gas phase studies of Katchalsky[28] and Manning[29] studying the potentials and colligative properties of polyelectrolytes, respectively. However, there is still much to discover about the binding properties of polyelectrolytes in aqueous solutions. Due to their highly charged surfaces and adaptability, they have great potential to become the forefront of artificial molecular recognition systems.

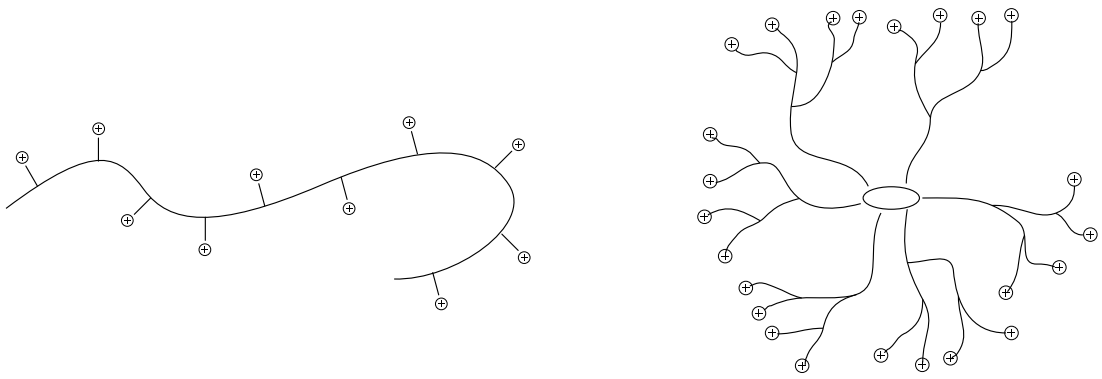

Figure 1.6. Structural representation of linear and branched polymer architectures. All representations are shown in the cation form.

Polyelectrolytes are available in a wide range of molecular weights and different polymer architectures (a few representative examples are shown in Figure 1.6). Examples of a linear and

randomly branched polyelectrolyte are shown in Figure 1.7. These polyelectrolytes specifically have the property of being polydisperse which makes them more difficult to study due to wide size distribution. Unlike these traditional polymers whose synthesis results in a Gaussian distribution of molecular weights, dendrimers can be synthesized in a much more controlled way.

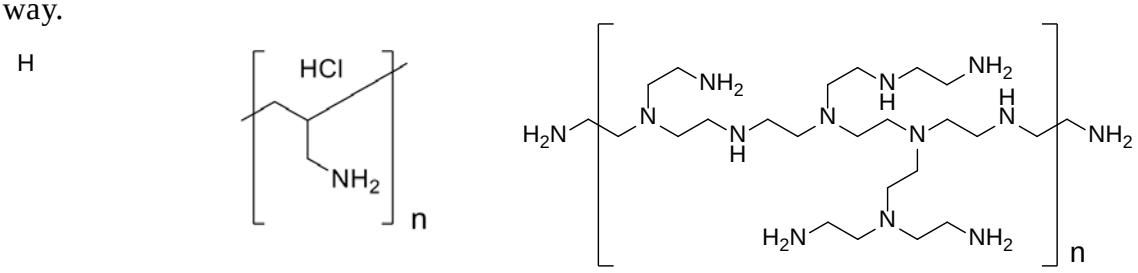

Figure 1.7. An example of a linear and random polyelectrolyte. Left: poly(allylamine), Right: poly(ethyleneimine).

1.4.1 Dendrimers

Dendritic structures are abundant in nature and range in size from blood vessel networks in mammals, to the much larger architecture in the branching of trees. The abundance of this motif in nature sparked interest in the replication of this functionality on the molecular level. Dendrimers themselves are regular hyperbranched polymers whose bonds stem from a central core. The name comes from the Greek word *dendron*, meaning tree, which represents the branching units that make up these macromolecules. During the late 1970's, dendrimers were introduced by Vögtle and coworkers[30] when they reported on low molecular weight amines synthesized by repetitive steps that were capable of binding ionic guests.

The precise synthesis of dendrimers allows control of their size, shape and functionality which has amplified the synthesis of many different structural classes of dendritic

macromolecules. These range from pure hydrocarbons, phenylacetylene dendrimers, to one of the most commonly used dendrimers, the poly(amidoamine) (PAMAM) dendrimers. Figure 1.8 depicts an example of a polyaryl ether dendrimer reported by Fréchet.[31] It was determined that these dendrimers have the ability to solvate hydrophobic molecules through non-covalent interactions. Since these dendritic macromolecules have been introduced only relatively recently, they are still a truly interesting topic for research and still have the potential for countless applications.

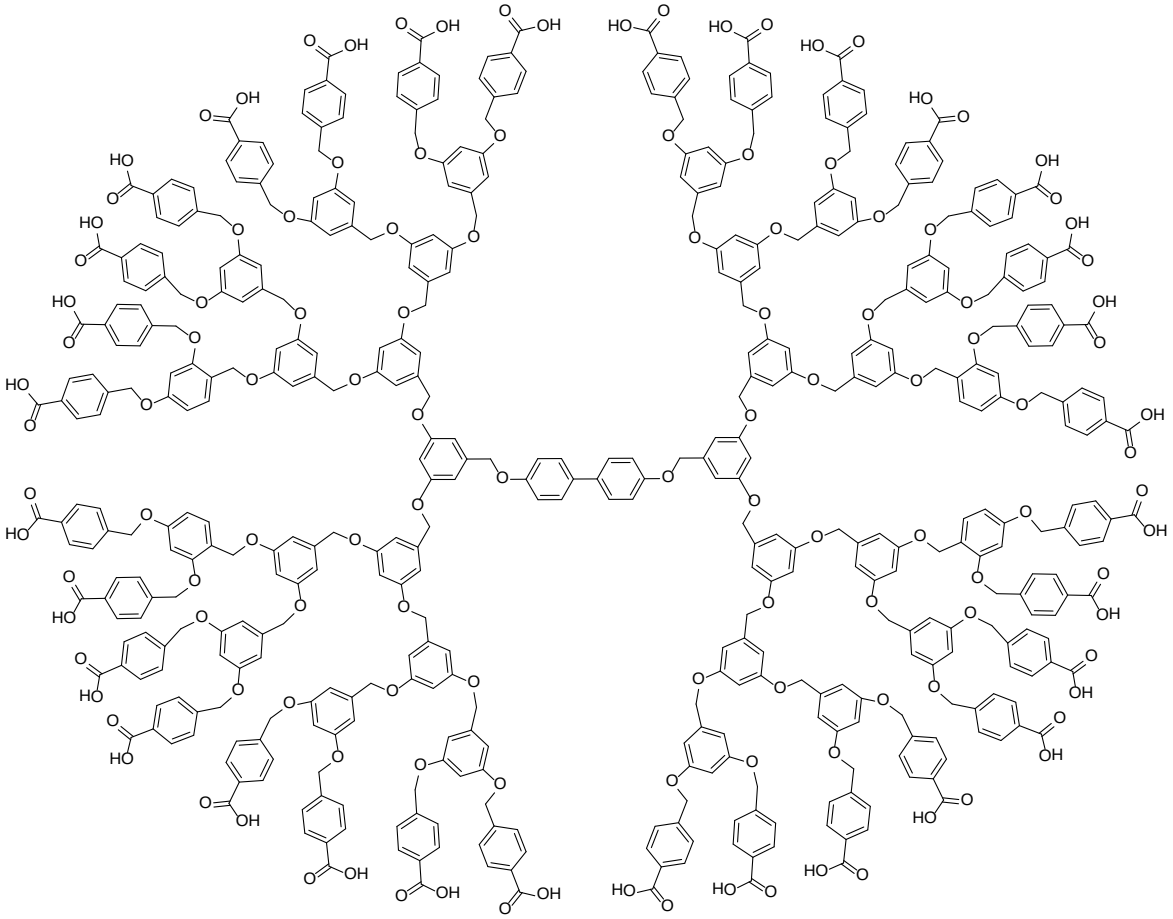

Figure 1.8. A water soluble polyaryl ether dendrimer reported by Fréchet.[31]

1.4.1.1 Dendrimer Synthesis

Dendrimers are synthesized in a controlled and stepwise fashion that offers control of their size, shape and functionality. The structure of a dendrimer starts with a central core. The core can consist of a central atom or a group of atoms, and then branches are added stepwise to the dendritic framework. The continuous branching results in repetitive layers called "generations". The moieties that make up the surface of the molecule are denoted as the end or terminal groups.

To date, two strategies have been developed for the synthesis of dendrimers (Figure 1.9). In the so-called divergent method, the growth of the dendrimer originates from the core while the alternative convergent method proceeds from the outer surface and works inwards towards the core. The divergent method has advantages such as the use of cheap reagents and a fast synthesis, but it has the issue of both side and incomplete reactions at the end-groups which makes purification more complicated.[32] In the convergent approach, fragments are built up separately and with successive coupling they are linked to a common core in the final step, thus minimizing the number of individual reaction steps that need to be taken.[32] Even though the convergent method provides better structural control, the divergent method is more amendable to large scale synthesis. As a result, the commercially available polyamidoamine (PAMAM) dendrimers that are the subject of the work in this dissertation are prepared commercially through the divergent protocol.

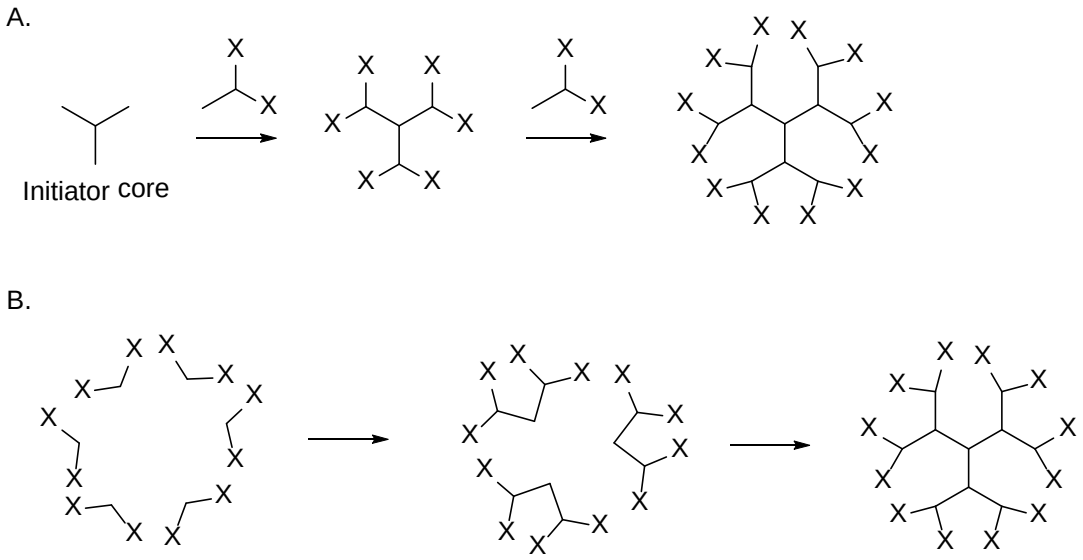

Figure 1.9. Synthesis of dendrimers. A. Divergent synthesis is initiated from the core and terminates at the dendrimer surface through a series of iterative reaction steps. B. Convergent synthesis proceeds from the surface and works inwards by linking surface units together until attaching to a core to generate the macromolecule.

1.4.1.2 PAMAM Dendrimers

First synthesized in the early 1980's by Donald Tomalia and coworkers,[33] poly(amidoamine) (PAMAM) dendrimers consist of a diamine core, amidoamine repetitive branching units, and most commonly carboxylic acid or amine terminal groups. Scheme 1.2 shows the schematic structure of a PAMAM first-generation dendrimer (G1) which demonstrates the conventional naming of the growth of layers in these macromolecules, commonly referred to as generations. PAMAM dendrimer's commercially availability, water solubility and high loading capacity make them a convenient test bed for the study of these hyperbranched materials, and are currently being explored for a wide range of applications.[34-37]

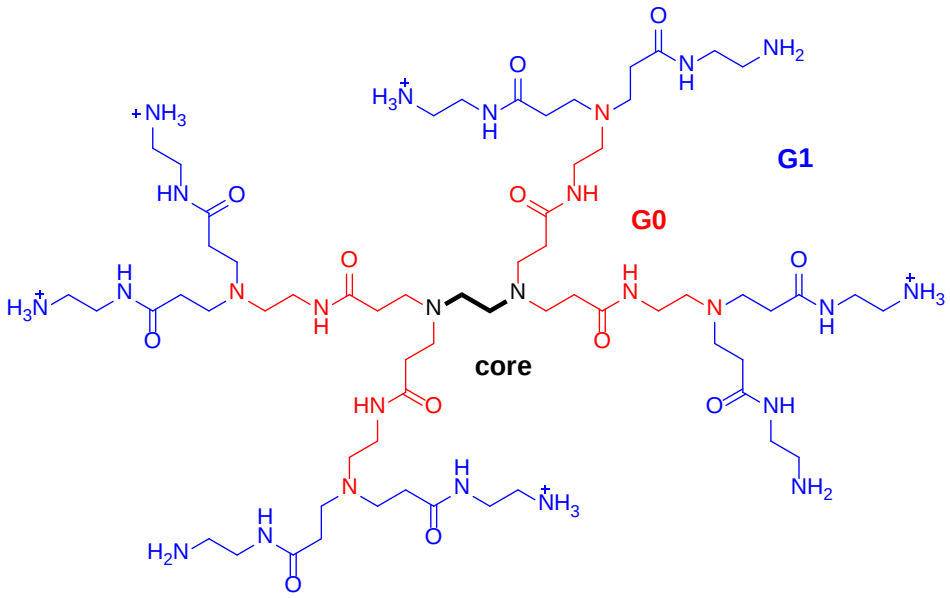

Scheme 1.2 Schematic structure of a first-generation (G1) amine-terminated poly(amidoamine) (PAMAM) dendrimer with a 1,2-diaminoethane core. The conventional naming of dendrimer generations is highlighted in color.

PAMAM dendrimers can be synthesized as half (X.5) or full generations (X.0), the former bearing carboxylic acid, whereas the latter has amine terminal groups. The synthesis focuses on a Michael addition followed by an amidation step with ethylenediamine as shown in Figure 1.10. Half generation dendrimers are prepared from hydrolysis of the esters following the Michael addition resulting in carboxylic acid terminal groups.

The full generation PAMAM class of dendrimers will be the focus of this research. Due to the protonation of a sizable portion of their surface amine groups it makes them good hosts that can bind small organic molecules in water. The protonation of these specific dendrimers has been studied through potentiometric titrations by the Borkovec group,[38] determining that the degree of protonation of surface charges was very close to 50% at a pH 7.5 in a solution with ionic strength I = 0.1 M, and almost independent of the dendrimer generation.

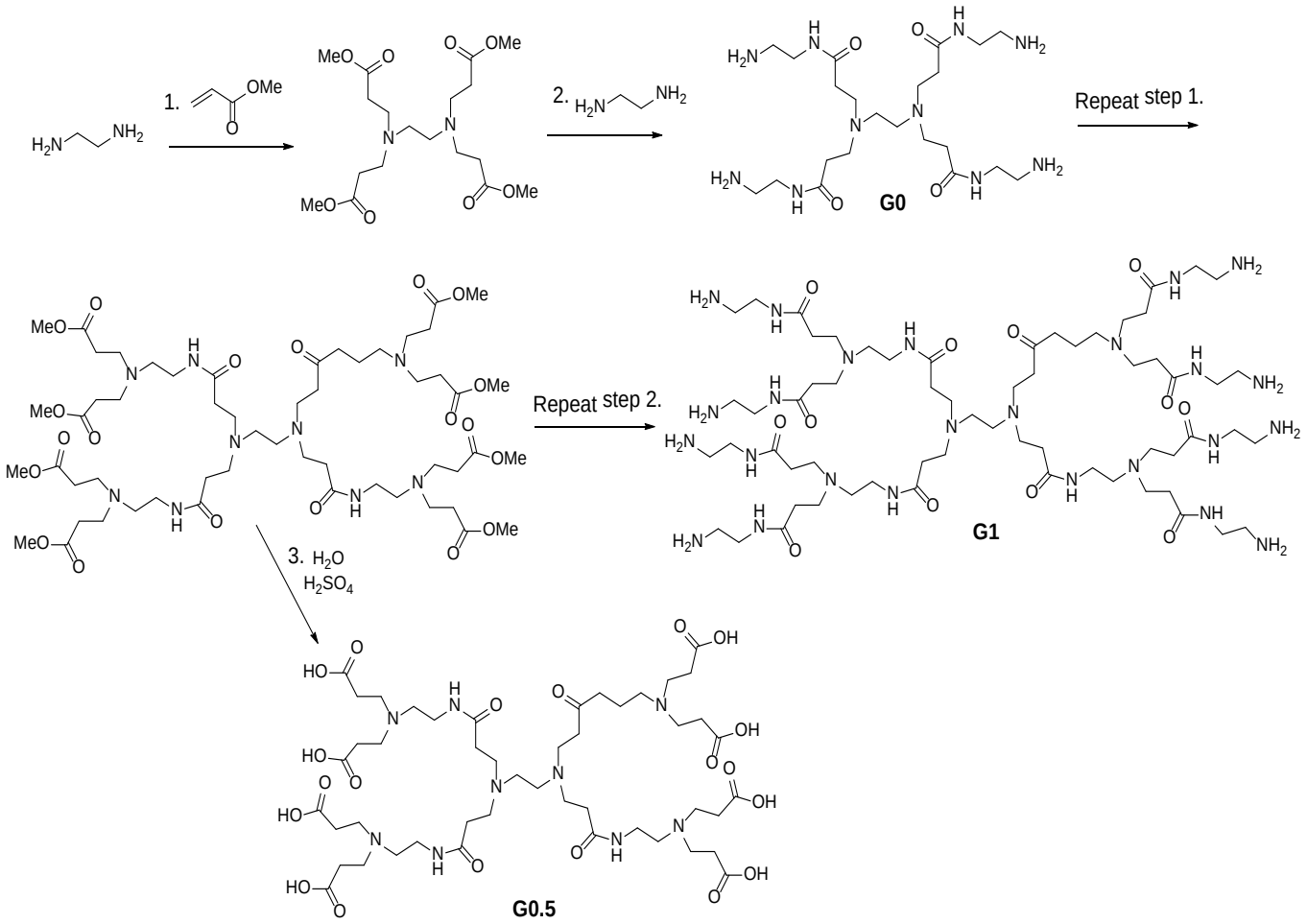

Figure 1.10. Divergent synthesis of a first generation PAMAM dendrimer. 1. Michael addition of acrylate ester. 2. amidation of the formed ester with ethylenediamine. 3. Hydrolysis of ester terminal groups.

1.5 COVALENTLY MODIFIED POLYELECTROLYTES AS SENSORS

Due to the presence of excellent synthetic handles on their polymer chains, polyelectrolytes can be easily covalently modified resulting in many types of polyelectrolyte derivatives. Attachment of sensing elements to polyelectrolyte structures enables the investigation of local environmental changes in close proximity to the modified surface. In many cases, the covalent attachment consists of a fluorescent molecule or dye that allows these macromolecules to work as optical sensors.

Interested in the development of a convenient method to detect sugar levels in diabetic patients, Shinkai and coworkers[39] synthesized a boronic acid based fluorescent sensor from a PAMAM dendrimer (Figure 1.11). A second generation PAMAM dendrimer was modified to contain the attachment of sensor elements consisting of eight boronic acids and anthracene units. Through monitoring fluorescence intensity, Shinkai determined that the flexibility of the dendritic scaffold and its increased number of binding sites allowed the saccharide to form 1:2 complexes with two boronic acids thus stabilizing the complex. They determined very low concentrations of saccharides such as D-galactose and D-fructose could be bound to the dendrimer forming significantly more stable complexes than monoboronic acid complexes which can only form a 1:1 complex

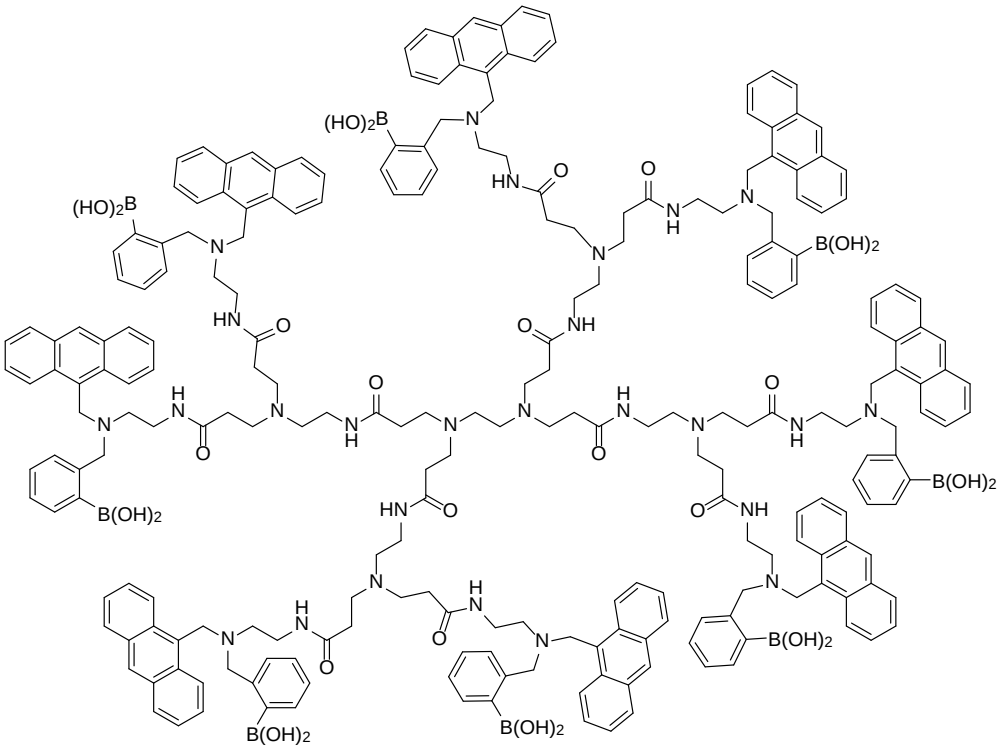

Figure 1.11. Structure of the dendritic boronic acid used as a sugar receptor developed by Shinkai and coworkers.[39]

1.6 POLYELECTROLYTE-DYE ASSEMBLIES

The synthesis of covalently modified polyelectrolytes discussed above is very time consuming and typically alters the properties of the macromolecule under study. Self-assembled complexes have been of great interest because they can be prepared without recourse to covalent architecture, and they can be designed to be quite stable due to their ability to self-organize when equilibrium condition is reached. The abundance of charged surface groups on polyelectrolytes has made them useful building blocks for self-assembly into various complex structures, allowing them to act as polyions that can interact with oppositely charged dyes.[40-42]

Fluorescent dyes have become popular molecular probes, used to not only determine microenvironmental parameters, but also their relocation and distribution dynamics in supramolecular systems can be followed. For instance, 8-anilino-1-naphthalenesulfonic acid (ANS) is a commonly used fluorescent probe (Figure 1.12). In polar media such as water, ANS is essentially non-fluorescent but its fluorescence intensity increases in nonpolar media or when buried in hydrophobic sites of proteins and membranes.[43] This unique fluorescence property of ANS makes it useful as a chemical microenvironment probe, as it provides structural information upon being encapsulated in other molecules.

Nagatani and coworkers[44] explored ANS's encapsulation properties with the generation 3.5 PAMAM dendrimer. Shown in Figure 1.12, they observed a fluorescence enhancement with a blue shift of the emission at pH values lower than 6 and greater than 1. The schematic drawing (Figure 1.12, C) depicts the proposed interaction between ANS and the dendrimer scaffold at a range of pH values. The authors concluded at pH values ranging between 3-6 where the interior of PAMAM G3.5 is cationic, anionic ANS can be electrostatically encapsulated in the dendrimer. However, we contend that the enhancement of fluorescence observed at pH 5 could

also be due to the hydrophobic environment of the dendritic core and not solely due to electrostatics, since at this pH we expect that a relatively small amount of the interior tertiary amines would actually be protonated.

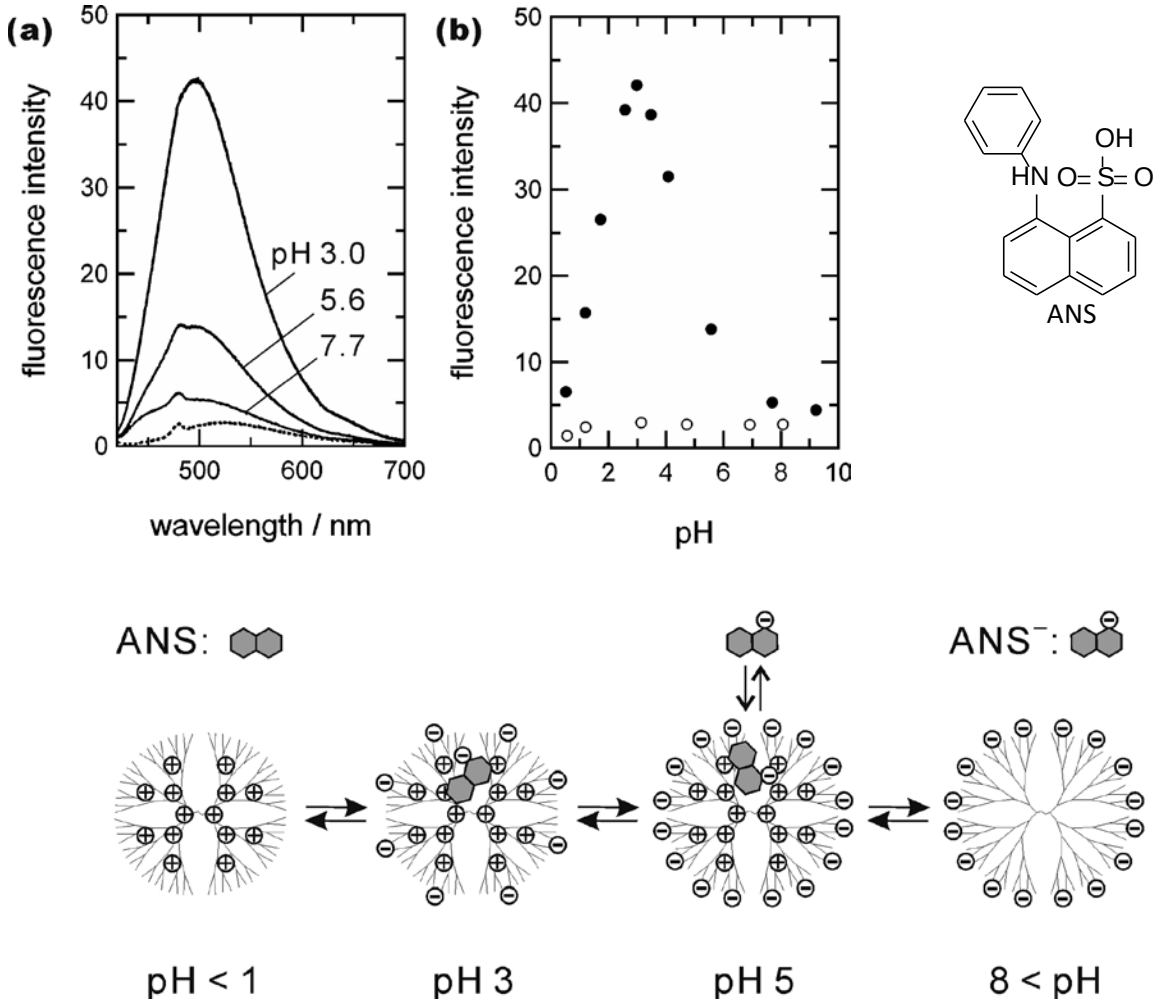

Figure 1.12. Schematic representation of the encapsulation behaviour of 8-anilino-1-naphthalenesulfonic acid (ANS) into the PAMAM G3.5 dendrimer.[44]

CHAPTER 2

PAMAM DENDRIMERS ACT AS SUPRAMOLECULAR HOSTS THROUGH NON-COVALENT INTERACTIONS

2.1 INTRODUCTION

As we discussed in Chapter 1, commercially available poly(amidoamine) (PAMAM) dendrimers are water-soluble, hyperbranched polymers that have attracted attention due to their interesting structural features.[33,45] They are currently being explored for a wide range of applications.[2,37,46] The full generation PAMAM dendrimers are polycations in aqueous solutions near neutral pH,[38] making them good hosts that can bind small organic molecules in water.

Previous studies have been reported in the literature by the Gröhn group,[2,40,41,47] and others,[34,48] on the binding of small organic molecules to charged polyelectrolytes. In this study, these binding processes were investigated in-depth, in hopes that we will contribute to a more complete understanding of these interactions. We approached this task by the study of the interactions established by the dendrimer with small organic probe molecules.

2.1.1 Spectroscopic Methods

Binding titrations of small molecules to the dendrimers were investigated by recording changes in absorbance, fluorescence emission intensity, and fluorescence anisotropy. Fluorescence anisotropy is a polarized fluorescence technique that reports on the rate of rotational diffusion of fluorescent molecules.[20] In fluid solution, fluorescein dye molecules display a fast rotational diffusion rate translating to low measured fluorescence anisotropy values

when excited with polarized light. In contrast, when bound to much larger molecules, such as the PAMAM dendrimers studied here, fluorescein molecules tumble at the much slower rate characteristic of the heavy polymers, resulting in an increased anisotropy value for their emission. We therefore can look at anisotropy as a valuable reporter for binding. As an added advantage, anisotropy measurements are carried out by taking the ratio of two independent fluorescence intensity readings taken with crossed polarizer settings, they are also largely insensitive to the fluorophore concentration. Therefore, anisotropy reports directly on the molar ratio of free vs. bound fluorophore and is a very valuable property in studying binding.

In the present context, optical spectroscopy has significant advantages over other conventional structural elucidation methods: it is faster, it can be carried out at very low concentrations, and it can be largely automated. Unfortunately, common methods to investigate intermolecular interactions such as nuclear magnetic resonance (NMR) and mass spectroscopy (MS) are not quite appropriate in this situation. For instance, at the higher concentration required for effective NMR studies the system's behavior may not be the same as it would be at the much lower concentrations relevant to current applications. Additionally, the most effective buffering system we have found so far (HEPES) is NMR active and it would swamp any signal. NMR would also prove daunting because concentrated dendrimer solutions are very viscous and equilibration is exceedingly slow, and also the amount of polymeric material necessary to complete these studies would be prohibitively high. On the other hand, MS studies would certainly consume very little sample, but the desolvation and ionization processes are likely to upset the balance of weak intermolecular interactions: although some of the limitations of MS methods in this respect have been overcome,[49] conclusions drawn from such methods may not translate to the dilute aqueous medium that we want to characterize.

It is important to note that full generation PAMAM dendrimers display fluorescence emission as shown by Wang et al.[50] However, it was concluded that their intensity was only strong under acidic conditions and the phenomena was only evident after exposure to oxygen.[50] We did not see any evidence of this phenomenon in the work presented in this dissertation. Also, stoichiometry information cannot be readily extracted from these studies: a combination of the low concentrations used and the complexity of the equilibria involved has made it impractical to determine accurate loading of the small organic dyes on the dendrimer hosts. Similar difficulties have been previously reported in the literature.[48] The problem of determining stoichiometry for systems with a large number of binding sites has been tackled in other fields, e.g., in binding metal ions[51] or drugs[52] to nucleic acids, but in those cases a definitive model of the binding interactions was available, which is unfortunately missing in the case at hand. Therefore, we restricted ourselves to presenting relative affinities. These qualitative results still carry a surprising amount of valuable information about the binding interactions.

2.1.2 Significance

The studies presented in this chapter focus on the binding process of amine-terminated polyamidoamine (PAMAM) dendrimers with ethylenediamine cores of generations G3-G6. The G3-G6 range of generations was chosen for study because it presents an excellent compromise between a size large enough to provide interesting binding behavior and good loading properties, while maintaining the system's economically affordable for practical applications. Although we do expect larger dendrimers to have improved loading capacity, their prohibitively high price would significantly hinder their use in most applications. The dendrimers used in these studies are commercially available from Dendritech, Inc. in high purity as H_2O and MeOH solutions.

We conducted binding studies in aqueous solutions buffered at pH 7.4 using 50 mM 4-(2-hydroxyethyl)-1-piperazineethanesulfonic acid (HEPES) maintained at a constant temperature of 25°C. We chose to work at the physiological pH of blood (pH 7.4) because this would be the conditions for many projected applications, i.e. drug delivery. Working at pH 7.4 also allows these polyelectrolytes to bear charged surfaces which is necessary for studying the binding of small organic molecules to their scaffolds in water.

We selected HEPES as a buffering agent because it displayed minimal interactions with our dendrimer hosts. Other buffers commonly used around neutral pH can interfere with the binding of small organic molecules. For instance, Figure 2.1 illustrates that the common phosphate buffer system is not viable for these experiments, because the phosphate anions compete effectively for the dendrimer binding sites at the concentrations necessary for affective binding. Figure 2.1 shows the binding experiment with PAMAM G4 and 5(6)-carboxyfluorescein in phosphate buffer. There was very limited binding of **CF** to the dendrimer scaffold observed over a range of concentrations that would otherwise result in complete binding when carried out in HEPES buffer. The phosphate anions saturate all the binding sites of the dendrimer, not allowing binding of **CF** to the dendritic scaffold.

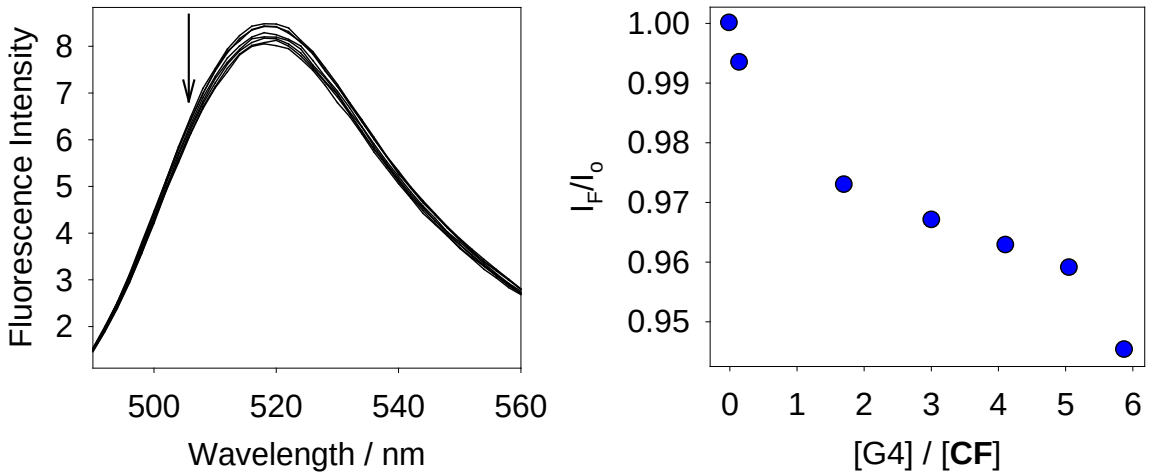

Figure 2.1. Comparison of the binding of 5(6)-carboxyfluorescein (**CF**) to a G4 PAMAM dendrimer using fluorescence intensity in phosphate buffered H_2O (pH 7.4). [**CF**] = 2.0×10^{-6} M.

2.1.3 Research Design

The amine-terminated PAMAM dendrimers only have spectroscopic signatures in the far UV region (where our buffering system also absorbs). In order to follow the binding of these systems, we established a way to move detection to the visible region. We report on the structural information extracted from the analysis of the binding of a series of anionic fluorescent probes to PAMAM dendrimers in buffered neutral water. The chemical structures of these dyes are shown in Scheme 2.1 in their calculated protonation states in dilute aqueous solution buffered to pH 7.4, as determined from literature data.[53-55]

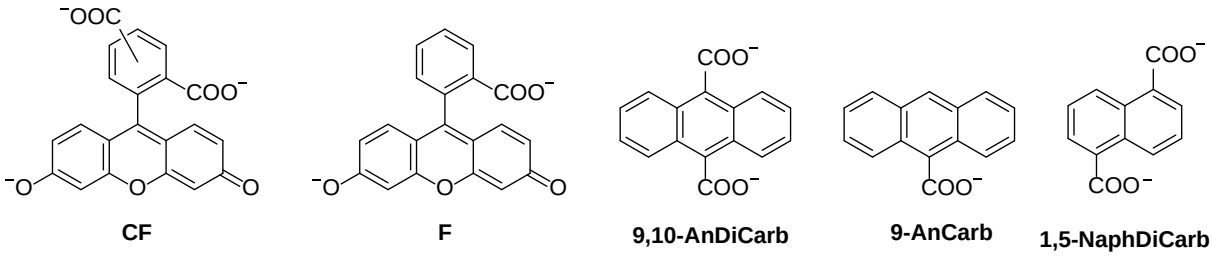

Scheme 2.1. Structure and protonation states of the fluorophores relevant to the present study when dissolved in dilute aqueous solution buffered to pH 7.4. From left: the 5(6)-carboxyfluorescein trianion (**CF**), the fluorescein dianion (**F**), the 9,10-anthracenedicarboxylate dianion (**9,10-AnDiCarb**), the 9-anthracenecarboxylate anion (**9-AnCarb**), and the 1,5-naphthalenedicarboxylate dianion (**1,5-NaphDiCarb**).

In this approach, a fluorescent indicator (**CF** in this example) is bound to the dendrimer (D) to form a dye-dendrimer complex (Scheme 2.2); we call this the binding process and the results obtained from it will be discussed in detail in this chapter. In this complex, the dyes display the typical optical properties of the bound species. This provided insight as to what structural features are significant for the binding to these dendritic structures.

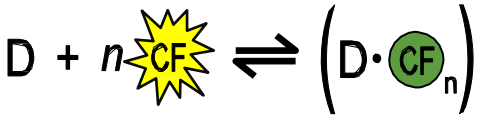

Scheme 2.2. Dye binding process.

2.2 MONO-ANIONIC SYSTEMS

We performed our first exploratory studies using 9-anthracenecarboxylate (**9-AnCarb**), but the apparent binding affinity of a monoanionic system was unfortunately too low to be practicable at the concentrations relevant to these studies (Figure 2.4). We hypothesized that due to **9-AnCarb**'s low molecular symmetry that it would be a poor fluorophore resulting in a low quantum yield, which would also make it harder to study its optical properties at relevant concentrations. The larger number of allowed vibrational modes translates into multiple non-radiative decay opportunities, which depress the fluorescence quantum yield.

In order to prove this, we determined the quantum yield of **9-AnCarb** and **9,10-AnDiCarb** using the comparative method which involves the use of a reference fluorophore of known quantum yield. The solutions of the reference and unknown samples with similar absorbance, when excited at the same wavelength, can be assumed to be absorbing the same number of photons.[20] Therefore, a ratio of the integrated fluorescence intensities of both solutions will yield the ratio of quantum yield values. The quantum yield of the unknown fluorophore is calculated by equation (1): where Φ is the quantum yield, I is the integrated

intensity, *OD* is the optical density, and *n* is the refractive index of the solvent. The quantities with the subscript *ref* refer to the reference fluorophore of known quantum yield.

$$\Phi = \Phi_{Ref} \frac{n^2}{n_{ref}^2} \cdot \frac{I}{OD} \cdot \frac{OD_{ref}}{I_{ref}} \quad (1)$$

We chose anthracene as a reference fluorophore that has a known Φ of 0.27 in ethanol, which has a refractive index of 1.36. Determining the Φ for **9,10-AnDiCarb** first, two solutions were made: one of anthracene in ethanol [2.02 x 10^{-5} M] and one of **9,10-AnDiCarb** in 50 mM HEPES buffer [2.02 x 10^{-5} M]. From the absorbance data shown to the left of Figure 2.2, the excitation wavelength was chosen to be 374 nm. The optical density of anthracene and **9,10-AnDiCarb** at this wavelength was 0.1203 and 0.1520, respectively. The integrated fluorescence intensities were determined to be 11744156 for anthracene and 36731356 for **9,10-AnDiCarb**. From the equation above, the Φ of **9,10-AnDiCarb** was calculated to be 0.64.

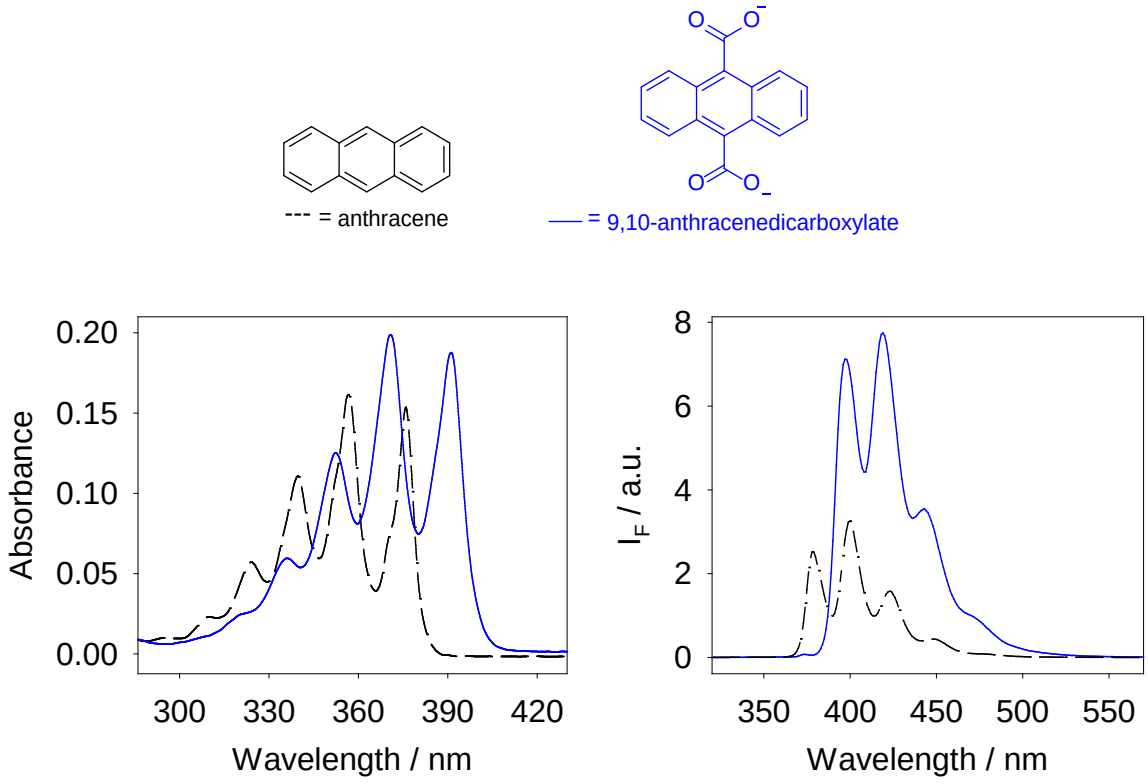

Figure 2.2. Absorbance and fluorescence intensity of anthracene in ethanol and **9,10-AnDiCarb** in buffered H_2O. λexc: 374 nm, λem: 300-600 nm, Slits, exc & em: 2 nm spectral resolution.

We then calculated the Φ for **9-AnCarb** using the same method and reference. From the absorbance data in Figure 2.3, the excitation wavelength was chosen to be 378 nm. The optical density of anthracene and **9-AnCarb** at this wavelength were 0.1203 and 0.1520, respectively. The integrated fluorescence intensities were determined to be 11744156 for anthracene and 36731356 for **9-AnCarb**. From the equation above, the Φ of **9-AnCarb** was calculated to be 0.10. The much smaller calculated quantum yield for **9-AnCarb** confirms why we have to work at higher concentrations when using it as a probe, compared to **9,10-AnDiCarb**.

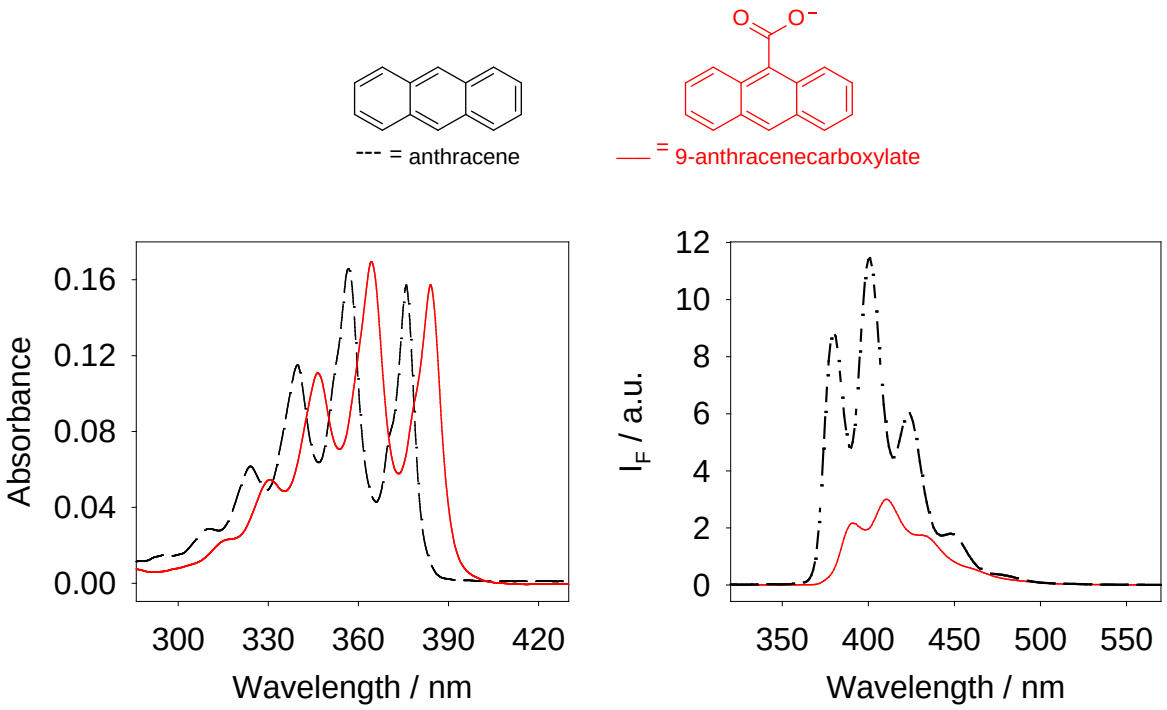

Figure 2.3. Absorbance and fluorescence intensity of anthracene in ethanol and **9-AnCarb** in buffered H_2O. λexc: 378 nm, λem: 300-600 nm, Slits, exc & em: 2 nm spectral resolution.

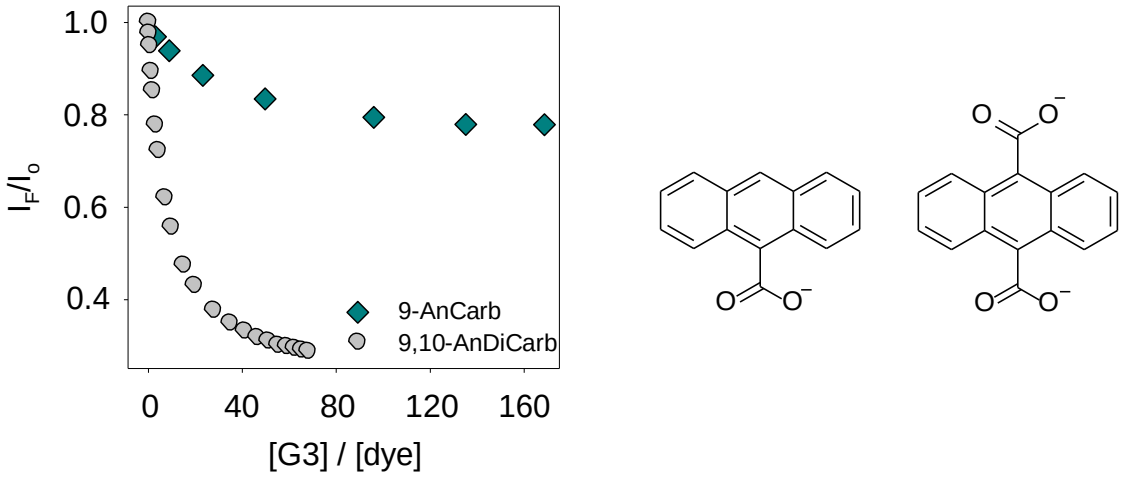

Figure 2.4. Comparison of the binding of 9-anthracenecarboxylate (**9-AnCarb**), and 9,10-anthracenedicarboxylate (**9,10-AnDiCarb**) to a G3 PAMAM dendrimer monitored through fluorescence intensity in buffered H_2O (pH 7.4). [dyes] = 2.0×10^{-6} M. Intensity was normalized to that of the free fluorophore in both cases.

In Figure 2.4 we present a comparison between the binding of **9,10-AnDiCarb**, a dianion, and **9-AnCarb**, a monoanion, with PAMAM G3 dedrimer. It is clear that the monoanion binds with much lower affinity than the dianionic fluorophore. Given these limitations, i.e. the lower "brightness" of this fluorophore and its lower binding affinity, we did not pursue the study of interactions involving **9-AnCarb** any further.

2.3 5(6)-CARBOXYFLUORESCEIN AS A BINDING PROBE

This work was previously published by other members of this group.[34] For comparison, I reproduced the binding profiles between PAMAM G3-G6 and CF shown in Figure 2.5. It is worth mentioning that all the experiments presented in this work were carried out at exactly constant dye concentration. In order to do so, aliquots of a solution containing the polymer were typically added to a solution of the dye to construct the binding profiles shown. The profiles are a function of the polymer to dye ratio in solution. A low [polymer] / [dye] ratio corresponds to an excess of dye; at high [polymer] / [dye] ratios, an excess of polymer is present in solution.

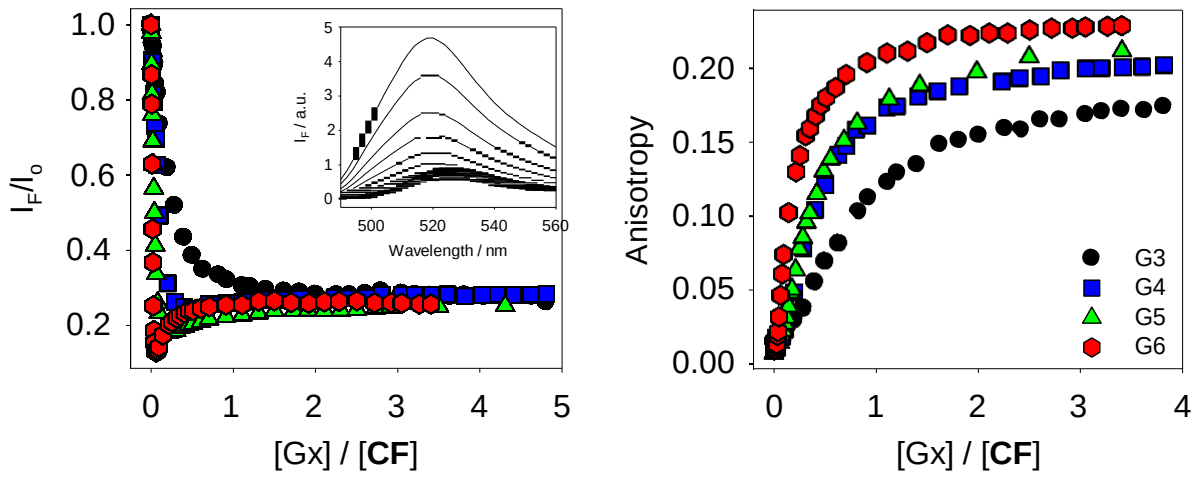

Figure 2.5. Generational trends in the fluorescence intensity and anisotropy signal: comparison between isotherms obtained from the interaction of 5(6)-carboxyfluorescein with PAMAM dendrimers of generations G3-G6. In buffered H_2O (pH 7.4), [**CF**] = 2.0×10^{-6} M. Inset: Family of spectra obtained from fluorescence intensity titration.

2.4 FLUORESCEIN AS A BINDING PROBE

We chose to begin our in depth binding studies using full generation PAMAM dendrimers which bear a positive charge. We, therefore, needed a negatively charged probe for adequate binding. We chose fluorescein (**F**) as our first dianionic fluorescent probe to study because it has high quantum yield, it is commercially available, and it is inexpensive. **F** also bears two negative charges in aqueous solution at neutral pH which is essential for binding with the positively charged dendrimer. Previous work in our group had also shown that the xanthene family of dyes have high affinity for the dendrimer scaffold.[34]

2.4.1 Fluorescein's Absorbance

Upon addition of aliquots of PAMAM dendrimers to a buffered aqueous solution of fluorescein (**F**, 2.0×10^{-6} M), a red shift occurs in the absorption spectrum of the dye and an isosbestic point is observed (Figure 2.6). At low [dendrimer] / [**F**] ratios, most of the dye is still

free in solution, giving an absorbance spectrum typical of the free anionic fluorophore, while at high [dendrimer] / [**F**] ratios we see an absorbance spectrum typical of the bound complex.

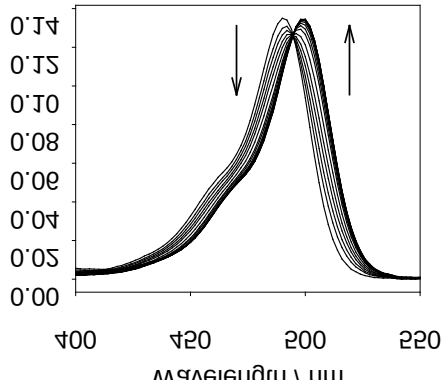

Figure 2.6. Family of spectra obtained from the titration of fluorescein ([**F**] = 2.0 x 10^{-6} M) with amine-terminated G5 PAMAM dendrimer ([dendrimer] = 0 → 1.3 x 10^{-4} M) in buffered H_2O (pH 7.4).

We have confirmed that the red shift observed in the absorbance spectra over the course of the titration is not due to a change in the protonation state of the fluorescein molecules. We accomplished this by making three solutions of fluorescein dye at 2.0 x 10^{-6} M from a stock in buffer and then modified the pH of the solutions by adding HCl or NaOH as appropriate, to reach pH 2.0, pH 7.4, and pH 12.0. The spectrum of fluorescein in very acidic water solution (pH 2.0) displays a band centered around 438 nm, which denotes the protonated structure of fluorescein (Figure 2.7). The spectrum of fluorescein in very basic water solution (pH 12.0) displays a band centered around 490 nm, which is compatible with the spectrum of the free dye in our titrations. This indicates to us that fluorescein is already fully deprotonated at the working pH (7.4) and the absorbance change observed upon binding to the polyelectrolyte is not due to further deprotonation. It therefore must be due to direct interaction with the PAMAM dendrimer.

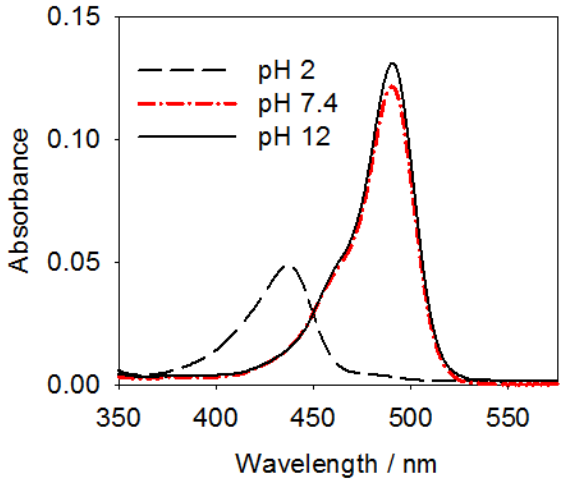

Figure 2.7. The absorbance spectra of three solutions of fluorescein dye at pH 2, 7.4, and 12. ([**F**] = 2.0 x 10^{-6} M)

When comparing the absorbance profiles obtained by the titration of different generations of dendrimers into fluorescein solutions, a generational trend is apparent (Figure 2.8): it is clear that the observed affinity of the dendrimer for the dye increases at higher generations. We ascribe this effect to the exponential increase in the number of surface charges present in dendrimers of higher generation. In particular, we contend that the most important structural effect is not simply the increase in charge, but rather the increase in charge density on these hyperbranched structures. In fact, the diameter of these molecules grows only slightly across the generations,[56] whereas the net charge approximately doubles with each generation.[8] As a point of reference, the effective diameter of G5 PAMAM dendrimer (~60 charges) is 5.4 nm, whereas that of G6 (~120 charges) is 6.7 nm.[57] Further discussion of this effect can be found in the context of fluorescence emission trends below.

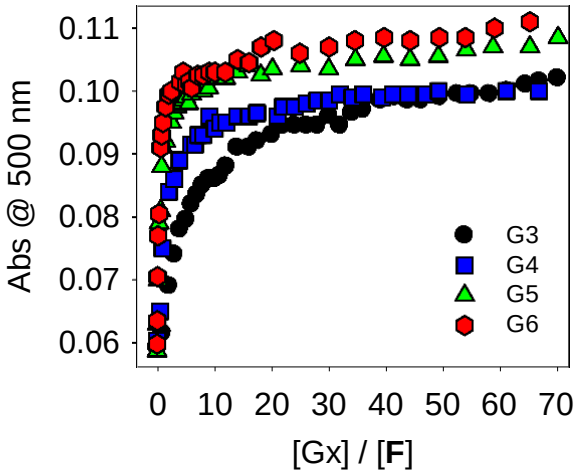

Figure 2.8. Generational trends in absorbance: comparison between isotherms obtained from the interaction of fluorescein with PAMAM dendrimers of generations G3-G6, in buffered H_2O (pH 7.4). [**F**] = 2.0×10^{-6}M.

2.4.2 Fluorescein's Fluorescence Emission

The fluorescence intensity profiles obtained over the course of the binding titrations described above are presented in Figure 2.9; fluorescence intensity has been normalized to that of the free dye for ease of comparison. These profiles may be interpreted on the basis of the [dendrimer] / [**F**] ratio as well.

At very low [dendrimer] / [**F**] ratios most of the dye molecules are still free in solution, a state characterized by fluorescein's high fluorescence emission. Conversely, towards the end of the titration, signal saturation is reached after the addition of a very large excess of dendrimer (high [dendrimer] / [fluorophore]), characterized by significant quenching of the fluorescein emission. In this situation, all the fluorescein must be in the bound state, i.e. each fluorescein molecule is bound to a different dendrimer molecule and isolated, in a one-dye-per-polymer binding state. We expect that an excess of unoccupied dendrimer molecules is also present in solution. Therefore, the emission quenching observed in these conditions is due solely to the interaction between the dendrimer and fluorescein. We hypothesized that the observed quenching is caused by a photo-induced electron transfer (PET) process from those tertiary amines in the

dendrimer's backbone that happen to be in close proximity of the bound fluorophore.[58]

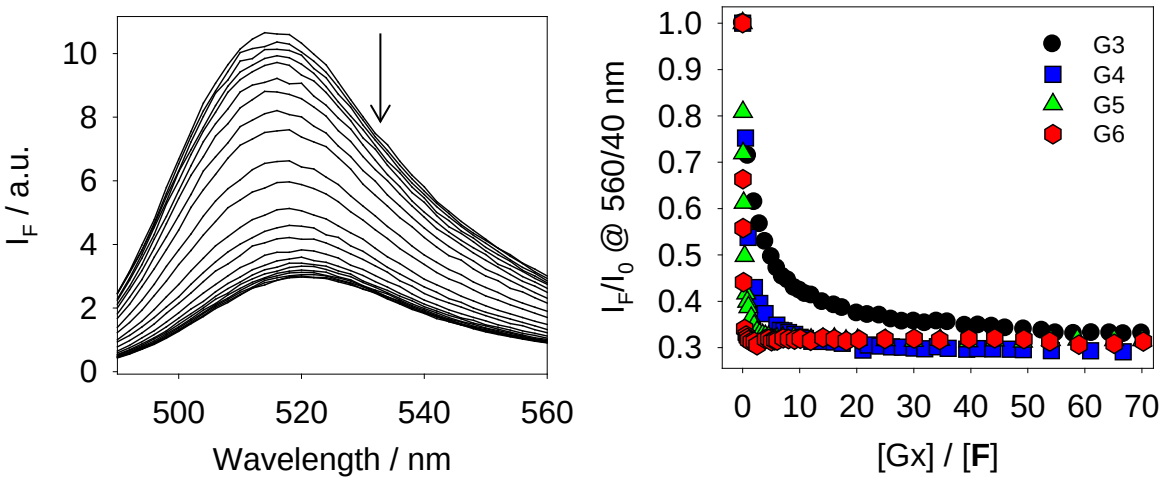

Figure 2.9. Left: Family of spectra obtained from the titration of fluorescein with amine-terminated G5 PAMAM dendrimer ([dendrimer] = 0 → 1.3 x 10^{-4} M). Right: Generational trends in the fluorescence intensity signal: comparison between isotherms obtained from the interaction of fluorescein with PAMAM dendrimers of generations G3-G6. In buffered H_2O (pH 7.4), [**F**] = 2.0 × 10^{-6} M.

The relative affinities displayed by each dendrimer generation for the fluorescein probe are comparable to those observed from the absorbance profiles discussed above: the observed affinity of the dendrimer for the dye is higher for larger dendrimers. We can once again ascribe this effect to the increase in charge density on these hyperbranched structures. Additionally, it is worth noting that the degree of quenching attained at saturation is very similar in all of these titrations (Figure 2.9), indicating that the final state must provide very similar immediate environments to the fluorophore molecules. This is in agreement with our hypothesis that, in the presence of an excess of dendrimer, each fluorophore molecule is bound and isolated. One must consider that even the smallest of the dendrimers used in the present study (G3, M_r ~6,900) is still very much larger than fluorescein (Mr ~330): when bound and isolated, the small organic fluorophore is essentially oblivious to the size of its partner, since its microenvironment is always the same, no matter which of the dendrimer generations it is bound to.

2.4.3 Fluorescein's Fluorescence Anisotropy

Anisotropy measurements were carried out concurrently with the fluorescence emission titrations present above. The shape of the fluorescence anisotropy profiles is also controlled by the [dendrimer] / [**F**] ratio (Figure 2.10). In fact, at a low [dendrimer] / [**F**] ratio most of the dye molecules are free in solution and rotating rapidly, a state characterized by low fluorescence anisotropy values. However, as the [dendrimer] / [**F**] ratio increases during the course of the titration, more of the dye molecules are bound to dendrimers, a state characterized by a significantly higher anisotropy signal for the fluorophore.

It is notable that the anisotropy profile reaches saturation at a different limiting value for each dendrimer generation. This is to be expected given the large difference in size between generations of these dendrimers. In fact, the saturation value of the anisotropy signal is ultimately determined by the rate at which the fluorophore-dendrimer complex tumbles in solution, and the latter rate is in turn overwhelmingly determined by the size of the much larger dendrimer. As discussed above, in the presence of a large excess of dendrimer, only 1:1 dendrimer-dye complexes are formed; the fluorophore's contribution to the mass of these 1:1 adducts is negligible. Larger dendrimers induce a lower tumbling rate of their dye adducts, and therefore a higher limiting value for the corresponding fluorescence anisotropy.

Once again, a clear trend is discernible in the relative affinities displayed by each dendrimer generation for the fluorescein probe (Figure 2.10, left). The fluorescence anisotropy of an ensemble of molecules has the convenient property of being the average of the anisotropy values of each component of the ensemble, weighted by that component's molar fraction. This consideration, combined with the important observation that a limiting value is clearly reached at the end of each titration in this data set, allows us to convert the anisotropy values into an overall

degree of binding $(r\text{-}r_0) / (r_{max}\text{-}r_0)$, where r is the measured anisotropy, r_0 is the anisotropy of the free dye measured at the start of the titration, and r_{max} is the limiting anisotropy recorded when binding is complete; the results are reported to the right of Figure 2.10. Inspection of these plots leads to the conclusion that the observed affinity of the dendrimer for the dye increases for larger dendrimers, an effect that we have previously observed and ascribed to the increase in charge density on these hyperbranched structures.

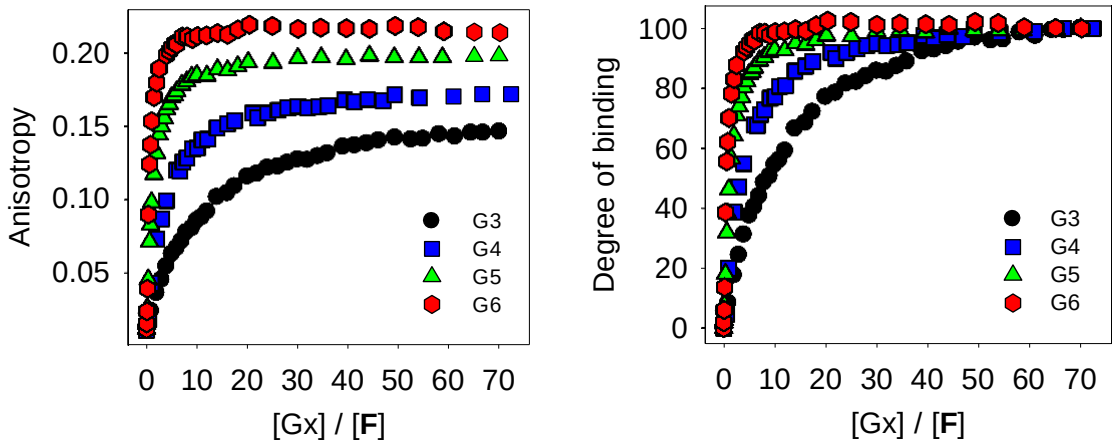

Figure 2.10. Generational trends in fluorescence anisotropy: left, anisotropy isotherms obtained from the interaction of fluorescein with G3-G6 PAMAM dendrimers; right, overall degree of binding of the fluorophore (%). All experiments in buffered H_2O (pH 7.4). [**F**] = 2.0×10^{-6} M.

2.5 9,10-ANTHRACENEDICARBOXYLATE AS A BINDING PROBE

In our quest to understand the behavior of PAMAM dendrimers as supramolecular hosts, we also studied their binding to the 9,10-anthracenedicarboxylate fluorophore (**9,10-AnDiCarb**). This fluorophore was chosen because it represents a significant departure from the xanthene fluorophores that we have studied so far. Additionally, both this dicarboxylate and fluorescein are dianionic in water solution around neutral pH, so we anticipated that any differences in their binding properties could be ascribed to those elusive non-electrostatic secondary interactions whose presence and nature it is our intent to elucidate.

In the case of this fluorophore, as it was with **F** and **CF** before, we collected absorbance (Figure 2.11), fluorescence emission (Figure 2.12), and fluorescence anisotropy information (Figure 2.13) during the course of binding titrations. Fluorescence data was obtained at a concentration of **9,10-AnDiCarb** = 2.0 x 10^{-6} M, for direct comparison to the results discussed above for the other fluorophore. Unfortunately, that concentration proved too low to obtain reliable absorbance data from the anthracene chromophore, since its molar absorptivity (≈ 9,000 M^{-1} cm^{-1}) is significantly lower than that of xanthene dyes (≈ 40,000 M^{-1} cm^{-1}); the absorbance data presented below was therefore obtained at a tenfold higher concentration ([**9,10-AnDiCarb**] = 2.0 x 10^{-5} M). A complete set of binding curves was obtained in this case as well, comparing the relative observed affinities of the PAMAM dendrimers of generations G3 through G6.

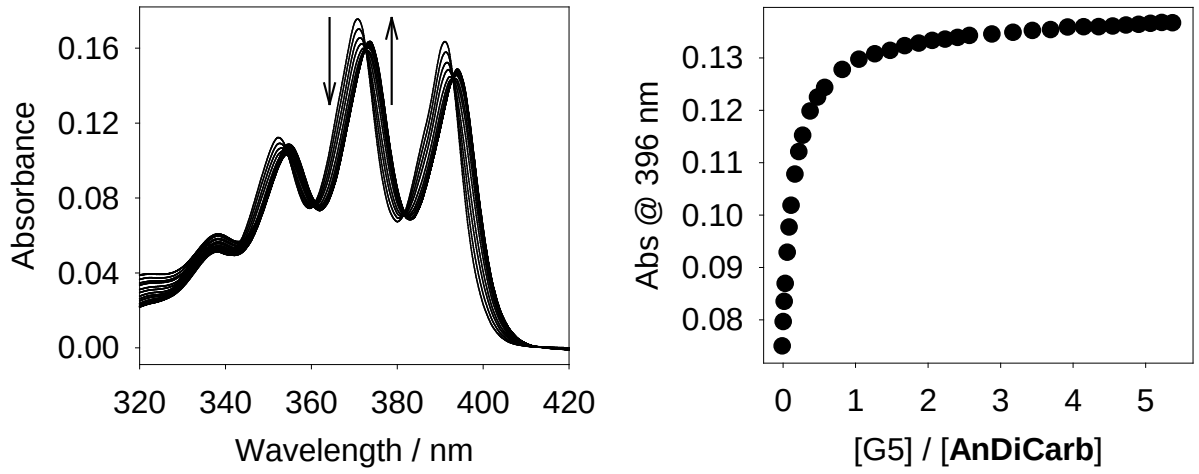

Figure 2.11. Titration of 9,10-anthracenedicarboxylate (**9,10-AnDiCarb**, 2.0 x 10^{-5} M) with G5 PAMAM dendrimer in absorbance. Left: family of absorbance spectra; right: titration profile at 396 nm as a function of the concentration of G5 dendrimer in buffered H_2O (pH 7.4).

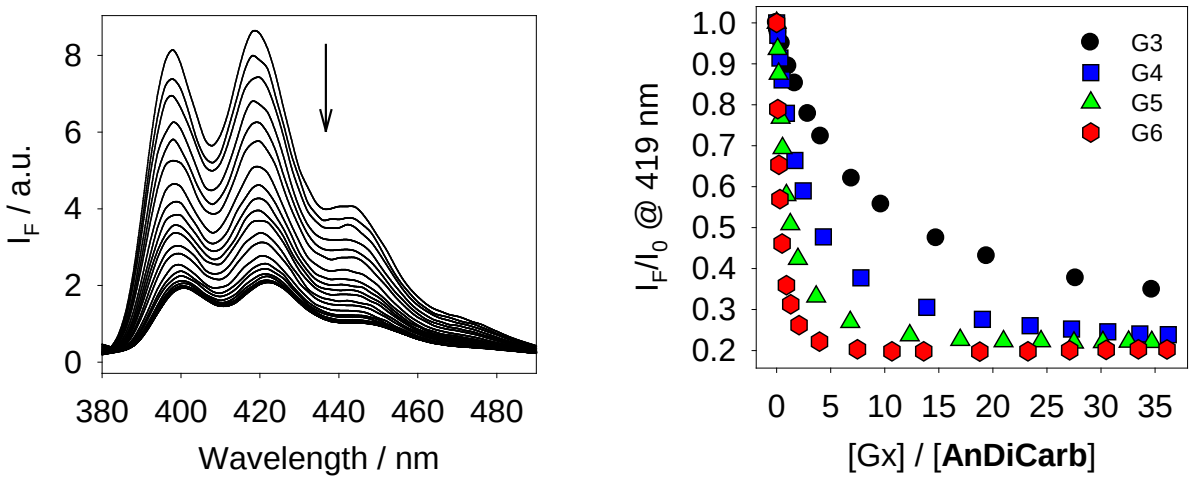

Figure 2.12. Left: Family of fluorescence emission spectra recorded over the course of the titration of 9,10-anthracenedicarboxylate with aliquots of G5 PAMAM dendrimer. Right: Fluorescence emission isotherms showing generational trends for binding of 9,10-anthracenedicarboxylate with G3-G6 PAMAM dendrimers. [**9,10-AnDiCarb**] = 2.0×10^{-6} M in buffered H_2O (pH 7.4).

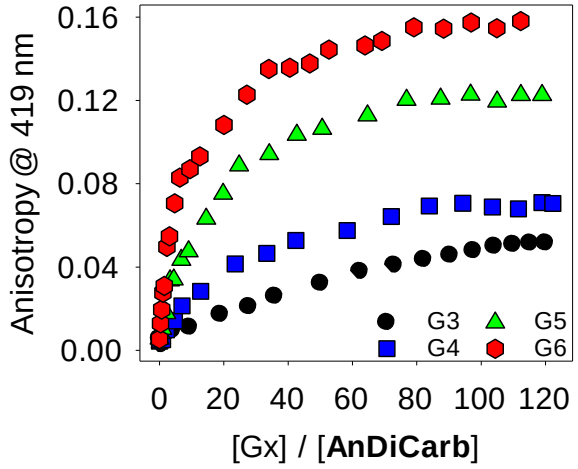

Figure 2.13. Fluorescence anisotropy isotherms showing generational trends in fluorescence for binding of 9,10-anthracenedicarboxylate with G3-G6 PAMAM dendrimers. [**9,10-AnDiCarb**] = 2.0×10^{-6} M in buffered H_2O (pH 7.4).

2.6 1,5-NAPHTHALENEDICARBOXYLATE AS A BINDING PROBE

We attempted to study the binding properties of 1,5-naphthalenedicarboxylate (**1,5-NaphDiCarb**). Our hope was that the binding interaction would be a good and direct comparison with **9,10-AnDiCarb**, the only difference being that of an extra aromatic ring in

9,10-AnDiCarb. We also hoped that **1,5-NaphDiCarb** would provide insight to the importance of flexibility and rotational freedom of the guest. However, from Figure 2.14 one can see that PAMAM dendrimers (G3 shown below) have significant absorbance at wavelengths in the range of the maximum of absorption for **1,5-NaphDiCarb.** Due to these results we could not obtain proper binding profiles and we did not pursue the study of interactions involving **1,5-NaphDiCarb** any further.

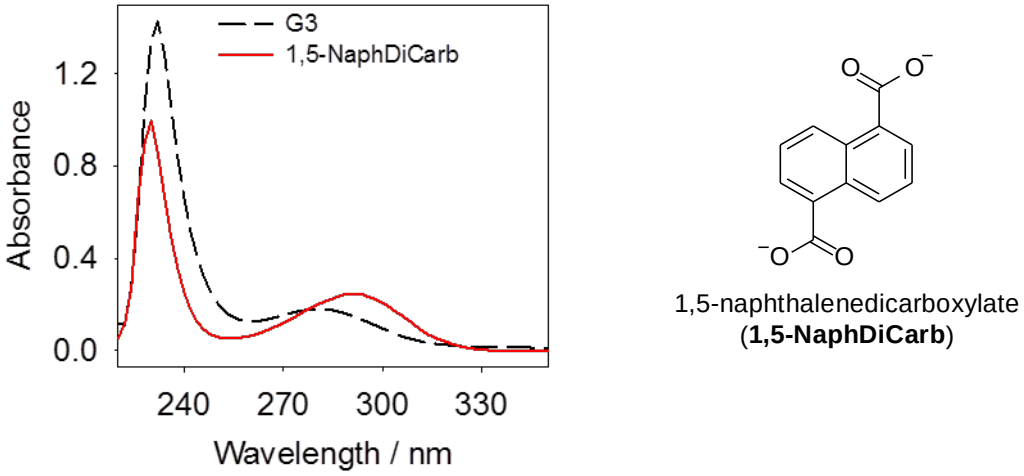

Figure 2.14. Absorbance scan of PAMAM G3 and 1,5-naphthalenedicarboxylate. [**1,5-NaphDiCarb**] = 2.0×10^{-5} M in buffered H_2O (pH 7.4).

2.7 COMPARING FLUOROPHORES

We are now positioned to compare the information obtained here from probing the binding of 5(6)-carboxyfluorescein (**CF**), fluorescein (**F**), and 9,10-anthracenedicarboxylate (**9,10-AnDiCarb**) to PAMAM dendrimers (Figure 2.17). We will focus first on the comparison between the two xanthene dyes, **F** and **CF**. We have previously shown that at pH 7.4 **F** carries two negative charges, whereas **CF** carries three.[34,53] A visual comparison of the overlaid fluorescence titration profiles for binding titrations of these two fluorophores to PAMAM dendrimers (Figure 2.15) immediately shows that **CF** has a much higher relative affinity for the dendrimer than **F** itself. For instance, we can observe that saturation is not quite reached for **F** in

the presence of two equivalents of dendrimer, whereas the **CF** titration is very near complete in the same conditions.

Quenching of the **CF** emission in these conditions does not arise simply from the discussed PET process induced by the dendrimer. In fact, our group has previously reported that at intermediate concentrations of dendrimer at which there is an excess of **CF** in solution with respect to the dendrimer, multiple molecules of **CF** are drawn in close proximity of the dendrimer surface.[34] In these conditions, self-quenching due to resonance energy transfer (RET) is very effective. This additional process gives rise to the characteristic "dip" in the fluorescence intensity profiles obtained as the concentration of dendrimer is increased in solution.

It is very interesting to note that such a trough in the profile is not observed at all in the case of the binding of **F**, as shown in Figure 2.15 for G5 and in Figure 2.9 for all generations considered. This is consistent with the lower affinity for **F** displayed by the dendrimers: the less powerful electrostatic interaction between the dendrimers and the dianionic **F** is not sufficient to overcome the repulsion between fluorescein molecules. Therefore, the molecules of this dye cannot be forced into as close proximity as those of the trianionic **CF**. Consequently, **F** molecules never come close enough to each other to interact through resonance energy transfer, so they do not self-quench as effectively as **CF** does, and ultimately they do not produce the characteristic "dip" at intermediate dendrimer concentrations.

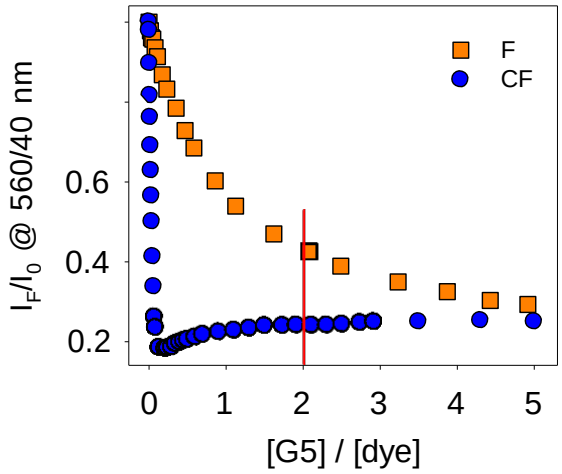

Figure 2.15. Overlay of fluorescence intensity isotherms obtained from titration of **F** or **CF** with G5 dendrimer. [**F**] and [**CF**] = 2.0×10^{-6} M in buffered H_2O (pH 7.4).

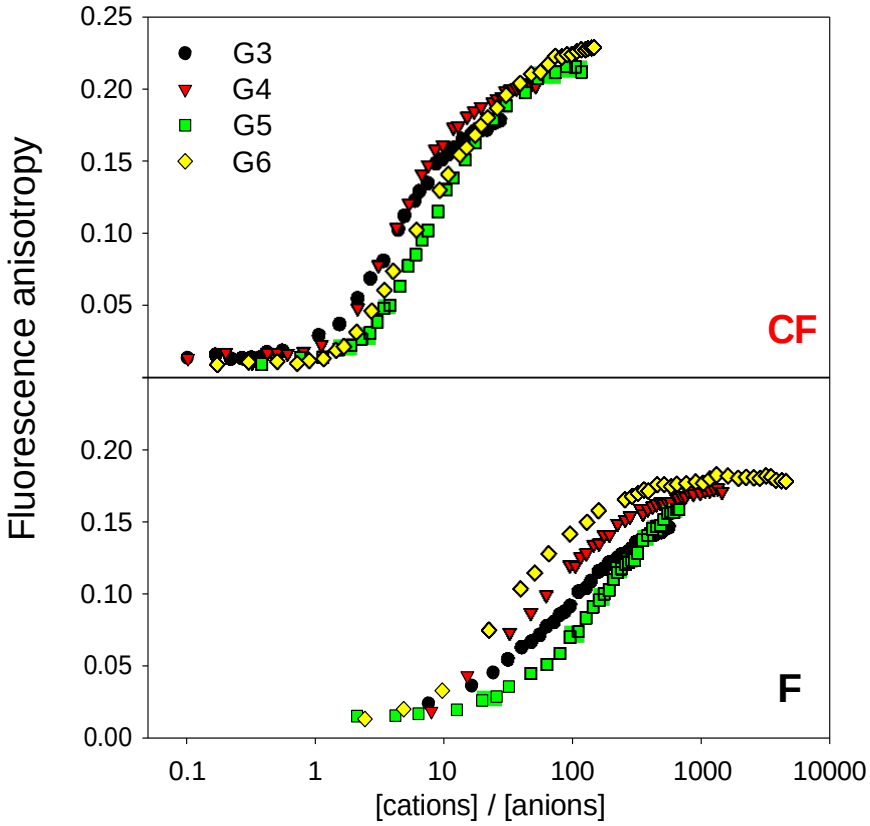

Figure 2.16. Comparison of relative affinities when electrostatic effects due to the different number of charges on various dendrimer generations and dyes are removed by normalization.

Figure 2.16 shows a comparison of generation trends in the fluorescence anisotropy for **F** and **CF** dyes binding to all studied dendrimer generations as a function of the ratio of the concentrations of positive over negative charges in the host and guest. Even when one accounts for the different number of charges on the **F** and **CF** dye molecules, there is still a difference in observed affinity between the two dyes that carries over across dendrimer generations. This suggests that dendrimers are sensitive to some structural parameters in the guest, such as its charge density.

We can now compare the binding behavior of the **F**, **CF** and **9,10-AnDiCarb** fluorescent probes to the charged PAMAM dendrimers. For the sake of brevity, here we will show comparisons based on the G5 dendrimer generation, but similar trends have been observed with all the generations under study. Furthermore, we will limit our discussion to fluorescence emission titrations carried out at a probe concentration of 2.0×10^{-6} M, because the absorbance signal of **9,10-AnDiCarb** was too low at this concentration to directly compare data. As shown in Figure 2.17, **CF** displays the highest affinity of the three probes studied so far. This is unsurprising, and accounted for by its three negative charges, whereas the other two probes only carry two negative charges each. More interestingly, however, **9,10-AnDiCarb** was found to bind with higher relative affinity than fluorescein, even though both probes bear two negative charges. As we had hoped at the onset of the study, secondary interactions must be at play in this case.

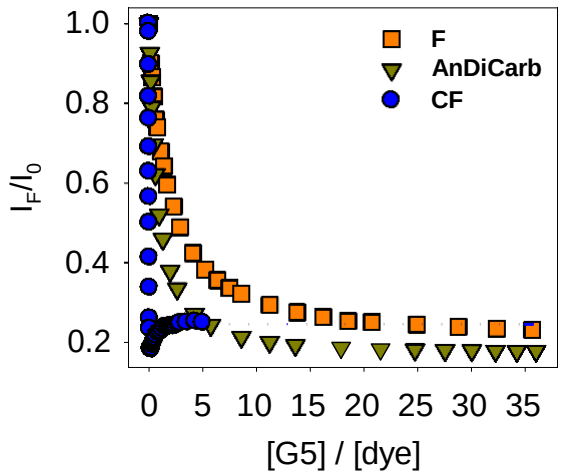

Figure 2.17. Comparison of the binding of fluorescein (**F**), 5(6)-carboxyfluorescein (**CF**) and 9,10-anthracenedicarboxylate (**9,10-AnDiCarb**) to a G5 PAMAM dendrimer monitored by fluorescence intensity in buffered H_2O (pH 7.4). [dyes] = 2.0×10^{-6} M.

We propose a twofold explanation for the anthracene probe's higher relative binding affinity. First, the difference could be ascribed to the existence of cation-π interactions between the surface ammonium groups in the dendrimer and the aromatic cores of the dye molecules. In his extensive studies on the origins of the cation-π interaction,[12] Dougherty established that although these interactions are not completely electrostatic in nature, electrostatics are nonetheless an excellent predictive tool when comparing strength of interaction of the same cation across a series of aromatics. In particular, electrostatic potential surfaces are a handy tool in these predictions. Additionally, Mecozzi and Dougherty have shown that the much more computationally affordable maps calculated from semi-empirical methods can also be used in this context.[59]

2.7.1 Electrostatic Potential Maps

In order to further understand the difference in binding affinity between **F** and **9,10-AnDiCarb**, we calculated electrostatic potential maps (ESP) for the extended aromatic systems that are present in both dyes, i.e. the xanthene and the anthracene moieties. The results

presented in Figure 2.18 show that the 9,10-anthracenedicarboxylate dye's carbon-only aromatic core would favor electrostatic interactions with a cation more than fluorescein's oxygen-containing xanthene moiety. Therefore, we expect that stronger cation-π interactions can be formed between the anthracene containing fluorophores and the dendrimers. This additional stabilizing contribution enhances the affinity of anthracene-based dyes for the cationic dendrimers and explains the higher relative affinity when compared to fluorescein. Additionally, further inspection of the ESP maps gave us a good idea of where these interactions might take place on these molecules, i.e. in the zones corresponding to the lowest (most negative) electrostatic potential. The maps suggest that the central ring would provide the most likely region of interaction with a cation in both structures.

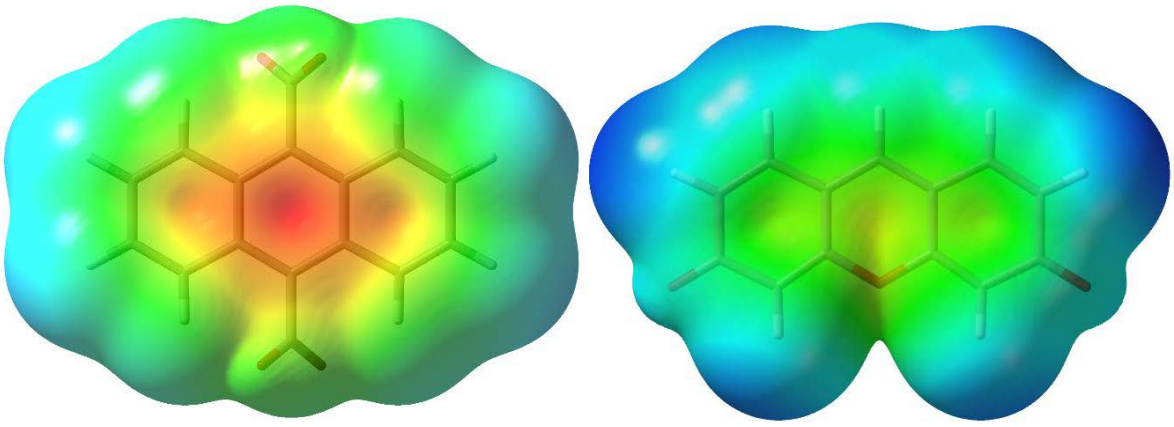

Figure 2.18. PM6 electrostatic potential surfaces for **9,10-AnDiCarb** (left) and the 6-hydroxy-*3H*-xanthene-3-one anion representing the lower aromatic portion of the fluorescein family of dyes (right).

2.7.2 Calculation of Electrostatic Potential Surfaces

The above calculation focused on the larger of the aromatic moieties present in the molecule. We thus considered the following three species shown in Figure 2.19. The geometrical structures of these molecules were optimized using the PM6 semi-empirical method[60] using *Gaussian*.[61] A vibrational frequency calculation was carried out to check that the resulting

geometry corresponded to an energy minimum. The Cartesian coordinates for each optimized structures are reported at the end of this chapter. The total electron density was sampled in space around each optimized structure, by generating an electron density cube from the total SCF density with the *cubegen* utility included in *Gaussian*. The cubes were generated with the parameters shown in Table 2.1.

.

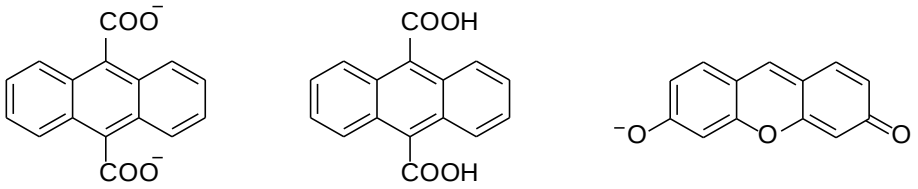

9,10-AnDiCarb **9,10-AnDiCarbH2** **Xanth**

Figure 2.19. 9,10-AnDiCarb and **Xanth**, were used to represent the aromatic moieties of the 9,10-anthracenedicarboxylate, and of fluorescein, respectively. **9,10-AnDiCarbH2**, i.e. the protonated form of **9,10-AnDiCarb,** was also considered as a point of comparison for the effect of the presence of charged species on the appearance of the ESP maps.

Table 2.1 Parameters used with the *cubegen* utility to obtain ESP maps from the SCF density.

Molecule:	**Number of points**	**Spatial resolution:**
9,10-AnDiCarb	81 x 147 x 162	0.09 Å
9,10-AnDiCarbH2	83 x 142 x 164	0.09 Å
Xanth	116 x 112 x 79	0.09 Å

The structures of the model compounds were optimized to a minimum with the PM6 semi-empirical method as implemented in the *Gaussian 09* program. The total electron density distributions from the optimized structures were used to calculate the electrostatic potential in space near the molecule. The values of ESP were then mapped onto an electron density surface with a density cutoff of 0.001. The colour mapping was chosen to highlight the difference between the **9,10-AnDiCarb** and **Xanth** systems, and the same mapping values were used for all

surfaces; in specific, the red colour (most negative) represents an ESP of -8.5, the blue colour (least negative) represents an ESP of -3.2 respectively. The ESP maps were then compared visually, as suggested by Dougherty. [59,12]

9,10-AnDiCarb and **Xanth**, however, carry different negative charges, the first being a dianion and the second being a monoanion. For us to conclude definitively that the difference in the calculated ESP is due to the electronic nature of the aromatic fragment, and not simply an accident of the difference in total charge, we also calculated an ESP map for the neutral 9,10-anthracenedicarboxylic acid (**9,10-AnDiCarbH2**), the protonated form of **9,10-AnDiCarb**. Upon comparison of the latter with **9,10-AnDiCarb**, we noted that the effect was minimal, as one can see in the comparison presented in Figure 2.20. We therefore concluded that the difference seen in the comparison with **Xanth** must indeed be due to the electronic nature of the aromatic fragment, and it is predictive of the ability of these compounds to form cation-π interactions.

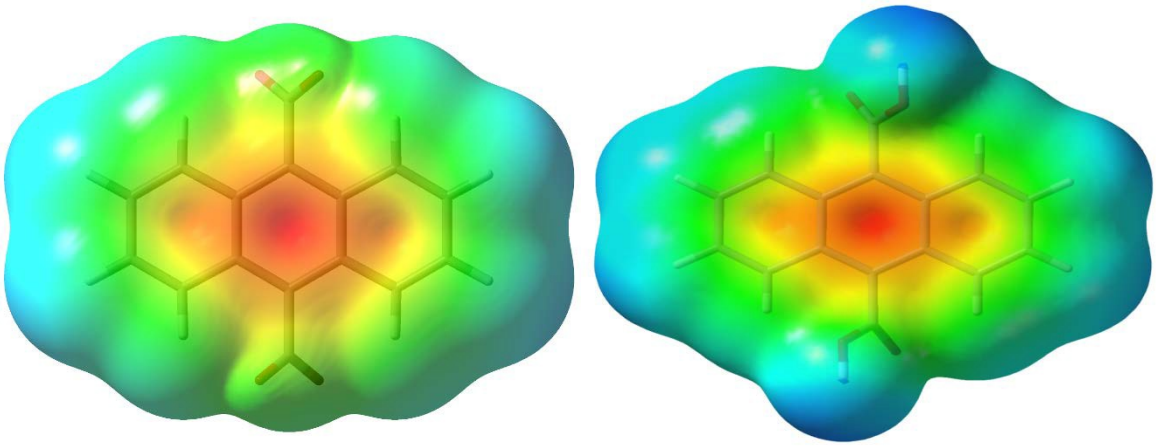

Figure 2.20. PM6 electrostatic potential surfaces for **9,10-AnDiCarb** (left) and the **9,10-AnDiCarbH2** (right).

2.7.3 Enthalpies of Hydration

A second explanation for **9,10-AnDiCarb**'s higher relative binding affinity can also be proposed on the basis of its calculated enthalpy of hydration compared to that of **F**. The optimized structures above were used to estimate the enthalpies of hydration of the anions through the QSAR estimation routine implemented in the *HyperChem 8.0* program.[62] Table 2.2 shows the parameters obtained (**9,10-AnDiCarb** = 9,10-anthracenedicarboxylate; **F** = fluorescein).

Table 2.2. Parameters obtained from HyperChem 8.0 program to determine the enthalpies of hydration for 9,10-anthracenedicarboxylate and fluorescein.

	9,10-AnDiCarb	**F**
Surface area / Å^2	419.13	508.52
Volume / Å^3	689.31	855.34
Hydration enthalpy / (kcal/mol)	-4.58	-8.53

On the basis of these values, **9,10-AnDiCarb** can be expected to be less efficiently solvated than **F** in aqueous solutions, as their calculated enthalpies of hydration suggest: in fact, **9,10-AnDiCarb** has an estimated ΔH_{hydr} = -19.2 kJ/mol, whereas that estimated for **F** is ΔH_{hydr} = -35.7 kJ/mol, (see Table 2.2). This is relevant to the binding process because both dianionic dyes must undergo at least partial desolvation in order to bind to the dendrimer, a process associated with an energetic penalty. This penalty is lower for the less effectively solvated anthracene dye, and the overall binding process is thereby made energetically more favorable, as reflected in the higher relative affinity observed experimentally.

Finally, it is worth noting that the fluorescence emission of **9,10-AnDiCarb** is also quenched upon binding, in line with what we observed for the xanthene dyes. The quenching of **9,10-AnDiCarb** is more pronounced than what was observed for **F** and **CF**. The extent of

quenching itself, however, is not an indication of relative affinity; instead, it is our opinion that it provides valuable hints as to the position of the bound fluorophore within the dendrimer. We have previously established that the dendrimer acts as a quencher for the bound fluorophore through its tertiary amines, and we expect deeper penetration of a fluorescent probe within the dendrimer's structure will be accompanied by more effective quenching because of closer proximity with those tertiary amines. We therefore interpret the higher extent of quenching of the anthracene dye when compared to **F** and **CF** as being due to its deeper penetration into the dendrimer's core. This behavior can be rationalized by referring once more to the hydrophobicity of the anthracene derivatives. Conversely, the more polar xanthene dyes (**CF**, **F**) endeavor to maximize their interaction with the solvent by remaining close to the surface of the dendrimer even while bound. The latter are therefore less exposed to the quencher moieties and their residual emission is higher even when bound.

2.8 HYPERBRANCHED AND LINEAR POLYELECTROLYTES AS HOST

Studying the binding properties of polyelectrolytes with differing architectures than the highly defined globular shape of the dendrimers was important and interesting, from the point of view of the determination of the likely origin of the fluorescence quenching we observe upon binding to fluorophores. Hyperbranched poly(ethyleneimine) (PEI), linear poly(allylamine) (PA), and polydiallyldimethylammonium chloride (PolyDADMAC) are commercially available cationic polyelectrolytes which are cheaper and more simple to produce compared to PAMAM dendrimers. These polyelectrolytes have also drawn a great deal of attention in the past years due to their wide range of industrial applications such as water treatment, cell encapsulation, and their ability to separate oil-in-water emulsions.[24,63,64] Unlike dendrimers, PEI, PA, and

polyDADMAC are more difficult to study due to their wide size distribution and less regular structures, but are desirable due to their low cost and wide use in commercial applications.

It is important to note that all polyelectrolytes studied contain the same binding motif as the PAMAM dendrimers (i.e. ammonium cations), and are comparable in size at least within reason. In order to compare the binding data, we performed interaction experiments of the same fluorophore with each polyelectrolyte in the same conditions as that of the PAMAM dendrimers. The studies presented here focus on using 5(6)-carboxyfluorescein (**CF**) as our fluorophore, kept at a constant concentration of 2.0×10^{-6} M for all experiments consistent with previous studies. As the previous data, these experiments were conducted in aqueous solutions buffered at pH 7.4 using 50 mM HEPES maintained at a constant temperature of 25°C.

2.8.1 Binding Hyperbranched Poly(ethyleneimine)

Randomly hyperbranched poly(ethyleneimine) (PEI) has a scaffold that is most similar to the dendrimer. It is the only other polyelectrolyte studied that contains tertiary amines in its backbone, thus allowing us to directly compare binding. PEI has an average molecular weight of 2,000 grams/mole. From the fluorescence intensity spectra obtained in Figure 2.21, we see that binding does occur and the fluorescence is quenched by about 85%.

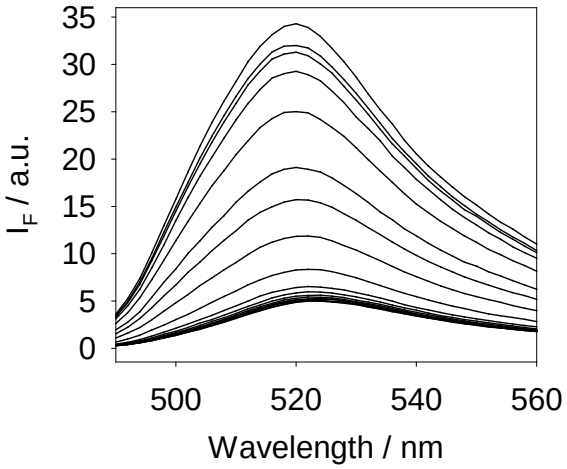

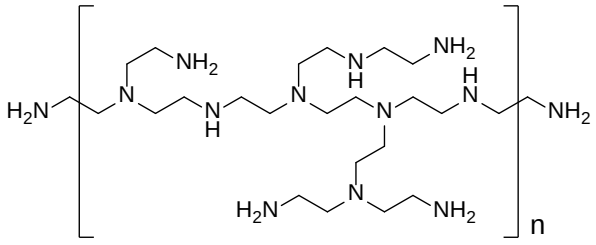

Figure 2.21. Family of emission spectra obtained from the titration of 5(6)-carboxyfluorescein ([**CF**] = 2.0×10^{-6} M) with poly(ethyleneimine) ([PEI] = 0 → 6.3×10^{-5} M) in buffered H_2O (pH 7.4). Right: PEI structure.

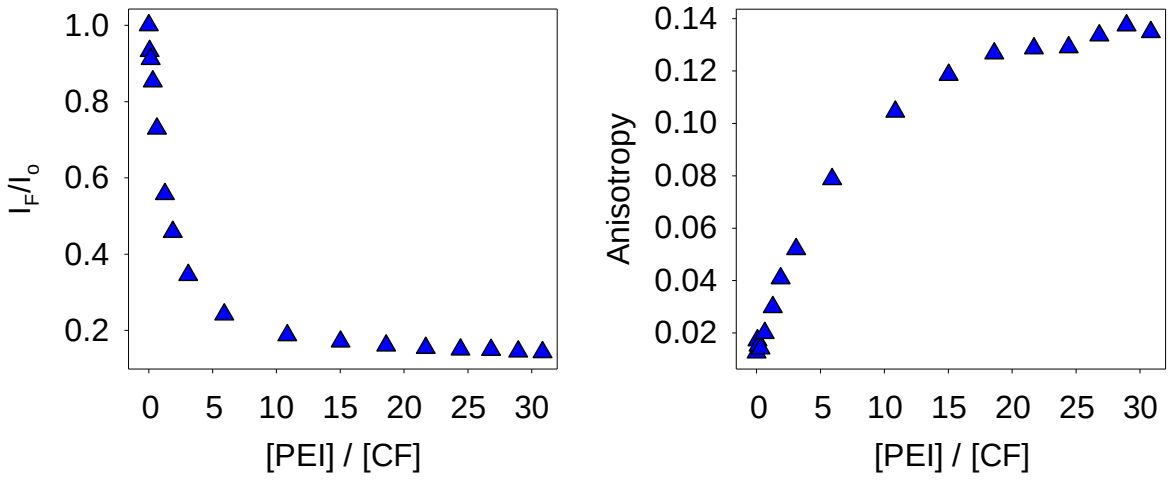

Figure 2.22. Normalized fluorescence intensity (left) and anisotropy (right) isotherms obtained from the interaction of **CF** with poly(ethyleneimine), in buffered H_2O (pH 7.4). [**CF**] = 2.0×10^{-6} M.

2.8.2. Binding Linear Poly(allylamine) and PolyDADMAC

Poly(allylamine) and PolyDADMAC are linear polyelectrolytes that are commercially available. They both contain the same binding motif as the PAMAM dendrimers (i.e. ammonium cations), nevertheless they do not contain any tertiary amine moieties. We can see from Figure 2.23 and Figure 2.25 that there is a much smaller extent of fluorescence quenching compared to the polyelectrolytes that contain tertiary amines in their backbones.

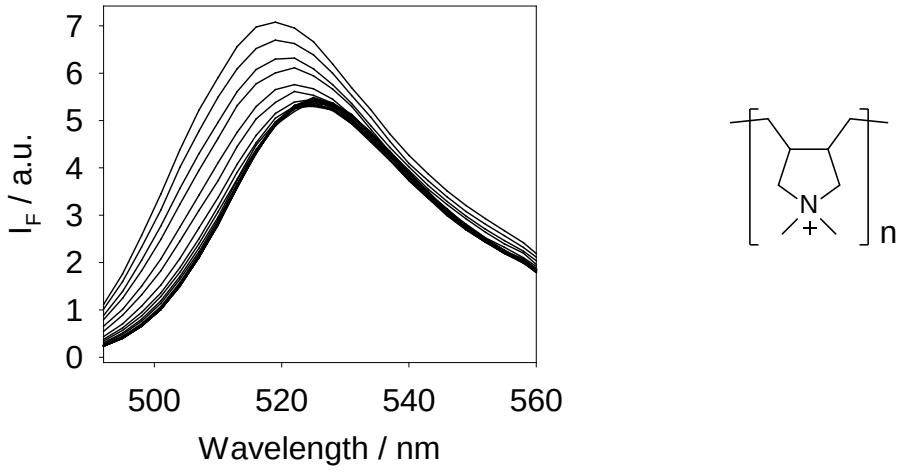

Figure 2.23. Family of emission spectra obtained from the titration of 5(6)-carboxyfluorescein ([**CF**] = 2.0 x 10^{-6} M) with polyDADMAC ([PolyDADMAC] = 0 → 2.4 x 10^{-6} M) in buffered H_2O (pH 7.4). Right: PolyDADMAC structure.

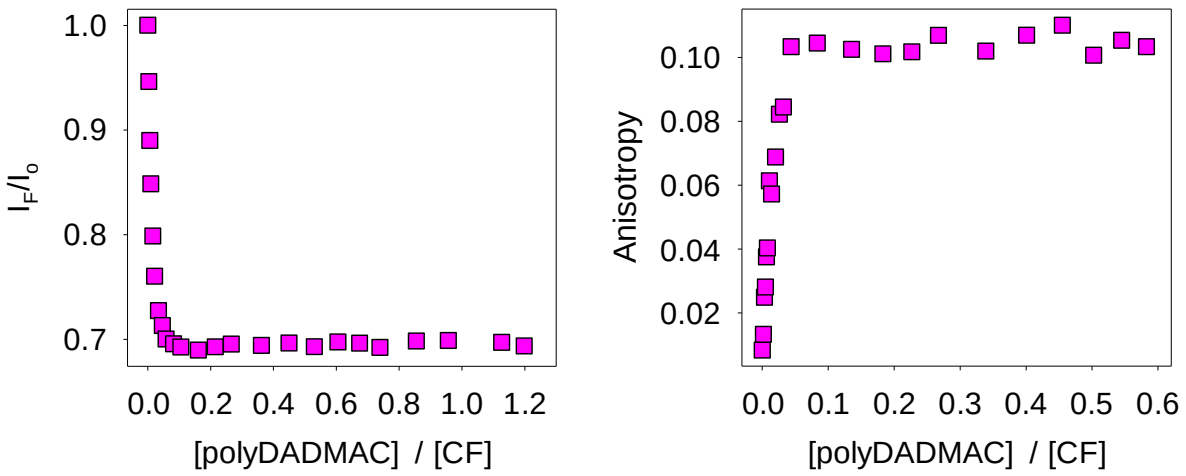

Figure 2.24. Normalized fluorescence intensity (left) and anisotropy (right) isotherms obtained from the interaction of **CF** with polyDADMAC, in buffered H_2O (pH 7.4). [**CF**] = 2.0×10^{-6} M.

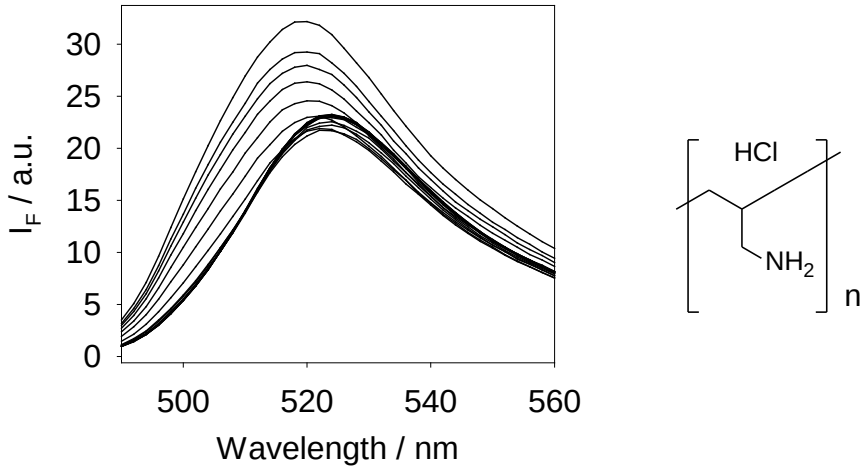

Figure 2.25. Family of emission spectra obtained from the titration of 5(6)-carboxyfluorescein ([**CF**] = 2.0 x 10^{-6} M) with poly(allylamine) ([PA] = 0 → 1.6 x 10^{-5} M) in buffered H_2O (pH 7.4). Right: PA structure.

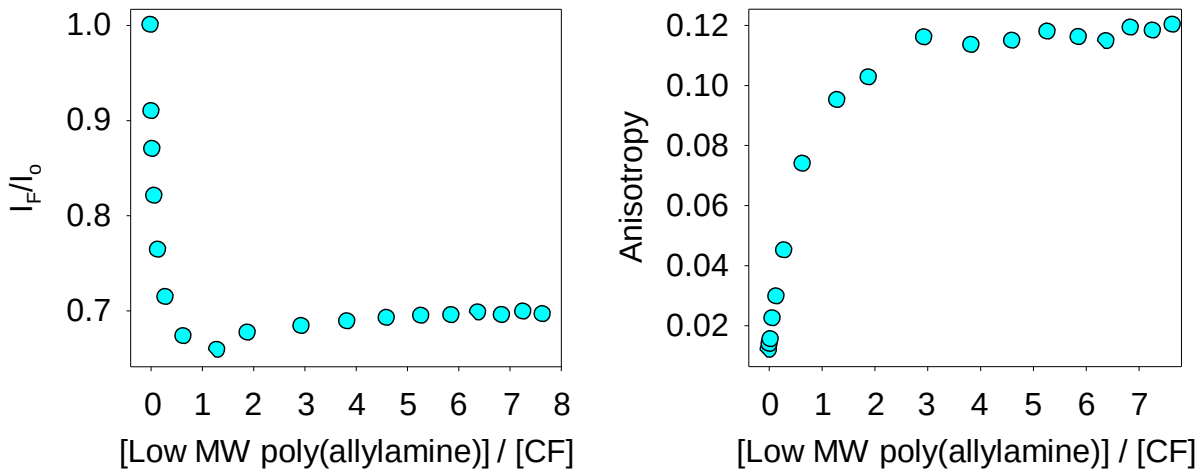

Figure 2.26. Normalized fluorescence intensity (left) and anisotropy (right) isotherms obtained from the interaction of **CF** with poly(allylamine), in buffered H_2O (pH 7.4). [**CF**] = 2.0×10^{-6} M.

2.8.3 Origin of PET quenching

The most interesting data came from the comparison of all the positively charged polyelectrolytes under study upon binding to **CF** (Figure 2.27). Earlier we proposed that the origin of quenching at high polyelectrolyte/fluorophore ratios is photoinduced electron transfer between excited **CF** molecules and the tertiary amines in the interior of the dendrimer scaffold. We can support our hypothesis by examining the extent of quenching of the dendrimer compared to the hyperbranched and linear polyelectrolytes. Even though PA and polyDADMAC contain the same binding motif as the PAMAM dendrimers (i.e. ammonium cations), neither contain tertiary amine moieties, and they are therefore unable to quench the fluorescence by the PET process postulated above for PAMAM dendrimers.

From Figure 2.27 we observe that the fluorophore's emission was only partially quenched upon binding with PA and polyDADMAC, showing the extent of quenching of 24% and 43%, respectively. On the other hand, poly(ethyleneimine) does contain tertiary amine moieties in its structure and we see that the extent of quenching is remarkably similar to the PAMAM dendrimers, 85% and 87% respectively. This further supports the assumption that PET

is the process associated with the large extent of quenching observed when these fluorophores bind to hosts containing tertiary amine moieties.

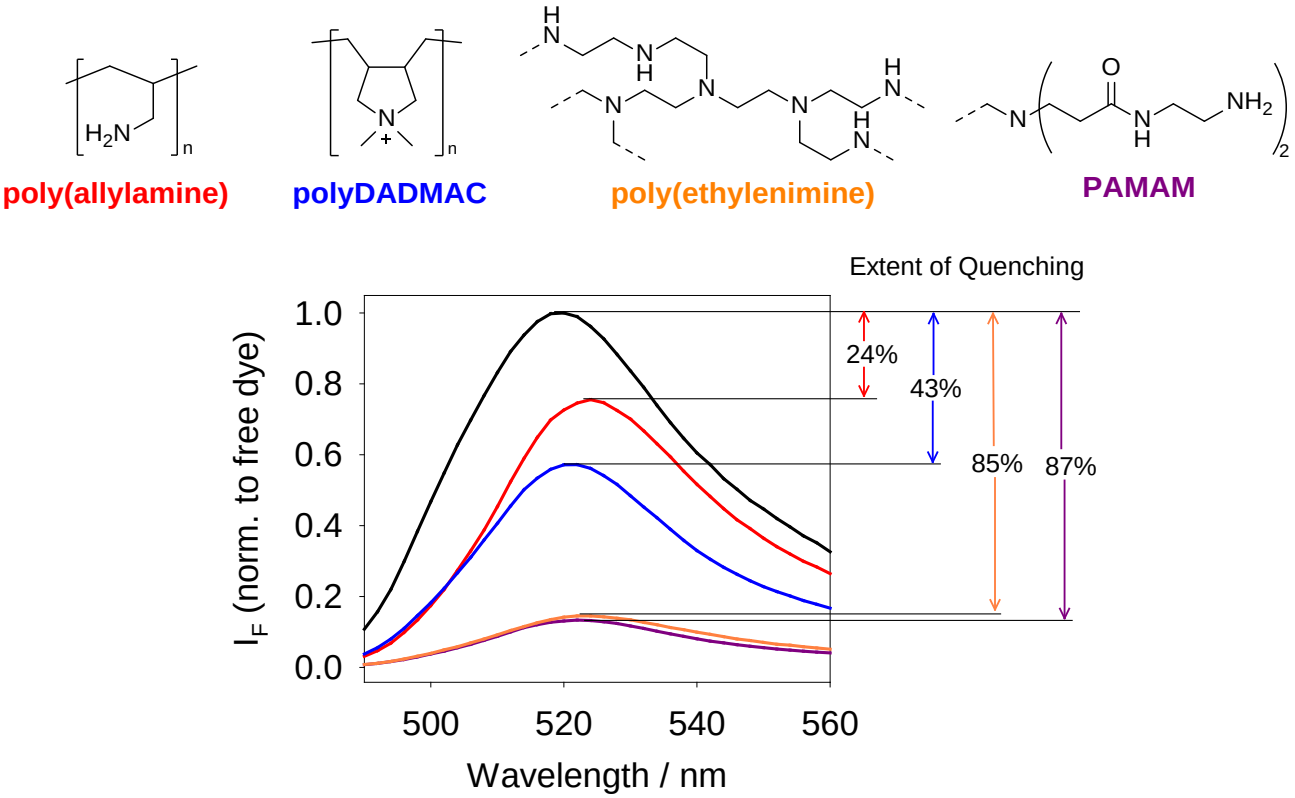

Figure 2.27. Quenching by polymer interactions. Fluorescence intensity spectra for the free fluorescein dye (black), the same dye in the presence of a large excess of poly(allylamine) (red), of polyDADMAC polymer (blue), of poly(ethyleneimine) (orange) and of G5 PAMAM dendrimer (purple). [polymers] = 8.0 x 10^{-5} M, [**F**] = 2.0 x 10^{-6} M in buffered H_2O (pH 7.4).

2.9 CONCLUSIONS

We have perfected a method to study the fundamental intermolecular interactions that allow water-soluble polyelectrolytes to act as supramolecular hosts. We utilize optical spectroscopy techniques, which are simpler and less time-consuming than most of the alternatives from classical physical organic chemistry. Contrary to most other structural elucidation methods, our approach is eminently suited to the very low micromolar concentrations that are common in established applications of these dendrimers (i.e. drug delivery,

multicomponent assembly). Results from our method are therefore inherently relevant to the design and optimization of such applications.

In particular, we have identified and rationalized the presence of the cation-π interaction in these intermolecular interactions, and we are beginning to unravel the role of the aqueous solvent as manifested through a desolvation penalty that has to be paid by each supramolecular guest, albeit to a different extent. We have also elucidated the origin of quenching at high polyelectrolyte/fluorophore ratios to be due to photoinduced electron transfer between **CF** molecules and the polyelectrolyte scaffolds which bear tertiary amines in their interior.

We do think that the insights gained in this chapter are crucial in order to use these macromolecules to their maximum capability. We are developing a detailed understanding of the fundamental nature of these binding interactions. We hope that these insights may encourage more widespread use of such powerful soft materials in the many fields of chemistry in which non-covalent encapsulation of small organic molecules is of interest.

2.10 EXPERIMENTAL SECTION

Binding studies

Materials. 4-(2-Hydroxyethyl)piperazine-1-ethanesulfonic acid (HEPES) buffer (free acid) was purchased from VWR. Poly(amidoamine) (PAMAM) dendrimers with ethylenediamine core and primary amine termination were used in these studies. The dendrimers were manufactured by Dendritech, Inc. and either purchased directly from the manufacturer or from their distributor (Sigma-Aldrich) as MeOH solutions of varying concentrations depending on the dendrimer generation. Dendrimer solutions were stored refrigerated at 4°C. Poly(diallyldimethylammonium chloride) (polyDADMAC, $M_w \approx 100{,}000$) was purchased from Sigma-Aldrich as a solution in water and used as received. The fluorescent probes fluorescein, 5(6)-carboxyfluorescein (as a

mixture of isomers), and 9,10-anthracenedicarboxylic acid were purchased from Sigma-Aldrich. All reagents were used as received. All experiments on dendrimer generations G3 and G6 were carried out using the same dendrimer lot, whereas G4 and G5 experiments were conducted from two lots of dendrimer. In the latter case, we confirmed lot-to-lot consistency by successfully replicating a number of fluorophore interaction experiments on both lots.

Instrumentation. Optical spectroscopy experiments were carried out on the following instrumentation:

- Biotek Synergy 2 **multimode plate reader**, capable of measuring absorbance spectra (through a monochromator) and steady-state fluorescence intensity and anisotropy (through bandpass filter sets and plastic sheet polarizers). Experiments were laid out onto the plate by hand using Eppendorf Research multichannel pipettors and VWR disposable plastic tips into Greiner BioOne 96-well nontreated (medium-binding) polystyrene plates with black walls and clear flat bottoms. The total volume of solution in each well (300 μL) was also kept constant, as this parameter controls the height of liquid in the wells and therefore the optical path length for absorbance experiments. Fluorescence readings were collected from the top of well; an appropriate dichroic mirror in the collection path was used to reject the excitation light. Temperature was internally controlled. Plate reading took approximately 45-50 min. Plates were never reused. No evaporation was ever apparent, so plates were not sealed.
- HP 8452A **diode array UV-Vis spectrophotometer**, recording spectra over the range 230-800 nm with a resolution of 2 nm; the cuvette holder temperature (25°C) was controlled by an external circulating water bath.

- ISS PC1 **spectrofluorimeter**, with manual calibrated slits and high-aperture Glan-Thompson calcite polarizers in the excitation and emission channels to measure steady-state fluorescence anisotropy. Excitation correction was carried out through a rhodamine B quantum counter with a dedicated detector. Excitation intensity was controlled by a manually operated iris (open/closed only). Detection was through red-sensitive PMT. Experimental temperature was controlled by external circulating water bath.

Titration conditions. All experiments were carried out in aqueous solutions buffered to pH 7.4 with 4-(2-hydroxyethyl)-1-piperazineethanesulfonic acid (HEPES, 50 mM). The concentration of all fluorophores was kept constant at 2.0×10^{-6} M throughout the fluorescence experiments. The concentration of 9,10-anthracenedicarboxylate was held at 2.0×10^{-5} M for UV-Vis absorption.

Instrumental parameters for fluorescence experiments.

Fluorescein and 5(6)-carboxyfluorescein, benchtop:

- Excitation wavelength: 480 nm
- Emission spectra: 490-560 nm
- Emission for anisotropy: 520 nm
- Slit, excitation: 4 nm spectral resolution
- Slit, emission: 2 nm spectral resolution
- Iris: open
- Polarizers: Glan-Thompson calcite, always in the light path:
  - set to the magic angle (54.7°) for intensity measurements
  - computer controlled for anisotropy measurements

Fluorescein and 5(6)-carboxyfluorescein, plate reader:

- Excitation filter: 485/20 nm
- Emission filter: 560/40 nm
- Dichroic mirror: 510 nm cutoff
- Polarizers: plastic, only used for anisotropy experiments
- Automatic detector gain adjustment

9,10-anthracenedicarboxylate, benchtop:

- Excitation wavelength: 373 nm
- Emission spectra: 385-500 nm
- Emission for anisotropy: 420 nm
- Slit, excitation: 4 nm spectral resolution
- Slit, emission: 4 nm spectral resolution
- Iris: open
- Polarizers: Glan-Thompson calcite, always in the light path:
  - set to the magic angle (54.7°) for intensity measurements
  - computer controlled for anisotropy measurements

9,10-anthracenedicarboxylate, plate reader:

No measurements were carried out on the plate reader with this fluorophore.

General binding titration protocol. All experiments were carried out in a buffered aqueous solution prepared in large batches to be used in multiple titrations. Its pH was adjusted by addition of NaOH or HCl solutions as needed. Combined glass electrodes were used to measure the pH of all solutions. The pH of the working solutions was also spot-checked during a titration to make sure that it had not drifted away from the desired value of 7.4.

We prepared multiple stock solutions of each dye that were used as starting points for multiple titrations. For example, a fluorescein stock solution was made by adding 1.69 mg of fluorescein solid to 25 mL of 50 mM HEPES buffer giving a concentration of 2.03×10^{-4} M.

All solutions used in binding experiments were made by dilution of aliquots of stock solutions of dyes or polymers. Binding experiments were carried out using two separate solutions, a "titrant" and a "cuvette" solution. "Titrant" and "cuvette" solutions were made fresh for each experiment.

A "**cuvette**" solution contained only the dye in buffer at its final working concentration; it was made by dilution of an aliquot of stock solution into buffer. The final working concentration of dye in these solutions was 2.0×10^{-6} M throughout, with the sole exception of 2.0×10^{-5} M for measurements of absorbance of 9,10-anthracenedicarboxylate, because of this chromophore's lower extinction coefficient.

A “**titrant**” solution contained both the dye and the polyelectrolyte under study. The dye concentration in this solution was always kept rigorously the same as the one in the corresponding “cuvette” solution, so that addition of the “titrant” to the “cuvette” solution would not change the overall concentration of the dye. “Titrant” solutions were made by dilution of an aliquot of dye stock and of an aliquot of polymer stock; the solution was then brought up to the final volume with buffer.

The pH of these solutions was checked with a calibrated glass electrode after their preparation and corrected to 7.4 by addition of NaOH or HCl if necessary.

The binding experiment was carried out by addition of aliquots of the “titrant” solution to the “cuvette” solution. The resulting mixture was then left to equilibrate briefly, then a measurement was taken. In the case of benchtop experiments, serial additions of “titrant” solutions were made to the same “cuvette” solution in a Starna Spectrosil quartz cuvette held in the temperature controlled cuvette holder of the instrument. The cuvette was not disturbed during the course of the titration to avoid artefacts due to changing background levels.

For a multiwell plate experiment instead, each point in a titration profile corresponded to a set of wells on the plate (normally two or three replicates). All points in the titration were laid out on a single plate and measured at the same time. Multiple experimental parameters (e.g. absorbance, fluorescence, anisotropy) could be measured on the same plate, ensuring greater internal consistency. The improved repeatability and multiple detection approach was the main reason multiwell plates were used in these experiments, as it saved significant time and effort.

Data treatment. Absorbance and fluorescence emission raw readings were blanked by subtracting the corresponding reading for the buffer. Replicate data points on a multiwell plate were averaged: the value reported for a titration point was the average of at least two readings.

The resulting data was plotted as a function of the [dendrimer] / [fluorophore] ratio to produce binding isotherms.

Table 2.3. Cartesian coordinates of the 9,10-anthracenedicarboxylate dianion, 9,10-anthracenedicarboxylic acid and the xanthene monoanion optimized structures.

9,10-AnDiCarb dianion - optimized geometry (PM6)

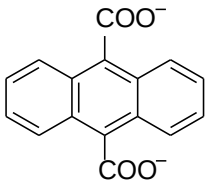

C	-0.05392753	0.71651464	3.66717634
C	-0.08840764	1.40069435	2.49000798
C	-0.02265956	0.71812471	1.21472730
C	0.02265956	-0.71812471	1.21472730
C	0.08840764	-1.40069435	2.49000798
C	0.05392753	-0.71651464	3.66717634
C	0.00004068	1.42627836	0.00000738
C	-0.00004068	-1.42627836	0.00000738
C	-0.02272230	-0.71812445	-1.21468879
C	0.02272230	0.71812445	-1.21468879
C	0.08859103	1.40068607	-2.48997737
H	0.19482231	2.49224557	-2.46198038
C	0.05404911	0.71651192	-3.66714035
C	-0.05404911	-0.71651192	-3.66714035
C	-0.08859103	-1.40068607	-2.48997737
H	-0.10783473	1.23105377	4.61889218
H	-0.19446401	2.49226145	2.46205098
H	0.19446401	-2.49226145	2.46205098
H	0.10783473	-1.23105377	4.61889218
H	0.10812064	1.23102982	-4.61885867
H	-0.10812064	-1.23102982	-4.61885867
H	-0.19482231	-2.49224557	-2.46198038
C	-0.00004068	-2.97280855	-0.00003869
O	-0.88052414	-3.53855647	-0.68122445
O	0.88039435	-3.53861364	0.68115610
C	0.00004068	2.97280855	-0.00003869
O	0.88052414	3.53855647	-0.68122445
O	-0.88039435	3.53861364	0.68115610

AnDiCarbH2 - optimized geometry (PM6)

C	1.65017000	-3.36204300	-0.04634700
C	2.00907500	-2.04883500	-0.01487300
C	1.01307200	-1.00066700	-0.03224200
C	-0.37257700	-1.37435400	-0.06024000
C	-0.70713900	-2.78039200	-0.10773100
C	0.26395000	-3.73507600	-0.10262300
C	1.35673000	0.36527500	-0.03604100
C	-1.35672200	-0.36511000	-0.03615800
C	-1.01308100	1.00081800	-0.03230700
C	0.37257700	1.37451800	-0.06011200
C	0.70704000	2.78058100	-0.10736400
H	1.76141100	3.06475800	-0.16902300
C	-0.26411600	3.73521700	-0.10230300
C	-1.65033200	3.36214600	-0.04637800
C	-2.00916500	2.04891000	-0.01511700
H	2.39955000	-4.15370400	-0.03133000
H	3.06187000	-1.76158000	0.04052400
H	-1.76155100	-3.06438100	-0.16963700
H	0.01359100	-4.79558100	-0.14310300
H	-0.01376800	4.79574200	-0.14258400
H	-2.39974000	4.15377400	-0.03144800
H	-3.06194800	1.76159100	0.03989900
C	2.78652300	0.77824600	-0.03604400
O	3.38134400	1.50843200	-0.79387600
O	3.46457200	0.21962300	1.02582300
H	4.41735800	0.51159700	1.06151800
C	-2.78649900	-0.77825000	-0.03608700
O	-3.38152700	-1.50764300	-0.79450100
O	-3.46401500	-0.22103500	1.02684000
H	-4.41679200	-0.51313900	1.06270300

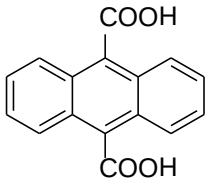

Xanth monoanion - optimized geometry (PM6)

C	3.63858267	-0.61149717	-0.00005631
C	2.32928358	-1.24592917	0.00019963
C	1.20691862	-0.47307662	0.00014042
C	1.20730175	0.96728604	-0.00001928
C	2.50736687	1.59546971	-0.00013458

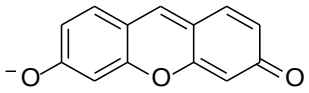

C	3.64861119	0.87123477	-0.00012085
C	-0.00000035	1.65992378	0.00000885
C	-1.20730172	0.96728597	0.00011098
C	-1.20691788	-0.47307742	0.00013552
C	-2.32928332	-1.24592872	0.00002269
H	-2.29293898	-2.32731189	0.00004192
C	-3.63858244	-0.61149745	-0.00014768
C	-3.64861113	0.87123471	0.00002577
C	-2.50736707	1.59546939	0.00013699
H	2.29294002	-2.32731215	0.00040924
H	2.53124327	2.68528753	-0.00022455
H	4.63243139	1.32513202	-0.00017977
H	-0.00000024	2.75137013	-0.00004153
H	-4.63243165	1.32513173	0.00003489
H	-2.53124305	2.68528715	0.00026049
O	-4.69160197	-1.24542085	-0.00035589
O	4.69160157	-1.24542105	-0.00021959
O	-0.00000027	-1.17402953	0.00031128

CHAPTER 3

A CLOSER LOOK AT THE INTERMOLECULAR FORCES DRIVING THE BINDING TO PAMAM DENDRIMERS IN WATER

3.1 SIGNIFICANCE

In the previous chapter we gathered as much information about the solution behavior of PAMAM dendrimers as supramolecular hosts as possible under the constraint that our probe molecules had to be colored and/or fluorescent. Unfortunately, these restrictions impose some requirements on the chemical nature of those probes such as small-molecule organic fluorophores are almost invariably rigid structures with extended aromatic regions. Multiple functional groups decorate these structures, whose effects on the binding to the polyelectrolyte are hard to separate and study alone. We therefore selected a series of smaller and much simpler probe anions, shown in Scheme 3.1. Comparison of small sets of these anions allows us to hone in on the contribution of specific interactions separately.

As shown in Table 3.1, the selected anionic probes differ by one key molecular element, so that comparison of the relative binding affinities provided us insight into a range of possible intermolecular interactions. For instance, one of the first interaction modes we studied was electrostatics. The probes selected were succinate, tricarballylate, and 1,2,3,4-butanetetracarboxylate which bear two, three, and four negative charges respectively. By comparing the binding behavior of these three probes, we obtained information on the influence of electrostatics on the binding process.

Table 3.1. Sets of anionic probes used to elucidate each intermolecular interaction phenomenon.

Feature under study:	**Anionic probes used:**
electrostatic interactions	succinate^{2-} vs. tricarballylate^{3-} vs. butanetetracarboxylate^{4-}
guest size	succinate (short) vs. pimelate (long)
guest conformation	maleate (*Z*) vs. fumarate (*E*)
hydrogen bonding	succinate (no OH) vs. malate (1x OH) vs. mesoxalate (2x OH); pimelate (no C=O) vs. ketopimelate (1x C=O) (vs. oxaloacetate)
guest steric effects	3° OH: tricarballylate vs. citrate; 2° OH: succinate vs. malate
charge-π interactions	cyclohexanetricarboxylate (aliphatic) vs. trimesate (aromatic)

However, monitoring the binding of optically silent species is much more challenging. We report here on a method allowing us to study the relative binding affinities of such spectroscopically silent species. Our method allows us to choose from a much wider assortment of molecules, permitting access to a broader collection of information in order to determine what structural features are valuable to enhance binding to these dendritic structures. In addition to the fundamental studies shown here, this method could also be applied to the construction of molecular sensing systems based on these polyelectrolytes in chemical recognition applications with spectroscopically active molecules.[65-71]

3.1.1 Experimental Details

The studies presented here focus on amine-terminated polyamidoamine (PAMAM) dendrimers with ethylenediamine cores of generations G3-G6. We will again present the results from studies conducted in aqueous solutions buffered at pH 7.4 using 50 mM 4-(2-hydroxyethyl)-1-piperazineethanesulfonic acid (HEPES) maintained at a constant temperature of 25°C. A number of small organic anions (Scheme 3.1) were selected as probes to isolate and

systematically investigate the fundamental intermolecular interactions involved when these polyelectrolytes behave as supramolecular hosts in solution. For comparison purposes, it is important to know the extent to which our probe anions are deprotonated at pH 7.4. The relevant pK_a values are shown in Table 3.2.

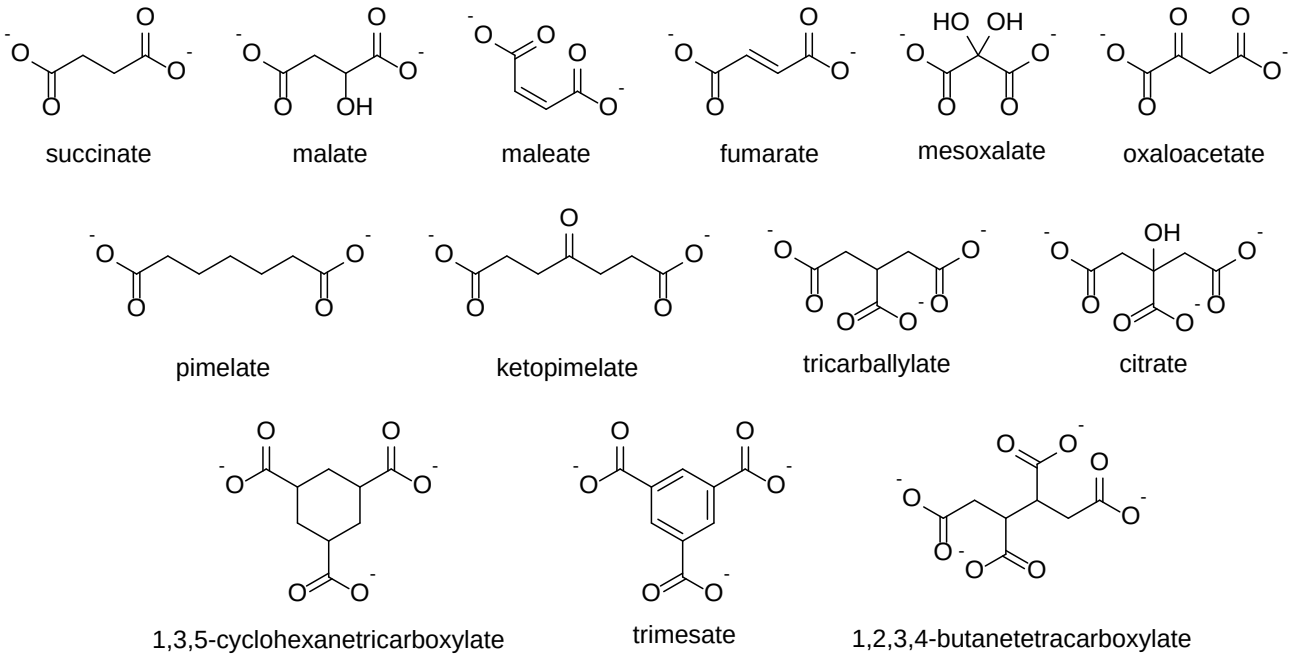

Scheme 3.1. Structures of the compounds used as anionic interaction probes in the present study, shown in their main protonation state in H_2O at pH 7.4.

Table 3.2. pK_a values for the conjugate acids of displacer anions.

	pK_a			
Acid	**1**	**2**	**3**	**4**
1,2,3,4-butanetetracarboxylic acid[72]	3.25	4.51	5.02	6.54
1,2,4,5-benzenetetracarboxylic acid[72]	1.87	2.71	4.97	5.80
Citric acid monohydrate[72]	2.93	4.23	5.09	16.13
Tricarballylic acid[72]	4.31	4.82	5.21	—
Trimesic acid[73]	3.12	3.89	4.70	—
1,3,5-cyclohexanetricarboxylic acid[74]	3.80	4.50	5.20	—
Succinic acid[73]	4.19	5.48	—	—
Malic acid[75]	3.40	5.20	—	—
Pimelic acid[73]	4.48	5.42	—	—
Oxaloacetic acid[75]	2.15	4.06	—	—
Maleic acid[73]	1.92	6.23	—	—
Fumaric acid[73]	3.02	4.38		

3.1.2 Indicator Displacement Assay

We conducted our studies using optical spectroscopy, as we have done in our direct binding studies reported in Chapter 2, and in previously reported work on similar systems.[34,67,76,77] As mentioned above, neither the organic probes nor the dendrimers contain any significant chromophore or fluorophore through which their binding can be directly monitored, requiring us to introduce a reporter in the system. In order to introduce a reporting system, we relied upon our elucidation of the binding properties of a number of dyes to positively charged PAMAM dendrimers of comparable generations (see Chapter 2).[34,76] Building upon that basis, we were able to set up a convenient dye displacement procedure[78] to monitor the binding of the spectroscopically silent anionic probes of interest.

An indicator displacement assay works by first binding an indicator to a receptor. Then, a competitive analyte, or displacer, is introduced into the system causing the displacement of the indicator from the host. The change in signal associated with the release of the indicator allows us to indirectly follow the binding of the silent displacer species. One major advantages of using IDAs is the fact that the system can be adapted to different receptors, indicators and analytes with simple changes, since no covalent synthesis is involved.[79]

In this approach (Scheme 3.2), a fluorescent indicator (in our case 5(6)-carboxyfluorescein, **CF**) is first bound to the dendrimer (**D**) to form a dendrimer-dye complex (**D•CF**$_n$ in Scheme 3.2, top). The dendrimer:dye ratio was chosen such that roughly 85-90% of the dye molecules are bound; the macroscopic optical properties of this solution are representative of the bound dye.[34,76] The non-fluorescent anionic probe of interest (**A**, see Scheme 3.1 for structures) is then added to displace the dye from its dendrimer complex and to form the probe-dendrimer complex (**D•A**$_m$), thus releasing the dye to the solution bulk, where its

spectroscopic signature reverts to that typical of its free state (Scheme 3.2, bottom). Although neither the **A** probes nor the **D•A**$_m$ dendrimer-probe complexes have any significant spectroscopic signatures, we can still monitor the complex formation process through the change in signal due to the displacement of the dye as it transitions from its bound to free state.

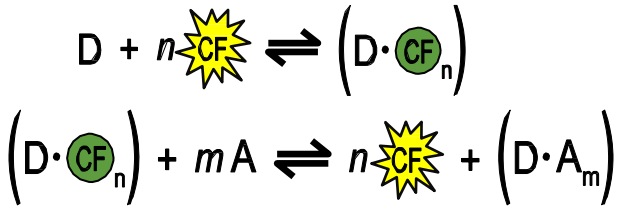

Scheme 3.2. The dye displacement assay used to detect binding of spectroscopically silent anionic guests **A** to the dendrimers **D** in the presence of the trianionic fluorescent dye 5(6)-carboxyfluorescein (**CF**). Top: dye binding process. Bottom: dye displacement.

The studies reported below were conducted by monitoring changes in the absorbance, fluorescence emission intensity, and fluorescence anisotropy of these systems. The comparison of isotherm profiles obtained from such titrations of **A** probes into a solution of the dendrimer-dye complex **D•CF**$_n$ provided immediate visual qualitative estimates of relative affinities which, in turn, indicated what structural features are significant for the binding to these dendritic structures and, ultimately, which intermolecular forces are at play in these systems. After a qualitative discussion, we will also present a semi-quantitative approach based on the relative amounts of probe anion necessary to cause a set degree of dye displacement (Table 3.3, located towards the end of this chapter).

The choice of the [dendrimer] / [dye] ratio to use in the displacement experiment is very important. If there is too little dendrimer present, the dye is not fully bound at the start of the experiment and we will not observe much signal change. On the other hand, too much dendrimer and the displacer probe will bind preferentially to the excess free host, without displacing the dye. On the basis of our previous experience and cited literature data,[67,79] we decided to work at

a [dendrimer] / [dye] ratio that gave us ca. 85% binding of the dye, which afforded us good sensitivity while maintaining a wide dynamic range for the measurement.

3.1.3 Indicator Displacement Kinetics

Throughout our studies, we always checked that we were conducting our measurements on fully equilibrated systems, to make sure that we were measuring true thermodynamic properties. In our experience, assembly and disassembly kinetics are fast on our experimental time scale. Because of our extensive use of a plate reader to streamline data acquisition, the fastest measurements practically available to us have a resolution around 30 seconds.

To check the kinetics of our system, we carried out the following experiment on a faster diode-array benchtop spectrophotometer instead. We first measured the absorbance of a solution of **CF** bound to a PAMAM G5 dendrimer at the concentration used for displacement experiments in the present work. We collected multiple spectra every 30 s for an extended time to ensure that no slow aggregation was taking place. No change was observed over 15 minutes (Figure 3.1, squares).

To the same solution we then added a large excess (60 equivalents) of 1,3,5-benzenetricarboxylate (trimesate) displacer while the measurement was ongoing (black spectra and circles below). The dye's transition from the bound to the free state was too fast to be observed in these conditions. After the addition of displacer, we continued to monitor the solution for another 15 minutes, over which no change was observed. We can conclude that the system is fully equilibrated by the time we carry out our measurements on a plate reader.

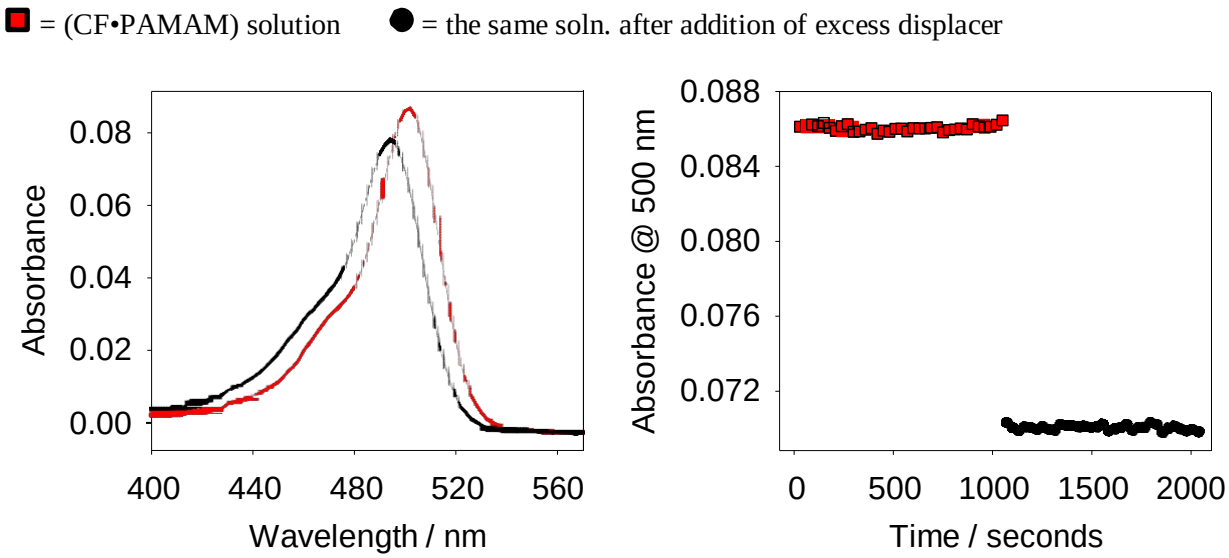

Figure 3.1. Kinetic studies of bound and displacement solutions. [**CF**] = 2.0 x 10^{-6} M, [PAMAM G5] = 4.5 × 10^{-7} M, [trimesate] = 1.2 × 10^{-4} M. (AJj-67)

3.2 PROBES TARGETING SPECIFIC BINDING INTERACTIONS

Careful comparison of the behavior of dyes carrying the same charge has made it clear that other non-covalent intermolecular interactions also play an important role in determining the affinity and influencing the selectivity of these dendritic polycationic hosts, as shown in Chapter 2. We therefore set out to study each interaction class separately and in closer detail: in particular, we will report here on the effect of molecular structure, overall charge, hydrogen bonding capabilities, and of the presence of aromatic moieties in the guest molecules.

In our experiments we measured absorbance, fluorescence emission and fluorescence anisotropy for all samples, but we will restrict ourselves to presenting only the fluorescence results for the sake of clarity as these are fully representative of the overall trends observed. As mentioned previously, fluorescence anisotropy is a very selective reporter as it is only sensitive to the rate of tumbling of the fluorescent moiety in solution.[20] An increase in the fluorescence anisotropy signal is uniquely associated with the binding of the small fluorophore to the much larger dendrimers. Conversely, as the fluorophore is displaced by probe anions **A**, the anisotropy

signal promptly returns to the value characteristic of the free dye, indicating the formation of a dendrimer-**A** complex.

For the comparison below on anion structure and shape (Figure 3.3 and Figure 3.4), we show results from all PAMAM dendrimer generations studied (G3-G6). However, to reduce repetitive graphs, other results will only report on the data obtained using fifth-generation (G5) PAMAM dendrimers, but we have carried out similar displacement studies with dendrimers of generations G3 through G6. The trends obtained from other generations were comparable to those obtained with G5. In the following work [DP] will indicate the concentration of the displacer probe anion.

3.2.1 Electrostatic Charge

We first investigated the effect of the electrostatic charge of the guest on the relative affinity for the dendrimer. We reported in Chapter 2 on the importance of this parameter in determining the affinities for the dendrimer of e.g. 5(6)-carboxyfluorescein (**CF**), a trianion in water at pH 7.4,[34] and fluorescein **(F)**, a dianion in the same conditions.[76] Here we compared the behavior of succinate, propane-1,2,3-tricarboxylate (tricarballylate), and 1,2,3,4-butanetetracarboxylate. These molecules respectively carry two, three and four negative charges in H_2O at pH 7.4. The results (Figure 3.2) show that the affinity of each guest for the dendrimer increases very significantly with an increase in overall charge of the guest. The quantitative observations summarized in Table 3.3 shows, on average, that adding one negative charge increases the relative affinity by one order of magnitude: this is by far the largest effect among those reported in the present study, once more highlighting the paramount importance of electrostatic interactions in these systems, even in water solutions where such interactions are typically diminished by water's high dielectric constant.

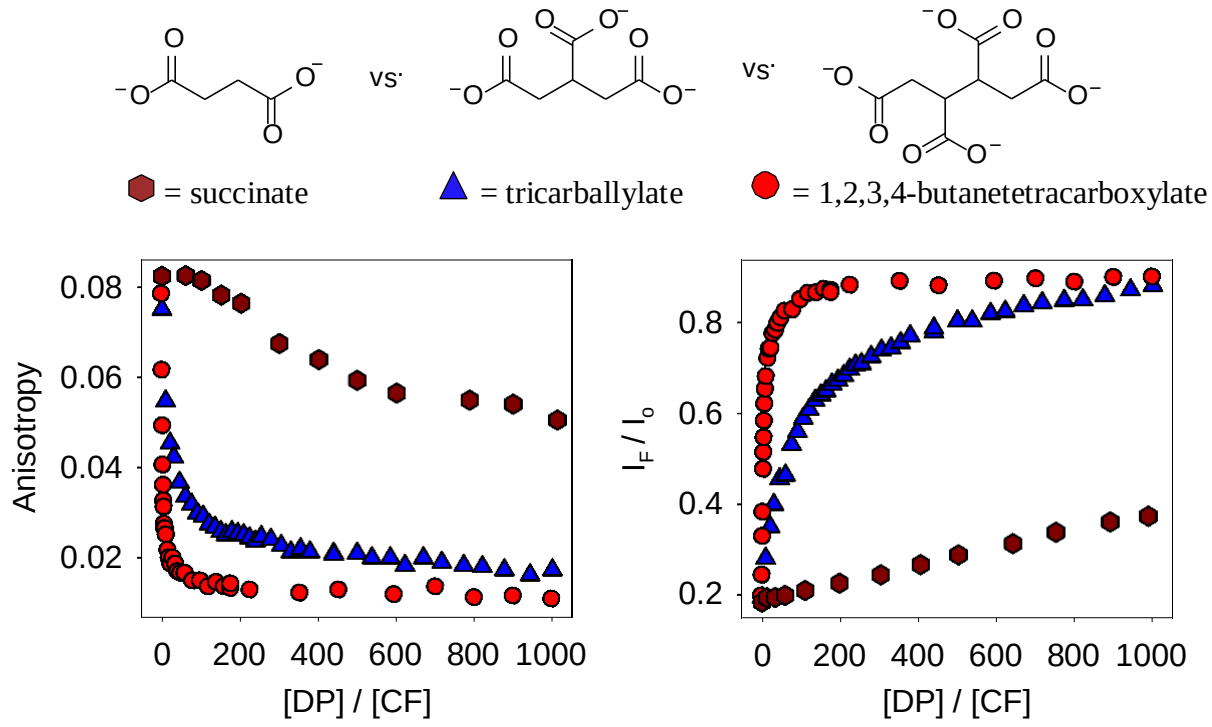

Figure 3.2. Guest charge: fluorescence intensity and anisotropy isotherms from titration of a G5•**CF**$_n$ complex with tetraanionic vs. trianionic vs. dianionic displacer (DP). [**CF**] = 2.0×10^{-6} M, [G5] = 4.5×10^{-7} M in buffered H_2O (50 mM HEPES at pH 7.4), λ_{exc} = 485/20 nm, λ_{em} = 560/40 nm.

3.2.2 Anion Structure and Shape

In order to explore the effect of the structure and flexibility of the guest anion on the overall affinity for the dendrimer, we compared the binding of tricarballylate and 1,3,5-cyclohexanetricarboxylate. Both anions carry three negative charges, so no contributions from electrostatic effects are expected, but the linear backbone of tricarballylate imposes no conformational restrictions, whereas cyclohexanetricarboxylate is much more rigid with a strong preference for its triequatorial conformation. Despite their structural differences, the two anions bind to the dendrimers with comparable affinity, as shown in the displacement isotherms in Figure 3.3, Figure 3.4 and numerically in Table 3.3. We conclude that structural differences alone do not significantly influence the binding. We ascribe this behavior to the conformational flexibility of the dendrimer: we surmise that the flexible multivalent dendrimer can rearrange to

accommodate virtually any spatial arrangement of charge required by its anionic guest.

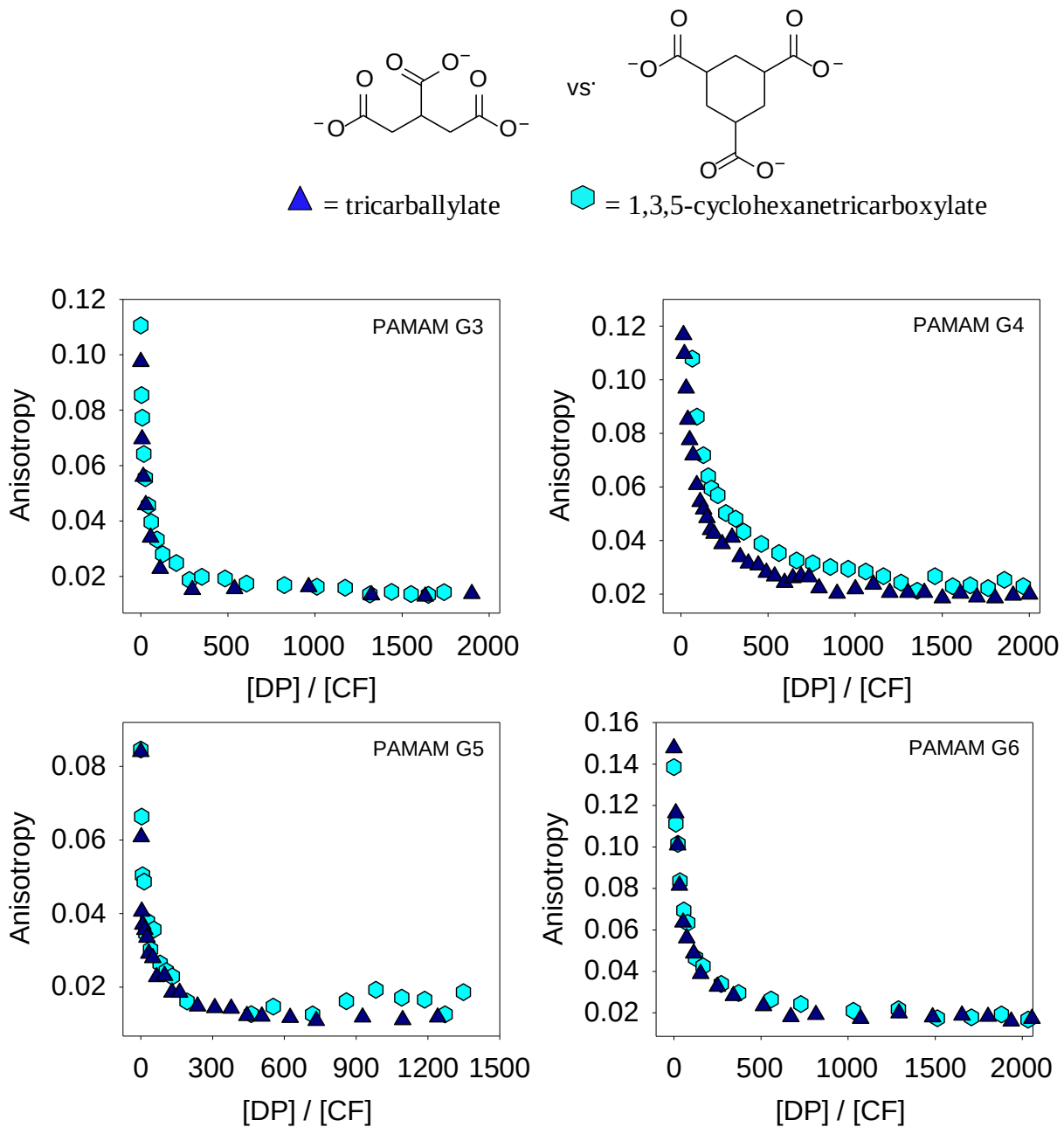

Figure 3.3. Guest shape: anisotropy isotherms from titration of a GX•**CF**$_n$ complex with trianionic displacers with different structural features. [**CF**] = 2.0 × 10^{-6} M, [G5] = 4.5 × 10^{-7} M in buffered H_2O (50 mM HEPES at pH 7.4), λ_{exc} = 485/20 nm, λ_{em} = 560/40 nm.

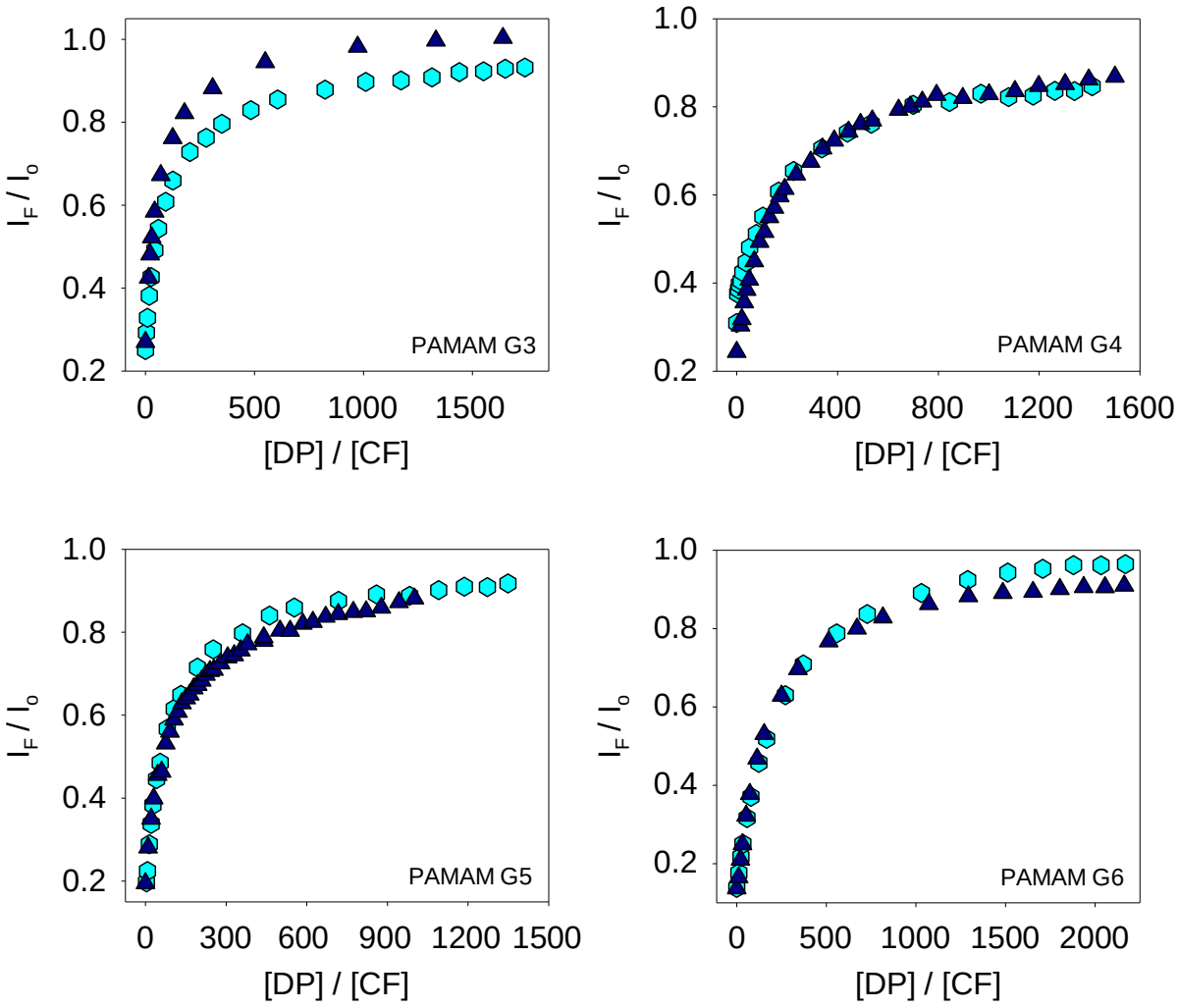

Figure 3.4. Guest shape: fluorescence intensity isotherms from titration of a GX•**CF**$_n$ complex with trianionic displacers with different structural features. [**CF**] = 2.0×10^{-6} M, [G5] = 4.5×10^{-7} M in buffered H_2O (50 mM HEPES at pH 7.4), λ_{exc} = 485/20 nm, λ_{em} = 560/40 nm.

Similarly, we found no difference in relative binding affinity between two linear dicarboxylates of differing chain length, succinate (four-carbon chain), and pimelate (seven-carbon chain), as shown in Figure 3.5. Again, both displacers carry two negative charges, therefore electrostatics contribute equally to their binding to the polycationic dendrimers; any difference in steric or configurational requirements between the two anions would be reflected in their relative affinity. We observed no distinguishable differences in their binding behavior,

further supporting our hypothesis that the guest's size and shape are essentially irrelevant in determining their binding affinity for the dendrimer.

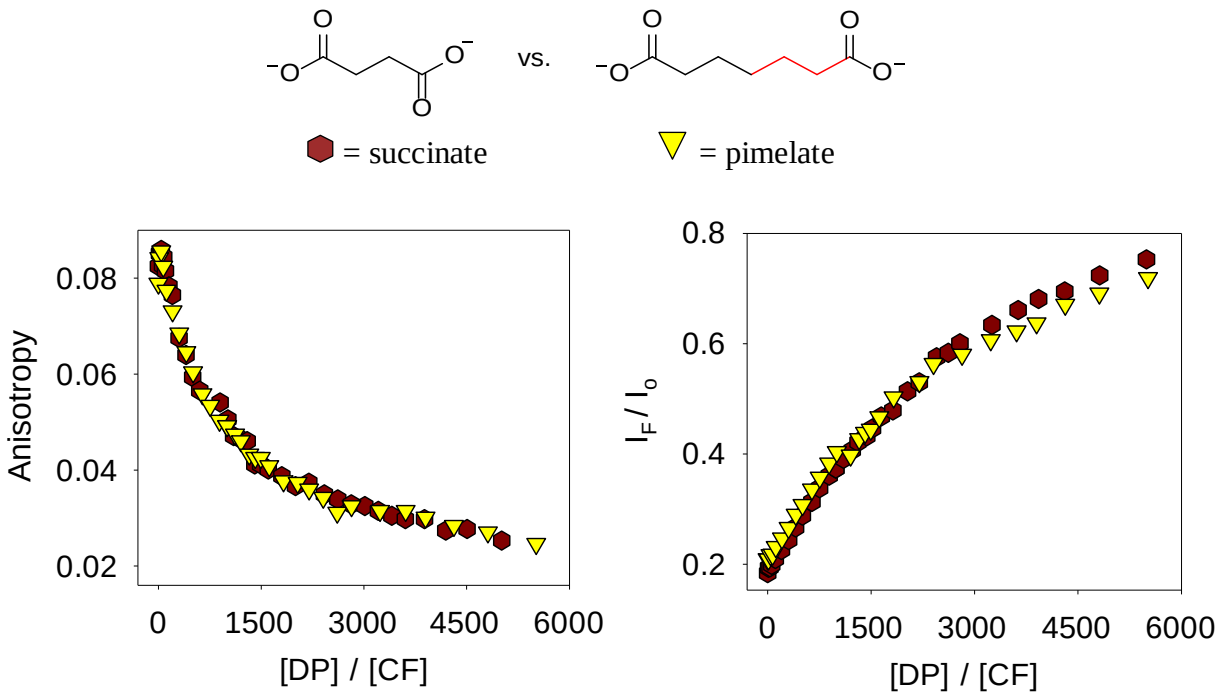

Figure 3.5. Guest size: fluorescence intensity and anisotropy isotherms from titration of a G5•**CF**$_n$ complex with displacers with different carbon chain lengths. [**CF**] = 2.0×10^{-6} M, [G5] = 4.5×10^{-7} M in buffered H_2O (50 mM HEPES at pH 7.4), λ_{exc} = 485/20 nm, λ_{em} = 560/40 nm.

To further confirm that the shape of the guest molecules are essentially irrelevant, we chose to look at the stereochemistry of our guest anions. We looked at maleate and fumarate, which both bear two negative charges. However, one contains a double bond in the *Z* conformation while the other is in the *E* conformation, respectively. As shown in Figure 3.6, the difference in conformation had no effect on binding affinity. Similar to the previous results, we further provided support to our hypothesis that the flexible multivalent dendrimer can accommodate nearly any spatial arrangement of charge required by its anionic guest.

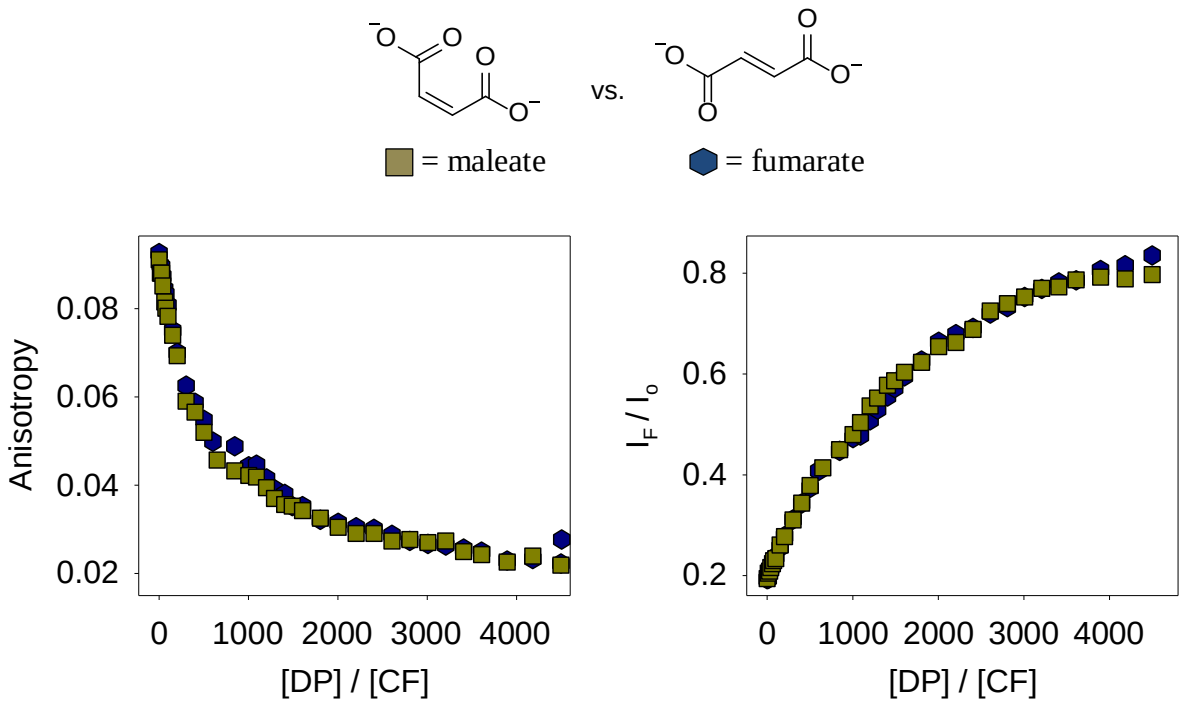

Figure 3.6. Guest shape – *E* vs. *Z* conformation: fluorescence intensity and anisotropy isotherms from titration of a G5•**CF**$_n$ complex with displacers with different stereochemistry. [**CF**] = 2.0×10^{-6} M, [G5] = 4.5×10^{-7} M in buffered H_2O (50 mM HEPES at pH 7.4), λ_{exc} = 485/20 nm, λ_{em} = 560/40 nm.

3.2.3 Hydrogen Bonding

Given the structure and its rich array of H-bond donors and acceptors, we expected the dendrimer scaffold to take part in hydrogen bonding interactions with its guests. On one hand, the carbonyl functionalities and the non-protonated amine groups in the scaffold may act as hydrogen bond acceptors (Figure 3.7, shown in blue); on the other hand, the protonated ammonium groups on its surface may act as hydrogen bond donors (Figure 3.7, shown in red). To test these hypotheses, we explored the two possible roles separately, using probe anions containing hydrogen bond donor and acceptor moieties, respectively.

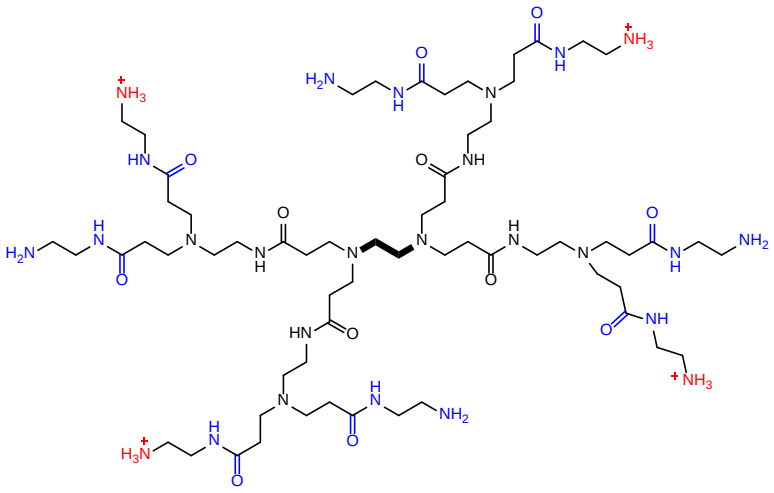

Figure 3.7. Partial structure of an amine terminated PAMAM dendrimer with possible H-bond donating groups shown in red and H-bond accepting groups highlighted in blue.

We first investigated displacers containing a varying number of hydroxyl groups that could act as H-bond donors, in order to test the behavior of the dendrimer as an H-bond acceptor. In particular, we compared the succinate, malate and mesoxalate dianions (Figure 3.8). Each displacer bears the same number of negative charges, so any difference observed in their binding affinity is due to the presence of the hydroxyl (OH) groups, which in turn reports on the ability of the dendrimer to act as a H-bond acceptor. Figure 3.8 shows that the observed affinity increases with the number of OH groups available: malate (one OH group) binds with a higher affinity than succinate (no OH), and mesoxalate (two OH groups) has even greater affinity than malate. We conclude that the dendrimer can act as an effective hydrogen bond acceptor to establish H-bond interactions of appreciable strength with its guests. The critical concentrations in Table 3.3 indicate that the establishment of one extra hydrogen bonding interaction leads approximately to a fourfold increase in the apparent binding affinity, a smaller effect than that generated by an increase in the guest's net charge: H-bonding is a lesser contributor to overall binding affinity than electrostatic interactions.

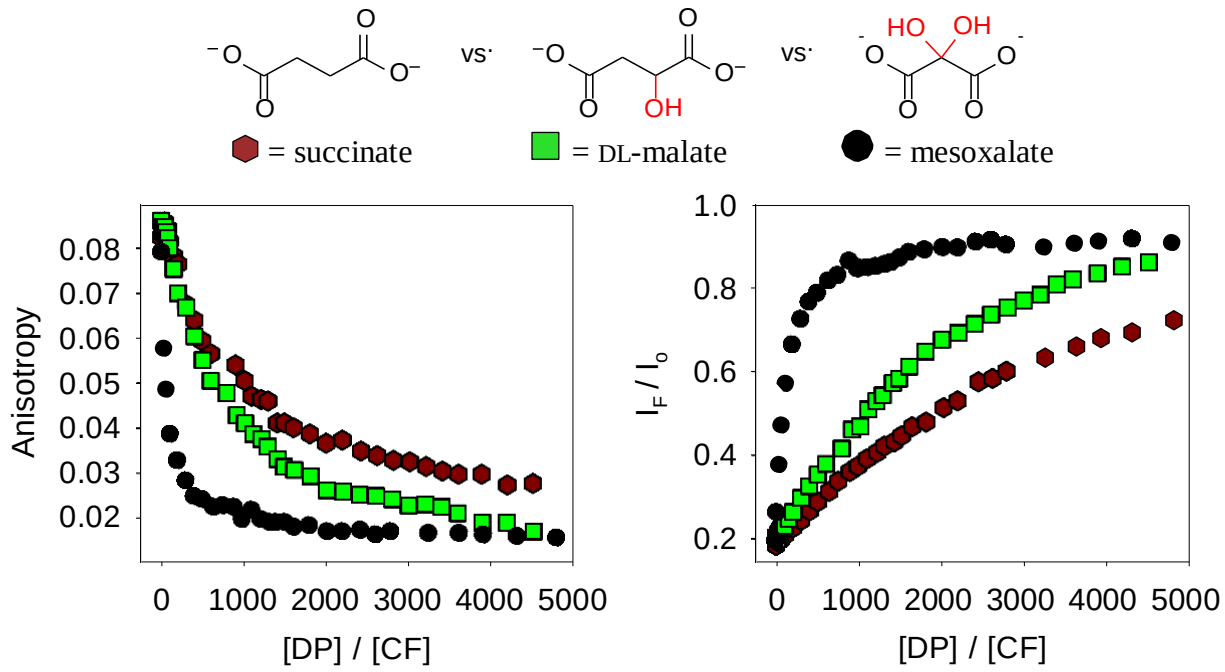

Figure 3.8. Dendrimer as H-bond acceptor: fluorescence intensity and anisotropy isotherms from titration of a G5•**CF**$_n$ complex with displacers with/without extra hydrogen bond donating groups. [**CF**] = 2.0×10^{-6} M, [G5] = 4.5×10^{-7} M in buffered H_2O (50 mM HEPES at pH 7.4), λ_{exc} = 485/20 nm, λ_{em} = 560/40 nm.

We subsequently turned to exploring the dendrimer's capability of acting as an H-bond donor by using probe anions containing a carbonyl moiety acting as H-bond acceptor. In particular, we compared the binding behavior of pimelate with that of 4-ketopimelate. These two anions each bear two negative charges: any differences in binding affinity among these anions can be ascribed to the involvement of the mid-chain C=O group present in ketopimelate. However, from examining Figure 3.9 it is clear that no difference was detected in the observed affinities of succinate and ketopimelate, leading us to the surprising conclusion that the dendrimers behave as poor H-bond donors. We suspect this is due to the extensive solvation of the surface amine groups that essentially tie those groups up in more strongly stabilizing H-bonds with water, a notoriously excellent H-bonding partner. Breaking the H-bonds with the solvent to form new ones with the guest molecules is apparently thermodynamically unfavorable.

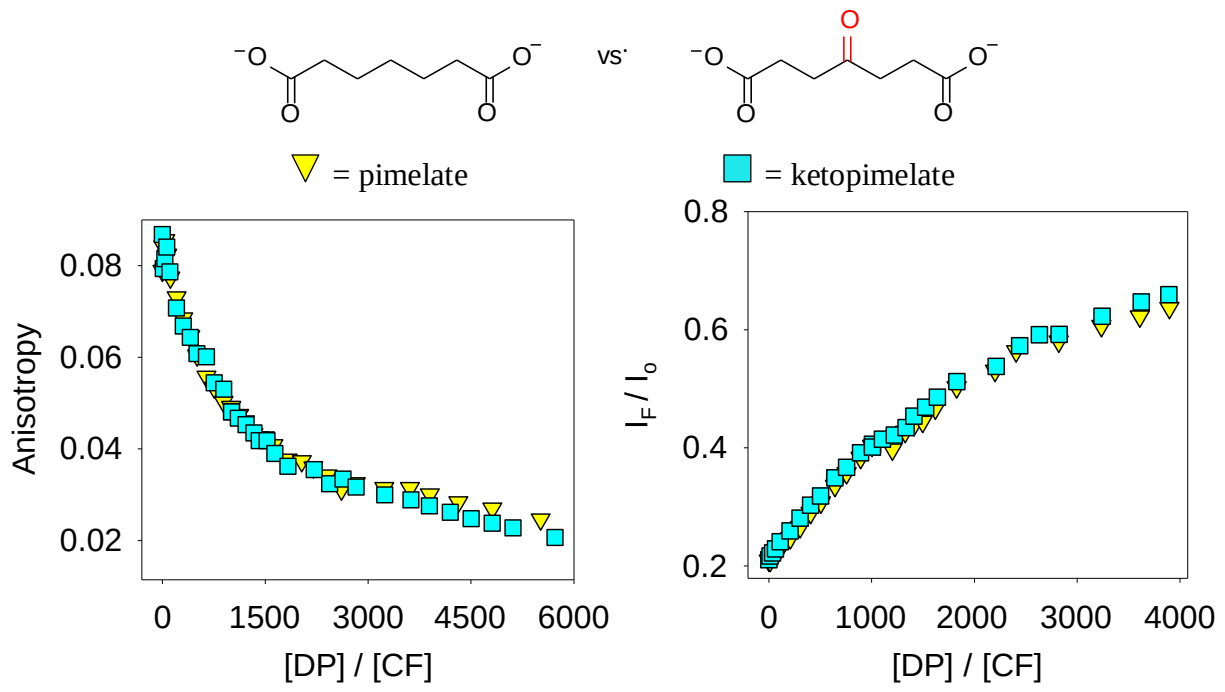

Figure 3.9. Dendrimer as H-bond donor: fluorescence intensity and anisotropy isotherms from titration of a G5•**CF**$_n$ complex with pimelate or 4-ketopimelate. [**CF**] = 2.0×10^{-6} M, [G5] = 4.5×10^{-7} M in buffered H_2O (50 mM HEPES at pH 7.4), λ_{exc} = 485/20 nm, λ_{em} = 560/40 nm.

A comparison between ketopimelate and oxaloacetate is interesting as well. In fact, both dianions formally contain an extra carbonyl moiety, so we were surprised to find that oxaloacetate displays significantly higher affinity than ketopimelate (Figure 3.10). However, ^{1}H-NMR experiments in D_2O indicated that the oxaloacetate anion actually exists primarily in its enol form in water solution, as shown in the literature with other similar carbonyl compounds.[80] This is due to the presence of a stabilizing intramolecular hydrogen bond interaction in the enol form (Scheme 3.3). The corresponding ketopimelate enol cannot form such a convenient intramolecular hydrogen bond, so ketopimelate exists in solution almost exclusively in the keto form (Scheme 3.4). Oxaloacetate is therefore more likely to behave as a hydrogen bond donor through its enol OH group rather than as an acceptor, in this respect being similar to the malate anion screened previously. In fact, the corresponding critical concentrations for 95% dye

displacement (Table 3.3) for malate (7.6 mM) and oxaloacetate (6.8 mM) are very similar, further confirming this hypothesis.

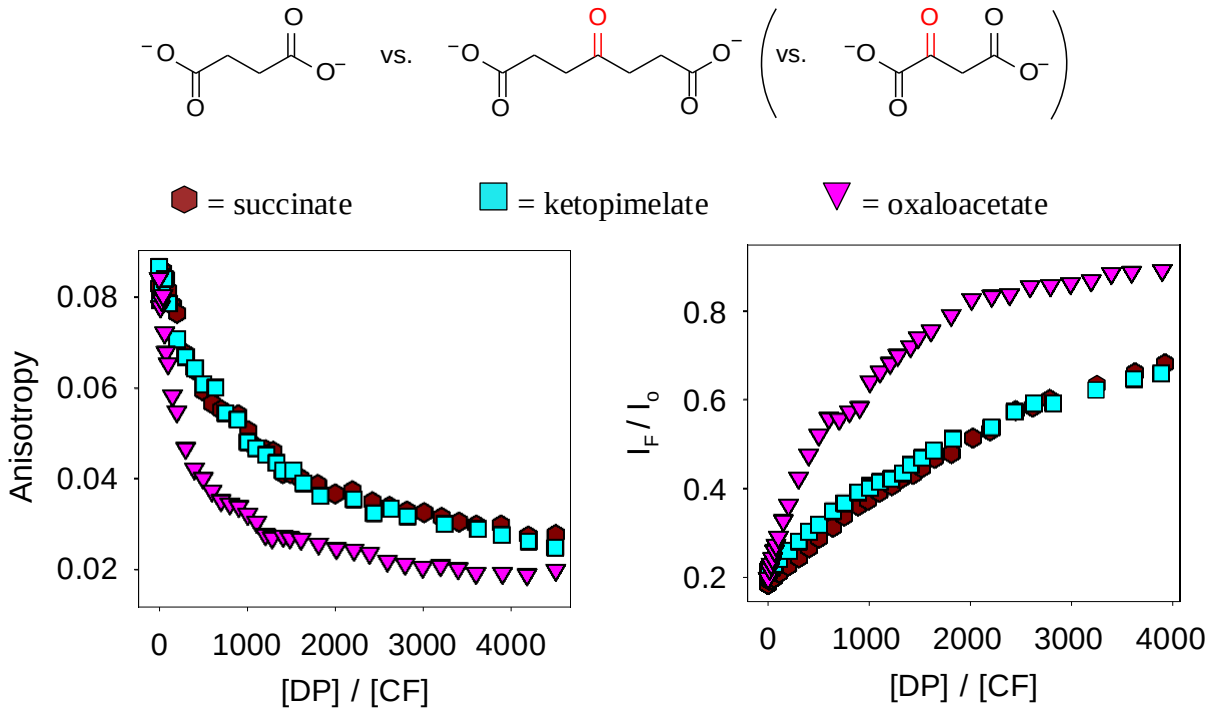

Figure 3.10. Enolizable anions: fluorescence intensity and anisotropy isotherms from titration of a G5•**CF**$_n$ complex with enolizable vs. non-enolizable displacers. [**CF**] = 2.0×10^{-6} M, [G5] = 4.5×10^{-7} M in buffered H_2O (50 mM HEPES at pH 7.4), λ_{exc} = 485/20 nm, λ_{em} = 560/40 nm.

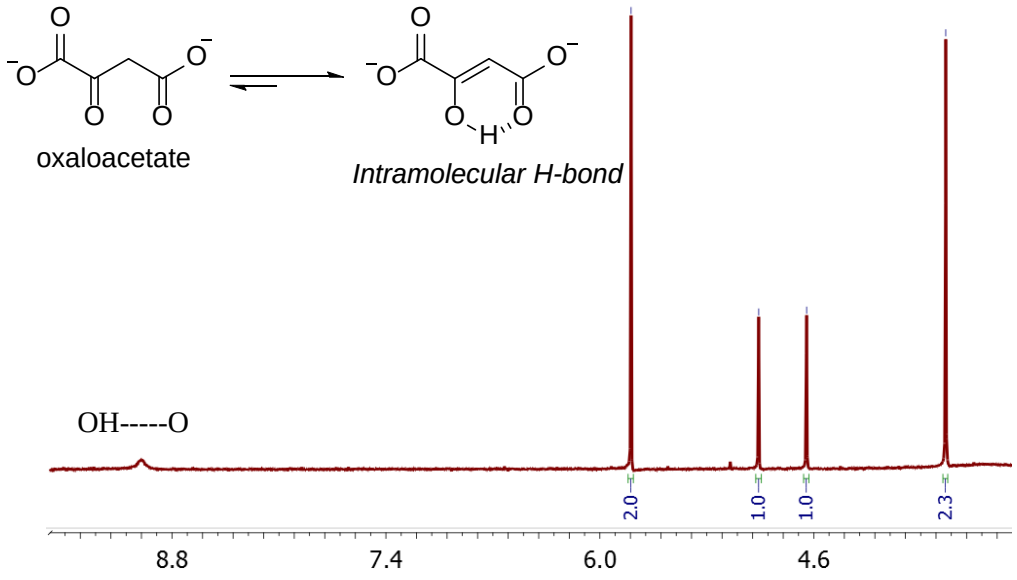

Scheme 3.3. Top: keto-enol tautomerism of oxaloacetate. Bottom: ^{1}H NMR of oxaloacetate in D_2O.

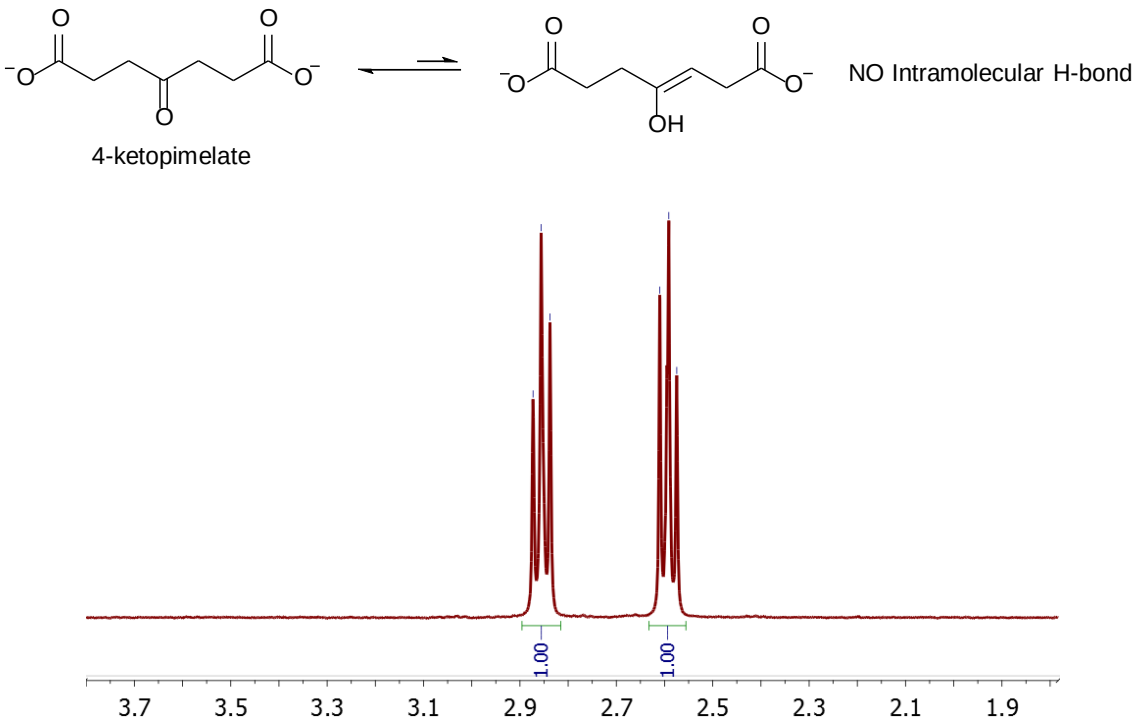

Scheme 3.4. Top: keto-enol tautomerism of 4-ketopimelate anion. Bottom: ^{1}H NMR of 4-ketopimelate anion in D_2O.

In order to further verify our hypothesis regarding the importance of enolization within our probe molecule, we thought that 1,3-acetonedicarboxylate could help clarify our results. This probe has a similar structure to oxaloacetate with the only difference being the addition of an extra carbon along its chain (shown to the right of Figure 3.11), and its enol form also has the ability to be stabilized due to an intramolecular H-bond interaction. However, 1,3-acetonedicarboxylate has the unfortunate disadvantage of being very hygroscopic. In order to determine if the purchased compound had absorbed moisture, we performed a displacement experiment with the compound as received (shown in grey diamonds), and then again after heating it in an oven overnight at 80^{o}C (shown in red inverse triangles). From the results depicted in Figure 3.11, we obtained significantly different binding isotherms, neither of which made sense when compared to the other anionic molecules under study. Due to the fact that

consistent data could not be obtained we were forced to abandon work with the 1,3-acetonedicarboxylate anionic probe.

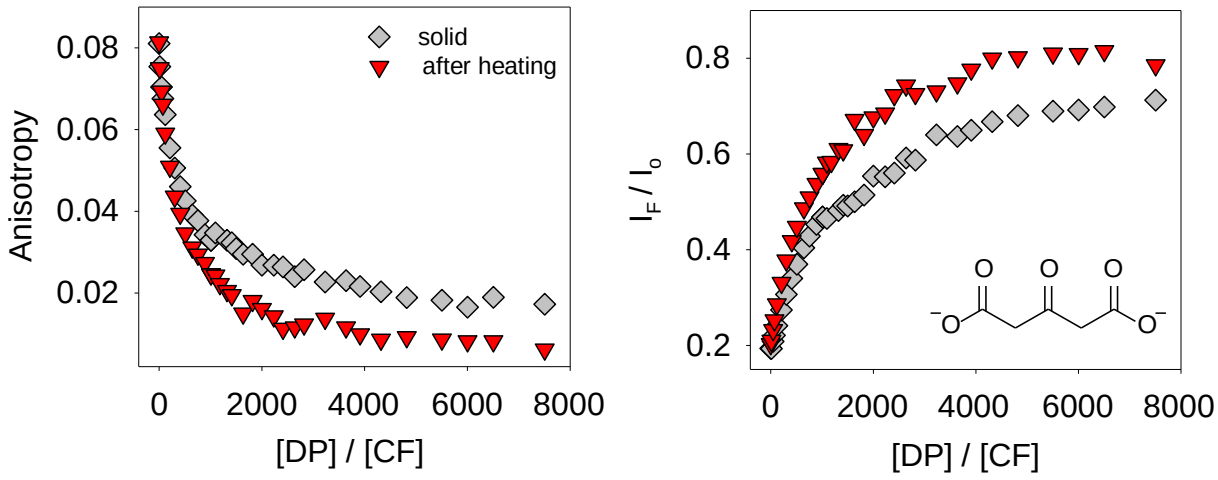

Figure 3.11. Potential enolizable anion: fluorescence intensity and anisotropy isotherms from titration of a G5•**CF**$_n$ complex with 1,3-acetonedicarboxylate. [**CF**] = 2.0 × 10^{-6} M, [G5] = 4.5 × 10^{-7} M in buffered H_2O (50 mM HEPES at pH 7.4), λ_{exc} = 485/20 nm, λ_{em} = 560/40 nm. (AJi-70)

We also tested the effects of hydrogen bonding in systems bearing three negative charges, by comparing the tricarballylate and the citrate trianions, which differ only in the fact that citrate contains a hydroxyl group. Based on our previous findings, we expected citrate to bind with higher affinity than tricarballylate because of its extra H-bond donating group. Surprisingly, the two anions were found to bind with essentially identical affinity (Figure 3.12). In this case, other factors are at play that prevent the OH from participating in the interaction effectively. For one, tertiary OH groups such as the one present in citrate are known to be highly sterically hindered and consequently to suffer from reduced availability of the OH group to intermolecular interactions.[81] Additionally, electrostatic interactions are much stronger for these trianionic systems than they are for the dianions discussed above, and the relative contribution of hydrogen bonding is consequently lower: in order to accommodate the dominant electrostatic interactions, citrate and tricarballylate are likely to assume a tripodal conformation that best exposes their

three charged groups to the surface of the dendrimer. In such a conformation, however, the OH of citrate is forced to point away from the dendrimer, thereby removing citrate's competitive advantage.

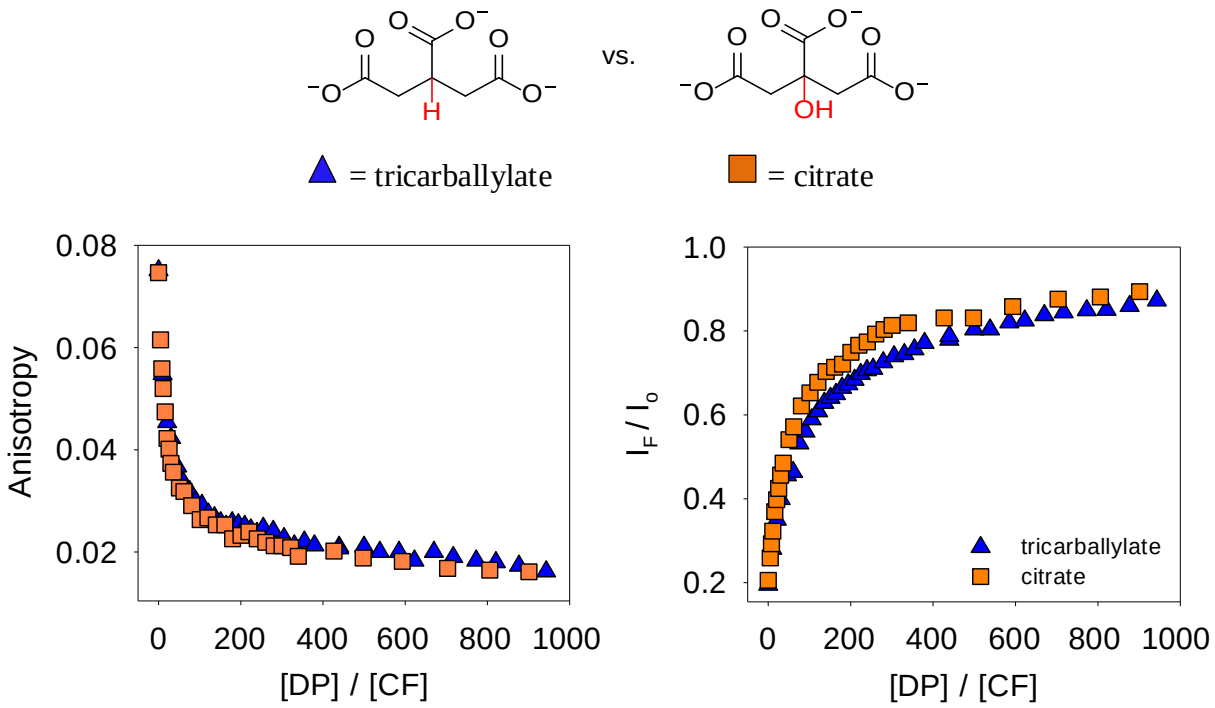

Figure 3.12. H-bonding in trianions: fluorescence intensity and anisotropy isotherms from titration of a G5•**CF**$_n$ complex with trianionic displacers with and without an OH group. [**CF**] = 2.0×10^{-6} M, [G5] = 4.5×10^{-7} M in buffered H_2O (50 mM HEPES at pH 7.4), λ_{exc} = 485/20 nm, λ_{em} = 560/40 nm.

3.2.4 The Effect of π Systems

As a final point, we probed the effect of the presence of aromatic systems in the guest species. The results of displacement titrations carried out with benzene-1,3,5-tricarboxylate (trimesate) and 1,3,5-cyclohexanetricarboxylate highlight a striking difference in the relative affinity of the two displacers for the dendritic polyelectrolyte (Figure 3.13). The two displacers carry the same charge and have similar size and spatial arrangement of charged groups, as shown by comparison of their estimated molecular surfaces and volumes. The molecular volumes and surface were estimated using the QSAR routines included in the *HyperChem* 8 software package. The molecular volumes were estimated to be 575 Å^3 and 533 Å^3, and the molecular surfaces

were 376 Å^2 and 361 Å^2, for cyclohexanetricarboxylate and trimesate respectively, which are found to be within 4% and 8% of each other. This consideration allows us to rule out charge density as a possible cause of the observed effect. The difference must then be ascribed to a secondary interaction that the trimesate anion alone is capable of establishing with the dendrimer scaffold.

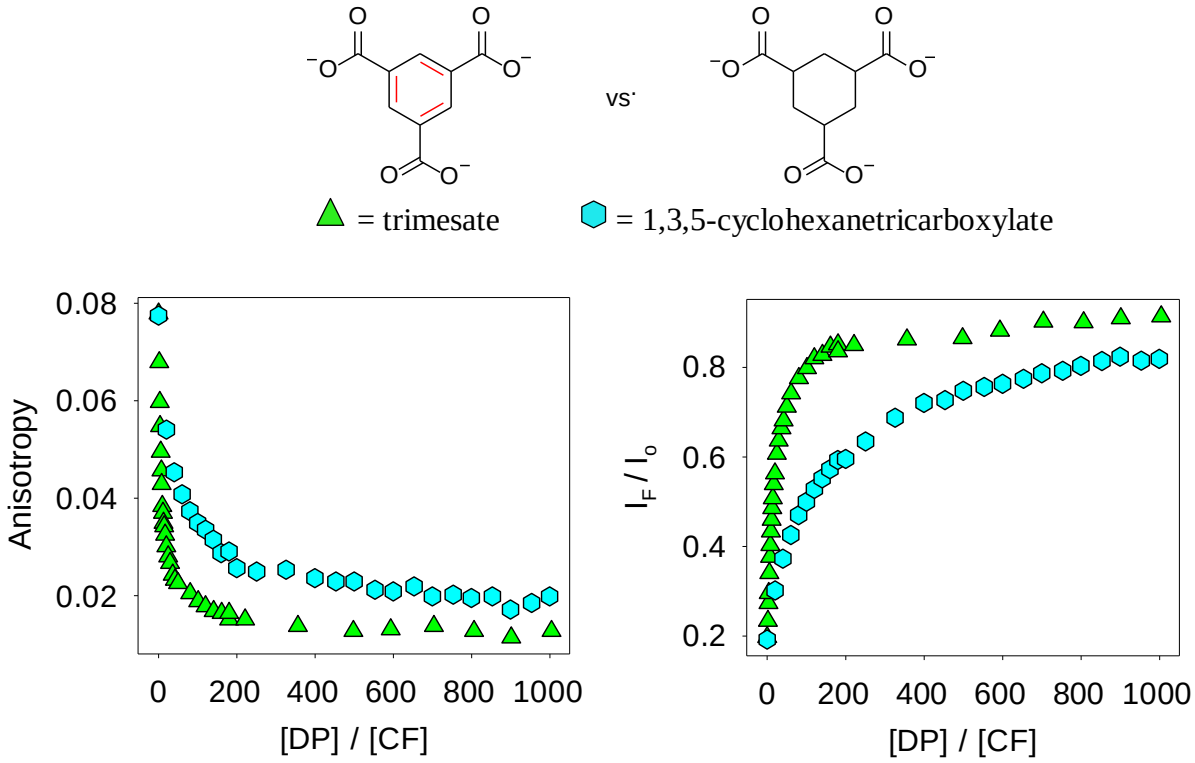

Figure 3.13. Interactions with a π-system: fluorescence intensity and anisotropy isotherms from titration of a G5•**CF**$_n$ complex with trianionic aliphatic and aromatic displacers. [**CF**] = 2.0 × 10^{-6} M, [G5] = 4.5 × 10^{-7} M in buffered H_2O (50 mM HEPES at pH 7.4), λ_{exc} = 485/20 nm, λ_{em} = 560/40 nm.

We propose that this extra contribution to the overall affinity is due to an interaction involving the aromatic core of the trimesate anion, promoted by the surface ammonium groups of the dendrimer (Scheme 3.5). The positive charge of the dendrimer's ammonium groups induces significant polarization of the C-H bonds on the carbon adjacent to it in the dendrimer backbone. One of these C-H bonds is positioned ideally to interact with the aromatic cloud of the guest in a CH-π interaction. The overall process is assisted by the electrostatic interaction

between the ammonium cation in the dendrimer and the carboxylate anion in the guest, as described in Scheme 3.5. This interaction is of course absent in the case of the cyclohexanetricarboxylate anion, which results in its lower apparent affinity.

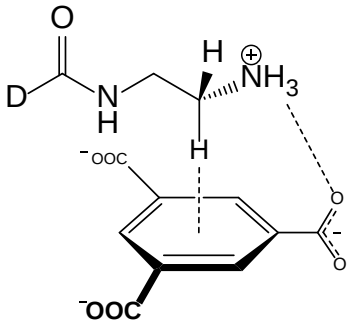

Scheme 3.5. Hypothesized CH-π interaction. An ammonium group of the dendrimer interacts with the carboxylate group of trimesate; this arrangement allows the aromatic core of trimesate to interact with the electron-poor H atom belonging to the CH_2 group adjacent to the ammonium ion. D = dendrimer scaffold.

3.2.4.1 Electrostatic Potential Maps

In order to support the proposed CH-π interaction, we calculated electrostatic potential maps for the 1,3,5-cyclohexanetricarboxylate and trimesate anions. The molecular structure geometries of these two molecules were optimized to an energy minimum using the PM6 semiempirical method as implemented in the *Gaussian* 09 software package.[61] A vibrational frequency calculation was carried out to check that the resulting geometry corresponded to an energy minimum. The total electron density was sampled in space around each optimized structure, by generating an electron density cube from the total SCF density with the *cubegen* utility included in *Gaussian*. The total electron density distributions from the optimized structures was used to calculate the electrostatic potential in space near the molecule. The values of ESP were then mapped onto an electron density surface with a density cutoff of 0.0004. The color mapping was chosen to highlight the difference between the aliphatic and aromatic systems, and the same mapping values were used for both surfaces; in specific, the red color

(most negative) represents an ESP of 5.0, the blue color (least negative) represents an ESP of 3.2 respectively.

The ESPs calculated for the two molecules are shown in Figure 3.14. The red region close to the aromatic ring in the trimesate anion is attractive for a positive charge and it can establish the stabilizing interaction with the dendrimer's backbone discussed above; the cyclohexanetricarboxylate possesses no such region, and cannot establish that interaction.

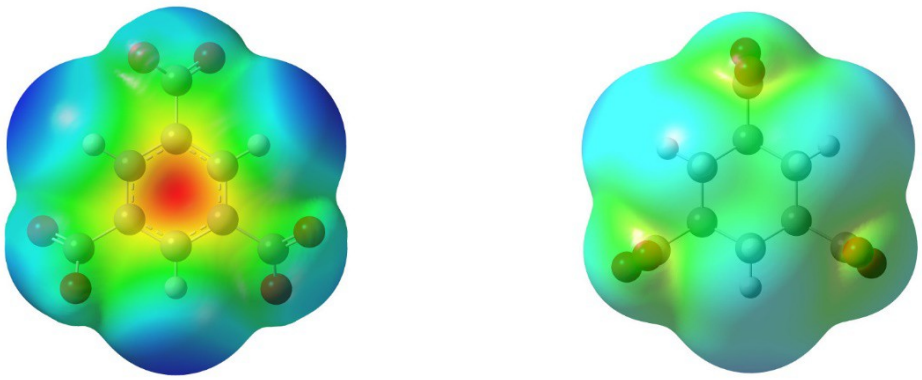

Figure 3.14. Electrostatic potential (ESP) maps for the trimesate (left) and the cyclohexanetricarboxylate (right) anions. These maps were drawn at the same mapping value boundaries; in particular, the red colour represents the regions of space most attractive for a positive charge, the blue colour represents those regions least attractive to a positive charge.

3.3 SEMI-QUANTITATIVE INSIGHTS

Finally, Table 3.3 summarizes quantitative insights into the relative affinities of the probe anions for the G5 PAMAM dendrimer. As discussed previously, thermodynamic binding constants are inaccessible for these systems, due to the complex equilibria involved and a lack of a viable model to conduct the fitting of experimental data. In lieu of those missing binding constants, each anion was assigned a "critical concentration", i.e. the concentration of the probe anion necessary to cause 95% displacement of the **CF** dye from its (G5•**CF**$_n$) complex, as measured from the anisotropy displacement isotherms. On this scale, a lower critical concentration corresponds to higher binding affinity of the corresponding probe anion for the G5

dendrimer. Using these values, we can readily rank the relative importance of each intermolecular interaction we studied. For instance, increasing the negative charge on the guest by one unit brings about a more than 10-fold increase in affinity, the largest effect among those studied. Most surprisingly, the presence of an aromatic moiety in the guest also leads to a similar increase in affinity, showcased here by the comparison of cyclohexanetricarboxylate and trimesate anions. This is an unexpected outcome of our study, and it opens interesting avenues in the use of these dendrimers for selective binding to aromatic over aliphatic guests (discussed in Chapter 4).

Table 3.3. Critical concentrations of probe anions necessary to cause 95% displacement of the **CF** dye from its (G5•**CF**$_n$) complex with the G5 PAMAM dendrimer. Lower critical concentrations correspond to higher affinity of the corresponding probe anion for the G5 dendrimer.

Probe anion:	**Critical concentration**
succinate	> 12 mM
pimelate	> 12 mM
4-ketopimelate	> 12 mM
tricarballylate	1.10 mM
citrate	0.70 mM
1,3,5-cyclohexanetricarboxylate	1.60 mM
1,2,3,4-butanetetracarboxylate	0.04 mM
trimesate	0.18 mM
malate	7.6 mM
mesoxalate	2.0 mM
oxaloacetate	6.8 mM

Furthermore, the presence of hydrogen bond donor groups (OH) in the guest has significant effects, inducing a 4-fold increase in affinity, as shown by the malate-mesoxalate comparison. Quite surprisingly, the dendrimer was found to behave as a much worse H-bond donor than it does as an acceptor, as implied by the much smaller influence of hydrogen bond

acceptor groups in the guest (e.g. pimelate vs. ketopimelate). Finally, shape and size of the guest have almost no effect on the affinity, thanks to the flexibility and multivalency of the dendrimer scaffold.

3.4 TERTIARY AMINE INTERACTION WITH FREE DYE

In all indicator displacement assays studied (IDAs) we used the free dye in solution as a reference point. When examining the fluorescence intensity displacement profiles using PAMAM dendrimers as the hosts, we noticed that we do not fully recover all the free dye. This result made us think that the free dye is still, to some extent, interacting with the dendrimer (left, Figure 3.15). We have determined from the binding experiments presented in Chapter 2 that some of the fluorophore's emission is quenched due to a photo-induced electron transfer (PET) process from the tertiary amines in the dendrimer's backbone that happen to be in close proximity to the bound fluorophore.

We further supported our hypothesis that PET was occurring by looking at the fluorescence intensity profiles shown in Figure 3.15. The profiles present similar displacement experiments using **CF** and 1,3,5-cyclohexanetricarboxylate in the same conditions, with the only difference being the host. Displacement of the anionic probe with the PAMAM G5 as the host is shown to the left of Figure 3.15, whereas polyDADMAC as the host is shown to the right in the same figure. From the two profiles, the dye emission is fully recovered after displacement when polyDADMAC is used as the host, but not in the case of PAMAM G5. It is significant to note here that although PolyDADMAC contains the same binding motif as the PAMAM dendrimers (i.e. ammonium cations), it does not contain tertiary amine moieties. This further verifies that the tertiary amines cause the quenching of the fluorescence intensity of **CF** due to the proposed PET process.

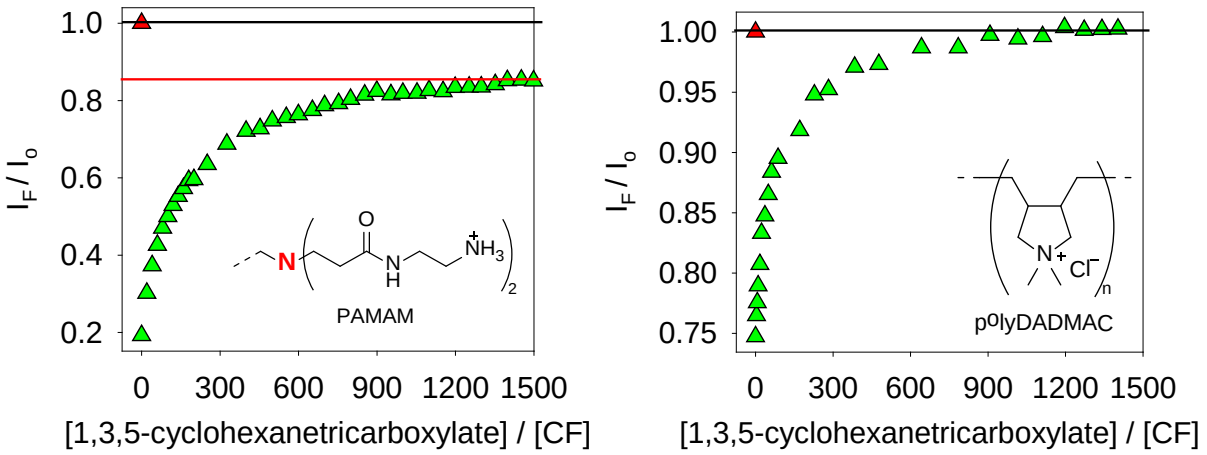

Figure 3.15. Titration of **CF** with G5 dendrimer and cyclohexanetricarboxylate, λ_{exc} filter = 485/20 nm, λ_{em} filter = 560/40 nm. Titration of **CF** with polyDADMAC and cyclohexanetricarboxylate, λ_{exc} = 480nm, λ_{em} = 520nm. [**CF**] = 2.0×10^{-6} M in buffered H_2O (50 mM HEPES at pH 7.4). Free dye reference point shown in red.

3.5 HYPERBRANCHED POLY(ETHYLENEIMINE)

We wanted to study the displacement properties of another polymer which bears a positively charged scaffold. Since the relatively high price of PAMAM dendrimers could be a significant hurdle in the path to their application, we chose a much less expensive polyelectrolytes. Hyperbranched poly(ethyleneimine) (PEI) is commercially available and significantly cheaper than the PAMAM dendrimer. This polyelectrolyte has a similar scaffold to the dendrimer and bears ammounium cations on its surface but does not have the well-defined shape of the previous studied dendritic macromolecules. We chose to study five highly relevant probes from our wide selection of anionic guests with this host. Figure 3.16 shows the fluorescence emission and anisotropy displacement data from all five anions studied using PEI as a host.

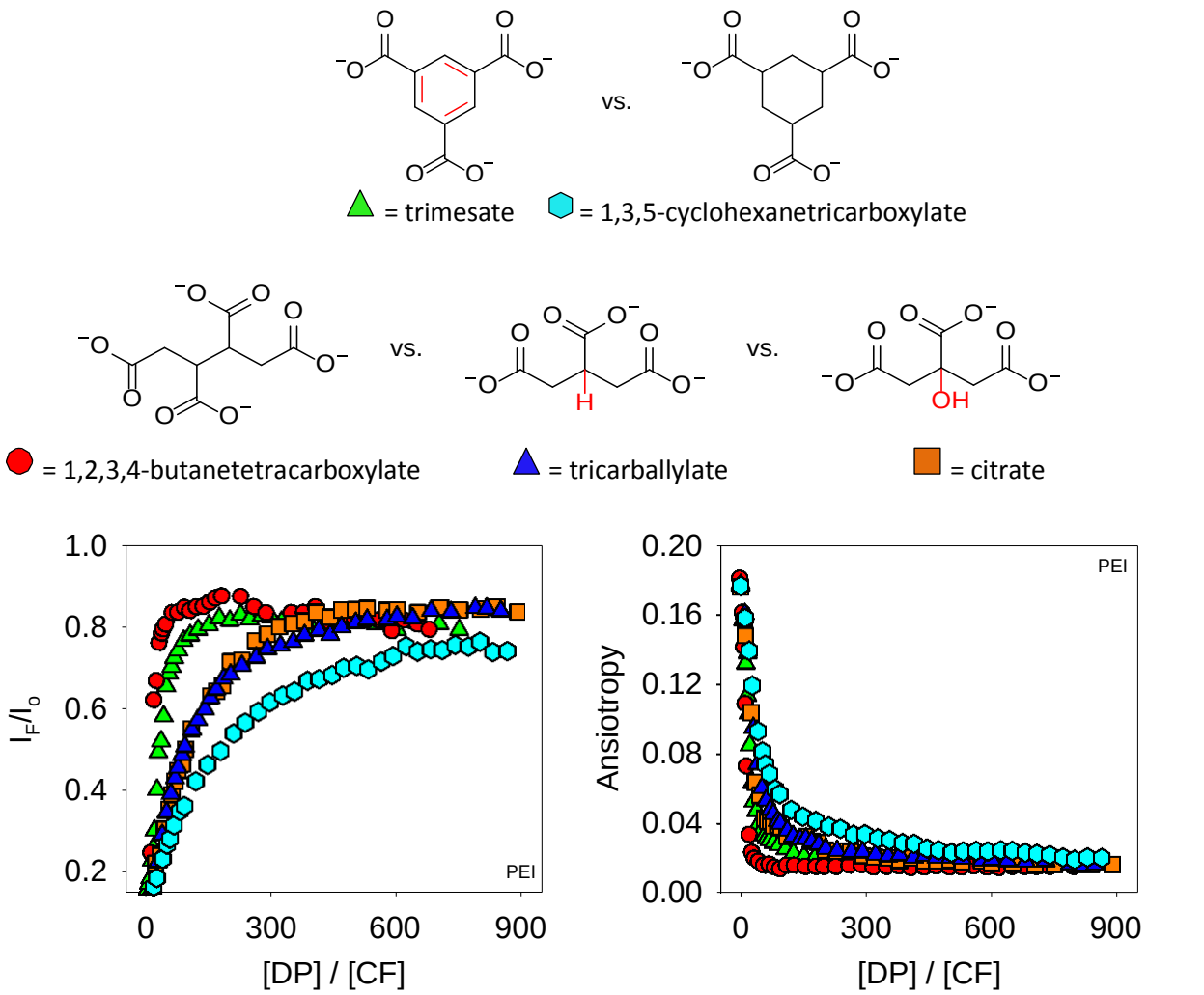

Figure 3.16. Guest charge: fluorescence intensity and anisotropy isotherms from titration of a G5•**CF**$_n$ complex with tetraanionic vs. trianionic vs. dianionic displacer (DP). [**CF**] = 2.0×10^{-6} M, [PEI] = 4.5×10^{-7} M in buffered H_2O (50 mM HEPES at pH 7.4), λ_{exc} = 485/20 nm, λ_{em} = 560/40 nm.

Table 3.4 summarizes quantitative insights into the relative affinities of the probe anions for the PEI polyelectrolyte. In order to compare to the data obtained from the dendrimers (Table 3.3), a similar "critical concentration", i.e. the concentration of the probe anion necessary to cause 95% displacement of the **CF** dye from its polyelectrolyte complex, was taken from the anisotropy displacement isotherms. Examining the critical concentrations of butanetetracarboxylate and tricarballylate, we see that increasing the negative charge on the guest by one unit brings more than a 10-fold increase in affinity. The presence of an aromatic

moiety in the guest, shown by the comparison of cyclohexanetricarboxylate and trimesate anions, leads to a similar increase in affinity. In both of these cases, we see similar results as those found by using the PAMAM dendrimer as a host.

Additionally, we see the same results when looking at citrate versus tricarballylate probes, where the tertiary OH group is expected to be sterically hindered and not available to participate in intermolecular interactions with the dendrimer scaffold. We see from Figure 3.16 that both molecules bind with similar affinity to PEI. However, the binding affinity of cyclohexanetricarboxylate compared to tricarballylate, both of which bear three negative charges, has yet to be fully understood. We can clearly see from Figure 3.16 that cycylohexanetricarboxylate binds with a lower affinity than tricarballylate, which is a problem that did not arise when examining binding to the PAMAM dendrimers. The cause for these differences is likely to be a complex interplay of factors such as the size and mass of the polyelectrolytes, their conformation in solution, and/or the role of the solvent. We have been unable to pinpoint any one leading factor so far, but further studies are ongoing in our lab.

Table 3.4. Critical concentrations of probe anions necessary to cause 95% displacement of the **CF** dye from its (PEI•**CF**$_n$) complex with poly(ethyleneimine). Lower critical concentrations correspond to higher affinity of the corresponding probe anion for the hyperbranched polyelectrolyte.

Probe anion:	**Critical concentration**
tricarballylate	1.02 mM
citrate	0.88 mM
1,3,5-cyclohexanetricarboxylate	1.56 mM
1,2,3,4-butanetetracarboxylate	0.07 mM
trimesate	0.36 mM

3.6 CONCLUSIONS

The role of various intermolecular interactions involved in the binding between polyanionic probes and cationic polyelectrolytes was explored using an indicator displacement method based on simple and sensitive optical spectroscopy techniques. The results of these experiments allowed us to evaluate the relative importance of various intermolecular interaction modes to the overall binding process. In doing so, the insights summarized here will provide valuable tools for researchers interested in using these attractive dendritic structures as molecular scaffolds and supramolecular hosts.

From studies conducted on the positively charged polyelectrolytes, PAMAM dendrimer and PEI, we found electrostatic interactions to be the most influential by far: the overall charge of the guest is a prime predictor of relative affinity. We also demonstrated that a significant stabilizing interaction exists between the dendrimer scaffold and the electron cloud of an aromatic system. Further information obtained from experiments with the PAMAM dendrimer, determined that hydrogen bonding interactions are also of importance. The dendrimer scaffold acts as an effective H-bond acceptor, therefore displaying higher affinity to molecules that can act as H-bond donors. However, we found poor results from H-bond donating probes which contained tertiary alcohols due to their high steric hindrance and reduced availability of the OH group to the hosts scaffold. Finally, shape and size of the guest have essentially no influence on the observed affinity, thanks to the high flexibility of the dendritic scaffold.

3.7 EXPERIMENTAL SECTION

Materials. 4-(2-Hydroxyethyl)piperazine-1-ethanesulfonic acid (HEPES) buffer (free acid) was purchased from VWR. Poly(amidoamine) (PAMAM) dendrimers with ethylenediamine core and primary amine termination were used in these studies. The dendrimers were manufactured by Dendritech, Inc. and either purchased directly from the manufacturer or from their distributor (Sigma-Aldrich) as MeOH solutions of varying concentrations depending on the dendrimer generation. Dendrimer solutions were stored refrigerated at 4°C. All experiments on dendrimer generations G3 and G6 were carried out using the same dendrimer lot, whereas G4 and G5 experiments were conducted from two lots of dendrimer. In the latter case, we confirmed lot-to-lot consistency by successfully replicating a number of fluorophore interaction experiments on both lots. The G5 stock solutions in MeOH received from Sigma and used throughout this work contained ~5% w/w dendrimer: the exact concentration depended on the specific lot, and was taken into consideration. Dendrimer solutions were stored refrigerated at 4°C. After dilution with buffer to obtain the desired working concentration of polymers, the final solutions used for titrations contained a negligible amount of MeOH (<0.2%). The fluorescent probe, 5(6)-carboxyfluorescein was purchased from Sigma-Aldrich as a mixture of isomers, and used as received. Displacer anion solutions were prepared from DL-malic acid, oxaloacetic acid, pimelic acid, sodium mesoxalate monohydrate, succinic acid and trimesic acid, (from Sigma), tricarballylic acid and 1,2,3,4-butanetetracarboxylic acid (Alfa Aesar), citric acid (Fisher Scientific), 1,3,5-cyclohexanetricarboxylic acid (TCI America), and 4-ketopimelic acid (Acros). All reagents were used as received.

Instrumentation. Optical spectroscopy experiments were carried out on the following instrumentation: Biotek Synergy 2 **multimode plate reader**, HP 8452A **diode array UV-Vis**

spectrophotometer, and ISS PC1 **spectrofluorimeter** whose details are discussed in Chapter 2 experimental sections.

Titration conditions. All experiments were carried out in aqueous solutions buffered to pH 7.4 with 4-(2-hydroxyethyl)-1-piperazineethanesulfonic acid (HEPES, 50 mM). pH was measured using a frequently calibrated glass pH combined electrode. The pH of the working solutions was adjusted prior to use by addition of NaOH or HCl solutions, and spot-checked during a titration to make sure that it had not drifted away from the desired value of 7.4. Drift was generally not a problem, but significant adjustments had to be made when preparing solutions of anions from their corresponding acids.

Instrumental parameters for fluorescence experiments.

5(6)-carboxyfluorescein, benchtop:

- Excitation wavelength: 480 nm
- Emission spectra: 490-560 nm
- Emission for anisotropy: 520 nm
- Slit, excitation: 4 nm spectral resolution
- Slit, emission: 2 nm spectral resolution
- Iris: open
- Polarizers: Glan-Thompson calcite, always in the light path:
  - set to the magic angle (54.7°) for intensity measurements
  - computer controlled for anisotropy measurements

5(6)-carboxyfluorescein, plate reader:

- Excitation filter: 485/20 nm
- Emission filter: 560/40 nm
- Dichroic mirror: 510 nm cutoff
- Polarizers: plastic, only used for anisotropy experiments
- Automatic detector gain adjustment

General displacement titration protocol. All experiments were carried out in a buffered aqueous solution prepared in large batches to be used in multiple titrations. The pH of the buffer was adjusted by addition of NaOH or HCl solutions as needed. Combined glass electrodes were

used to measure the pH of all solutions. The pH of the working solutions was also spot-checked during a titration to make sure that it had not drifted away from the desired value of 7.4.

We prepared multiple stock solutions of the **CF** dye that were used as starting points for multiple titrations. For example, a 5(6)-carboxyfluorescein stock solution was made by adding 7.90 mg of 5(6)-carboxyfluorescein solid to 50 mL of 50 mM HEPES buffer giving a concentration of 4.20×10^{-4} M.

All solutions used in displacement experiments were made by dilution of aliquots of stock solutions of dyes or polymers. Displacement experiments were carried out using two separate solutions, a "titrant" and a "cuvette" solution. "Titrant" and "cuvette" solutions were made fresh for each experiment.

A "**cuvette**" solution contained the [dendrimer] / [fluorophore] ratio used as our bound solution in buffer at its final working concentration; it was made by dilution of an aliquot of dye stock and of an aliquot of polymer stock into buffer. The final working concentration in these solutions of [PAMAM G5] / [**CF**] was [4.5×10^{-7} M] / [2.0×10^{-6} M] throughout.

A "**titrant**" solution contained the PAMAM G5 and **CF** at the same concentrations mentioned above and the displacer anion under study as well. The [**D•CF**$_n$] complex concentration in this solution was always kept rigorously the same as the one in the corresponding "cuvette" solution, so that addition of the "titrant" to the "cuvette" solution would not change the overall concentration of the dye or of the dendrimer. "Titrant" solutions were made by dilution of an aliquot of dye stock, of an aliquot of polymer stock and an aliquot of displacer stock; the solution was then brought up to the final volume with buffer.

The pH of these solutions was checked with a calibrated glass electrode after their preparation and corrected to 7.4 by addition of NaOH or HCl if necessary.

The displacement experiment was carried out by addition of aliquots of the “titrant” solution to the “cuvette” solution. The resulting mixture was then left to equilibrate briefly, then a measurement was taken. In the case of benchtop experiments, serial additions of “titrant” solutions were made to the same “cuvette” solution in a Starna Spectrosil quartz cuvette held in the temperature controlled cuvette holder of the instrument.

Multiwell plate experiments. Each point in a titration profile obtained in a multiwell plate corresponded to a set of wells on the plate (normally two or three replicates). All points in the titration were constructed from appropriate “titrant” and “cuvette” solutions (see displacement titration protocol above) laid out on a single plate and measured at the same time. Multiple experimental parameters (e.g. absorbance, fluorescence, anisotropy) were measured on the same plate, ensuring greater internal consistency, and a significant speedup in data acquisition. Absorbance and fluorescence emission raw reads were blanked by subtracting the corresponding reading for the buffer. Replicate data points on a multiwell plate were averaged: the value reported for a titration point was the average of at least two readings. The resulting data was plotted as a function of the [displacer] / [fluorophore] ratio to produce binding isotherms. Results obtained from the plate reader were in excellent agreement with those obtained on the standard benchtop instruments.

Data treatment. Absorbance and fluorescence emission raw readings were blanked by subtracting the corresponding reading for the buffer. Replicate data points on a multiwell plate were averaged: the value reported for a titration point was the average of at least two readings, and typically more. The resulting data was plotted as a function of the [displacer] / [fluorophore] ratio to produce binding isotherms.

Table 3.5. Cartesian coordinates of the 1,3,5-cyclohexanetricarboxylate anion and trimesate anion optimized structures.

1,3,5-cyclohexanetricarboxylate anion – PM6 optimized structure

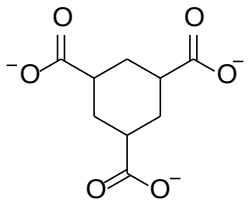

C	-1.44583	0.07805	0.11051
H	-1.44734	0.118762	1.217186
H	-2.50077	0.1179	-0.20569
C	-0.79944	-1.24036	-0.35884
H	-0.83829	-1.27688	-1.47252
C	0.676981	-1.29238	0.081388
H	0.736127	-1.29083	1.187231
H	1.14126	-2.2333	-0.25566
C	1.453223	-0.08509	-0.48095
H	1.409973	-0.12386	-1.59438
C	0.800015	1.22983	-0.01123
H	1.352347	2.093971	-0.41456
H	0.862678	1.303454	1.091968
C	-0.67603	1.289498	-0.45174
H	-0.71513	1.24804	-1.56523
C	2.96059	-0.14467	-0.10106
O	3.318185	-0.1181	1.097447
O	3.764454	-0.21954	-1.07212
C	-1.34322	2.633748	-0.04202
O	-1.44295	2.955549	1.162763
O	-1.76103	3.347547	-0.99632
C	-1.59266	-2.4798	0.145749
O	-1.71888	-2.70137	1.370486
O	-2.08129	-3.2175	-0.75525

Trimesate anion – PM6 optimized structure

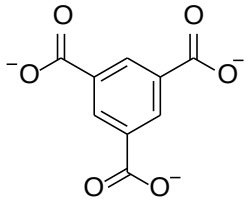

C	1.18654	-0.75895	0.00003
C	1.24002	0.64267	0.00001
C	0.064	1.40705	-0.00002
C	-1.17658	0.75255	-0.00001
C	-1.25054	-0.64811	-0.00001
C	-0.06344	-1.39522	0
H	2.21113	1.14594	0.00001
H	-2.09798	1.34192	0
H	-0.11316	-2.48785	-0.00001
C	-2.60434	-1.34975	-0.00003
O	-2.6244	-2.60717	-0.00029

O	-3.6433	-0.64121	0.00021
C	0.13325	2.93029	-0.00006
O	-0.94567	3.57638	0.00033
O	1.26634	3.47579	-0.00049
C	2.47109	-1.58054	0.00009
O	2.37697	-2.83459	-0.0002
O	3.57005	-0.96919	0.00044

CHAPTER 4

HYPERBRANCHED POLYELECTROLYTES AS SOLUBILIZING AGENTS FOR HYDROPHOBICS IN WATER

4.1 INTRODUCTION

Cationic polyelectrolytes (Scheme 4.1) including dendrimers and micelles have been extensively studied as encapsulating agents.[82,83] As mentioned previously, some of the fundamental properties of linear polyelectrolytes have been long modeled theoretically: for instance, Katchalsky[28] and Manning[29] have conducted pioneering work in this field. However, many aspects of the behavior of these polyelectrolytes in solution are still in need of clarification, especially regarding their interactions with smaller organic molecules in aqueous media and their possible application as solubilizing agents.

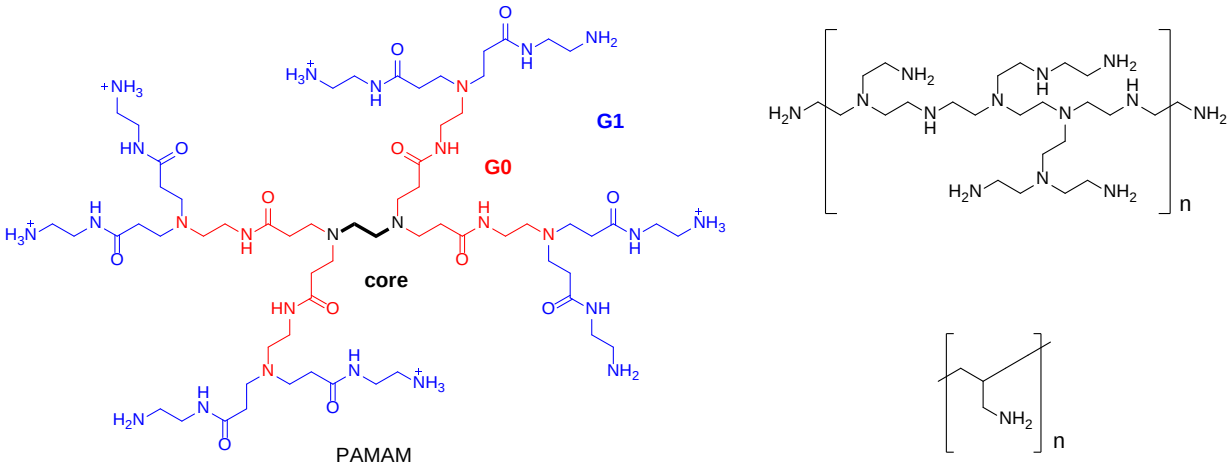

Scheme 4.1. Left: Structures of polyelectrolytes. Left: Schematic structure of a first-generation (G1) amine-terminated poly(amidoamine) (PAMAM) dendrimer. The conventional representation of dendrimer generations ishighlighted in color. Right, top: A partial structure of randomly hyperbranched poly(ethyleneimine) (PEI). Right, bottom: Structure of linear poly(allylamine) (PA).

Other researchers have previously considered the use of dendritic polymers or their derivatives as drug vectors, e.g. for the delivery of silibinin, a hepatoprotective drug,[84] or for *in vitro* gene delivery.[37] Similar randomly hyperbranched or linear polyelectrolytes, such as poly(ethyleneimine) and poly(allylamine) (Scheme 4.1, right), have also been considered for these purposes, because they are relatively inexpensive, and rather better known thanks to existing industrial applications.[27] These macromolecules, however, are typically more difficult to study due to their wider size distribution and less regular structures compared to PAMAM.

Our group has conducted extensive studies in the last few years on the fundamental interactions responsible for the encapsulation of small molecules inside large polyelectrolytes, as previously reported in this dissertation[85] and elsewhere.[34,76] Our reported results gave us deeper insight into the nature and relative importance of the fundamental intermolecular interactions that are responsible for the encapsulation of small molecules in these linear and globular charged polymers. More recently, we have been working to apply that expertise to the problem of solubilizing hydrophobic compounds in water, a significant practical challenge that impacts many fields of applied chemistry, among which the drug discovery process.

In fact, enhancement of drug dissolution and improvement of the bioavailability of poorly soluble drug candidates are major challenges in drug delivery.[86] Drugs with low water solubility tend to be eliminated from the gastrointestinal tract before they can be absorbed in blood circulation, resulting in poor bioavailability.[87] One approach to solving this issue is to encapsulate the drug into macromolecular hosts, e.g. to increase the drug's solubility in aqueous media, or to improve its pharmacokinetics.[88] Our overall goal is to apply the knowledge we have

accumulated on the binding properties of these polyelectrolytes to the problem of the solubilization of hydrophobic materials in aqueous solution. Furthermore, we have recently reported that aromatic compounds partition into these structures preferentially over aliphatics.[85] This surprising finding paves the way for very interesting applications for these polymers in separation science. For instance, micelles and other large macromolecules providing hydrophobic pockets have been previously used as pseudo-stationary phases for capillary electrophoresis. In this context, these structures add a further dimension to the separation capabilities of the technique, based on their unique binding preferences. We report here on results contributing to establishing the groundwork for such applications for the polyelectrolytes under study.

We present results from our studies on the ability of several cationic polyelectrolytes to increase the solubility of water insoluble molecules. We took a two-pronged approach to this problem. On the one hand, we used a dissolution testing approach to study the solubilization of hydrophobic compounds in water solution. On the other hand, we used standard titration techniques to explore the behavior of molecules whose water solubility is appreciable even in the absence of a solubilizing agent. Dissolution testing is an analytical technique used to measure the amount of a molecule of interest that can be dissolved in a known volume of liquid medium at a fixed time.[89] We used optical spectroscopy to carry out these studies as we have done previously in reported work on similar systems.[76,85]

We investigated the fluorescence response of two polycyclic aromatic hydrocarbons (PAHs), anthracene and pyrene (Scheme 4.2), upon interaction with the amine-terminated PAMAM dendrimers. Multiple reasons make these dyes an ideal choice for such studies: they are representative of polycyclic aromatic hydrocarbons, a class of compounds of great

importance in environmental chemistry applications; they are similar in size to common therapeutics; they have very low solubility in aqueous media; and the dependence of their fluorescence emission on environmental factors is very well understood.[90,91] In fact, anthracene was previously used by another group as a probe for solubility enhancement in similar studies.[92]

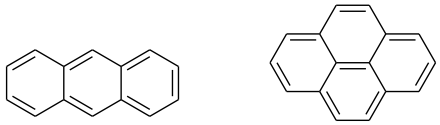

Scheme 4.2. Structures of the fluorescent hydrophobic hydrocarbons used as solubility probes. Left: anthracene, right: pyrene.

4.2 RESULTS AND DISCUSSION

This study focused on multiple families of polyelectrolytes. We will explore the behavior of PAMAM dendrimers with ethylenediamine cores, both with anionic (carboxylate) surface decorations (generation G3.5), and with cationic (ammonium) terminations (generations G3.0 through G5.0). We also compared the properties of the PAMAM dendrimers under study to that of cationic hyperbranched poly(ethyleneimine) and linear poly(allylamine). The dendrimers used in these studies are commercially available from Dendritech, Inc. as solutions in H_2O or MeOH. Dendrimers of generations G3 to G5 were chosen for this study because they strike an optimal balance between large size and affordable cost for practical applications, and therefore their properties are most relevant to study. From our experience, dendrimers smaller than G3 do not display high enough affinity to be viable in applications at micromolar concentrations, an observation confirmed by the work of Silber and coworkers.[92] On the other hand, larger dendrimers might perform better than those reported here, but they are exponentially more expensive than the smaller generations due to the difficulty in obtaining them in high purity.

All aqueous solutions used in this study were buffered at pH 7.4 using 50 mM 4-(2-hydroxyethyl)-1-piperazineethanesulfonic acid (HEPES). We were interested in neutral aqueous solutions because of the general relevance of such conditions to both physiological and environmental applications. However, the Trejo group has previously reported that increased ionic strength reduces the solubility of PAHs in aqueous solution.[93] Therefore the results reported here represent a worst case scenario; any solubility enhancements due to the presence of polyelectrolytes would be even more significant for low ionic strength applications. Temperature also plays a significant role in determining solubility, so we conducted experiments at a carefully controlled temperature of 25°C.

4.2.1 Dendrimers Solubilize Anthracene in Water

We recently reported on the surprising importance of CH-π interactions between positively charged PAMAM dendrimers and molecules containing an aromatic core.[85] On the basis of that study, we speculated that dendrimers could show the same interaction with the π-core of plain aromatic hydrocarbons, thereby increasing the solubility of these hydrophobic compounds in aqueous media, even without the assistance of electrostatic interactions, an impressive result for such a relatively simple system.

We chose to use anthracene as our first solubility probe because of its hydrophobic nature, low water solubility, and electron-rich π system. Anthracene is also an efficient fluorophore, so we were able to use highly sensitive fluorescence spectroscopy to monitor changes in the concentration of this hydrocarbon even in very dilute solutions.

The required solubility enhancement experiments were conducted in two ways. The first method described below has been used extensively in similar experiments in the literature. We have used this dissolution method to offer a point of comparison with previously published

results,[84] but we contend that this method may be prone to overestimating any solubility enhancement effect, as we discuss in more detail. Therefore, we have also proposed an alternative experimental setup that in our opinion alleviates this limitation.

In order to detect the solid – solution phase transfer according to the first method of study, a constant amount of anthracene was deposited as a thin film onto a series of cuvettes by evaporation of a solution in hexanes. We took care to deposit an excess of anthracene onto the cuvettes to ensure that only a fraction of the available anthracene would be brought into solution by the polymer. Identical volumes of solutions containing increasing concentrations of the polyelectrolyte under study were then added to each cuvette, the cuvettes were sealed, and left to equilibrate overnight at constant temperature. The fluorescence emission from the anthracene in the aqueous phase was then recorded upon excitation at 350 nm.

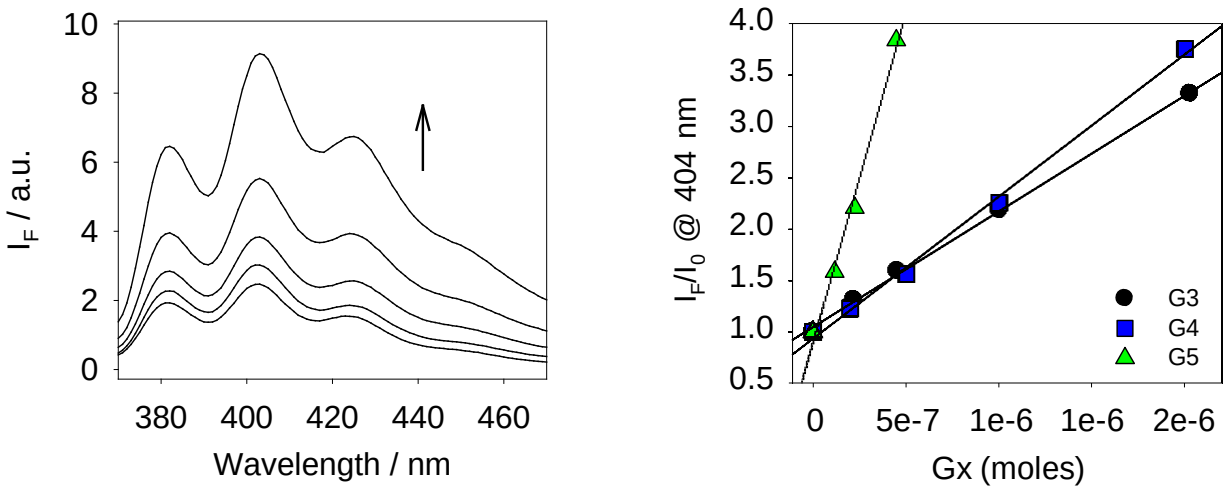

Figure 4.1. Comparing fluorescence emission spectra and profiles corresponding to increasing amounts of PAMAM G3-G5 in the presence of anthracene as a thin film. G3 = 0 to 2.03 x 10^{-6} moles, G4 = 0 to 2.00 x 10^{-6} moles, G5 = 0 to 4.47 x 10^{-7} moles, anthracene = 1.12 x 10^{-6} moles.

Experiments were conducted with cationic PAMAM dendrimers of generations G3 to G5 (G3, M_w ~7,000 g/mol; G5, M_w ~29,000 g/mol, Figure 4.1). The fluorescence emission of the water phase observed in these experiments increases linearly with the amount of solubilizing

agent added (Figure 4.1). This points unequivocally to the role of the macromolecule in increasing the total amount of hydrocarbon present in the water phase, thereby effectively increasing the solubility of that hydrocarbon. Additionally, the linearity of the response with the amount of dendrimer in solution also seems to indicate that the interaction between the solubilizing agent and anthracene does not display cooperative behavior. This is in agreement with results reported by the Yu group on the solubilization of silibinin in water using similar polyelectrolytes.[84]

These results strongly suggest that the increase in solubility is due to anthracene binding to the dendrimer structure. That said, however, other factors may be contributing to this outcome. For instance, one could hypothesize that increasing concentrations of large polyelectrolytes may influence the behavior of the solvent itself: larger polyelectrolytes may tie up more solvent molecules for their own solvation, thereby intensifying hydrophobic effects and changing the effective dielectric constant of the medium. This effect, in turn, may cause the observed change within the emission properties of anthracene independently of its binding to the PAMAM dendrimer.

4.2.2 Pyrene Excimer Formation Supports Binding Hypothesis

We wanted to confirm that the observed effects described above with anthracene are indeed a consequence of the binding of this PAH to the PAMAM dendrimer. To do so, we studied the behavior of pyrene, another representative polycyclic aromatic compound. As a fluorophore, pyrene displays unique emission characteristics due to its ability to form excited-state dimers (excimers) when a molecule of pyrene in its excited state happens to find itself in close proximity to another molecule in its ground state.[20] Excimer formation is therefore a direct indication of the close proximity of multiple fluorophore molecules in solution.

Thin-film solubilization experiments with pyrene were carried out as previously

described: a constant, large amount of pyrene was deposited onto a series of cuvettes. Equal aliquots of solutions containing increasing concentrations of dendrimer solubilizing agent were then added to each cuvette, and the fluorescence emission of the aqueous phase was recorded after equilibration.

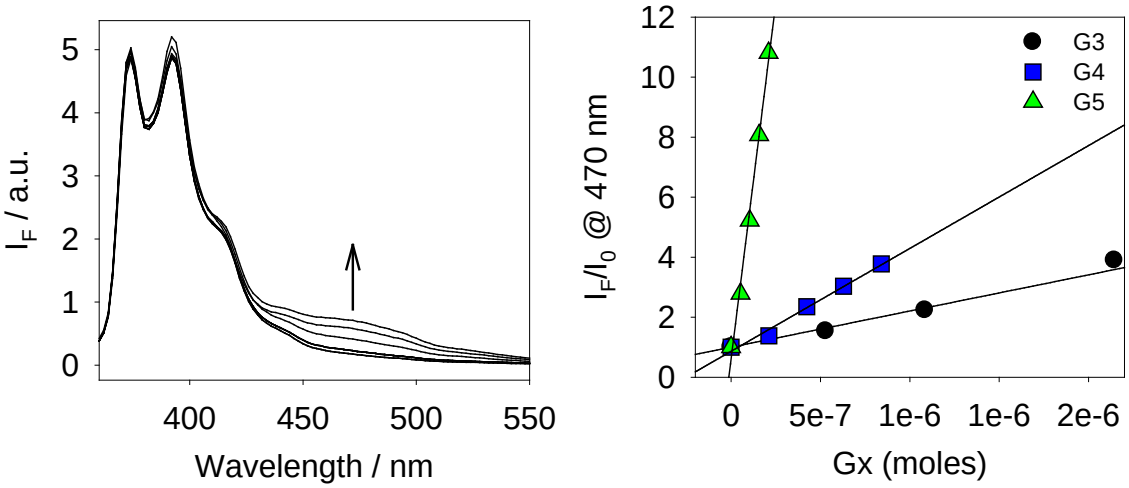

Figure 4.2. Comparing fluorescence emission profiles of solutions containing increasing amounts of PAMAM G3-G5 in the presence of a pyrene thin film. G3 = 0 to 2.14 x 10^{-6} moles, G4 = 0 to 8.41 x 10^{-7} moles, G5 = 0 to 2.10 x 10^{-7} moles, pyrene = 1.07 x 10^{-6} moles.

Upon excitation at 338 nm, pyrene displayed its typical emission bands centered at 374 nm and 392 nm attributed to the monomeric species. On addition of increasing amounts of dendrimer, a new band became prominent in the emission spectra of the aqueous phases. This broad, featureless band, red shifted from the monomer emission and centered around 470 nm, can be attributed to the formation of the pyrene excimer.[20] Its intensity was found to be linearly dependent on the concentration of polyelectrolyte in solution, as it had also been the case for the anthracene fluorescence emission spectra discussed previously (Figure 4.2). In contrast to the case of anthracene, however, formation of the pyrene excimer at such low overall concentration of pyrene can only be explained through the intermediacy of the dendrimer: multiple molecules

of pyrene must be brought into close proximity by their binding to the dendrimer molecules in solution so that when one of these molecules is excited, excimer formation is greatly facilitated by the presence of close neighbors.

In our opinion, these observations strongly support the hypothesis that the increased fluorescence signals are in fact due to an increase in concentration of the PAH in the aqueous solution, which is made possible by the formation of a non-covalent complex of the hydrocarbon with the dendrimer.

4.2.3 Improved Experimental Conditions for Dissolution Testing

The experimental setup described above still suffers from the changing nature of the aqueous medium through the course of the experiment. The interpretation of results from the method outlined above may be clouded by these "hidden variables". To sidestep this limitation, we devised a simple alternative setup described below.

We prepared thin layers of anthracene using much smaller and variable amounts of the dye. These samples were then exposed to aliquots of an aqueous solution with a constant concentration of polyelectrolyte, so that all aqueous phases exhibited the same properties (e.g. polarity). This approach also allowed us to very easily measure the amount of hydrophobic compound needed to saturate the polymer, i.e. the loading capacity of that polymer. The extent of phase transfer of anthracene into the aqueous phase was once again measured by monitoring the fluorescence emission of that phase upon excitation at 350 nm. Figure 4.3 shows the increase in anthracene emission from PAMAM G4 solutions exposed to increasing amounts of anthracene. The plateau observed in this interaction profile is attained when no further anthracene can be taken up and solubilized by the constant amount of polymer present in solution.

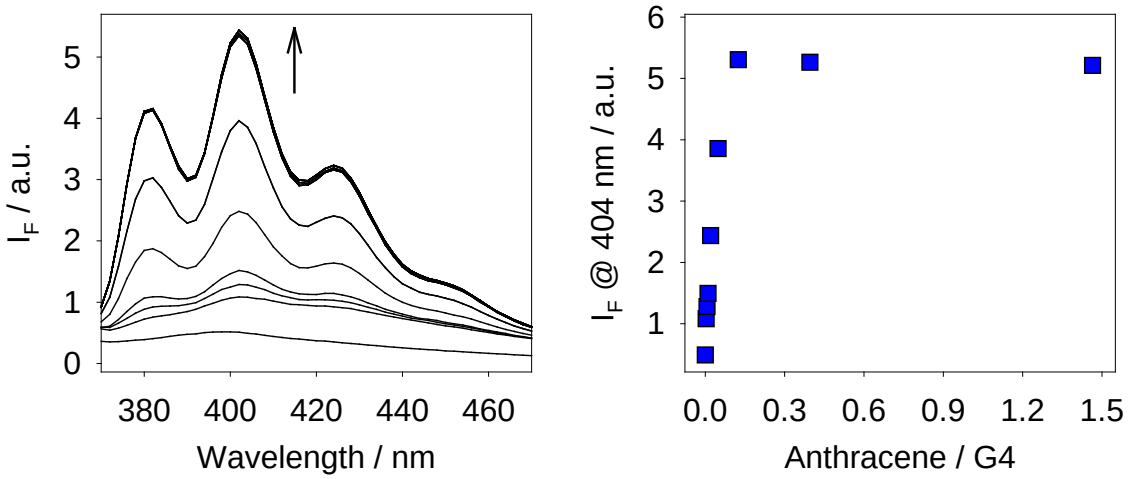

Figure 4.3. Fluorescence emission spectra and profile of solutions containing a constant amount of PAMAM G4 in the presence of increasing amounts of solid anthracene as a thin film. [G4] = 2.25 x 10^{-4} M, anthracene = 0 to 5.61 x 10^{-7} moles. (AJk-128)

From these results we were able to calculate the extent to which the solubility of anthracene was increased by the presence of PAMAM dendrimers (SE_{An}, solubility enhancement for anthracene, see eq. 1 below). First, we accounted for the background emission due to the amount of anthracene intrinsically soluble in the buffer, whose contribution cannot be ignored because of anthracene's relatively high quantum yield.[94] This parameter was readily measured by preparing a saturated solution of anthracene in buffer, whose characteristic emission (I_{satAn}) was used in the following calculations.

We also had to take into account the change in quantum yield of the anthracene fluorophore when free in the bulk solution ($\Phi_{free,\ An}$) vs. encapsulated in the dendrimer ($\Phi_{bound,\ An}$), which can be radically different.[10] An appropriate correction factor ($\Phi_{free,\ An}$ / $\Phi_{bound,\ An}$) is included in the expression for the solubility enhancement factor SE_{An}. Unfortunately, however, this parameter is difficult to access because of the low solubility of anthracene in plain buffer, which makes the determination of $\Phi_{free,\ An}$ very cumbersome. Instead, we approximated that

correction factor using the value measured for 9,10-anthracenedicarboxylate (AnDiCarb), a very similar fluorophore in molecular and electronic structure. The latter is much more soluble in water than plain anthracene, so a direct binding titration with PAMAM dendrimer allowed us to determine that the extent of quenching induced by binding is constant at 78.1% and does not depend on the dendrimer generation.[10] Considering this approximation (i.e. $(\Phi_{free}/\Phi_{bound})_{anthracene} \approx (\Phi_{free}/\Phi_{bound})_{AnDiCarb}$), we obtained the expression for the solubility enhancement of anthracene in the presence of PAMAM dendrimers shown in equation 1 below, which was used to generate Figure 4.4.

$$SE_{An} \approx \frac{\Phi_{free,\,\mathrm{AnDiCarb}}}{\Phi_{bound,\,\mathrm{AnDiCarb}}} \frac{I_F - I_{satAn}}{I_{satAn}} \qquad (eq.\,1)$$

These experiments were carried out with amine-terminated cationic PAMAM dendrimers of generations G3 through G5. The results (Figure 4.3) clearly indicate a transition between two regimes. When small enough amounts of anthracene are present, the deposited hydrocarbon is quantitatively brought into solution by the polyelectrolyte; in this regime, an increase in the total amount of available hydrocarbon causes a directly proportional increase in the amount brought into solution, and a corresponding linear increase in the emission response, as shown in the leftmost portion of Figure 4.4. When more anthracene is present than the dendrimer can solubilize, however, only a constant fraction of the available anthracene is brought into solution; an increase in the total amount of deposited hydrocarbon has no further effect on the concentration of the anthracene in solution. This limiting response corresponds to the *plateau* regions in Figure 4.4, and it indicates the maximum loading of that dendrimer generation with the hydrocarbon under study in our working conditions.

The solubility enhancement effects were very significant, ranging from a tenfold increase in solubility with the smaller G3 up to a 35-fold increase observed for G5, the largest PAMAM dendrimer included in this study (Figure 4.4).

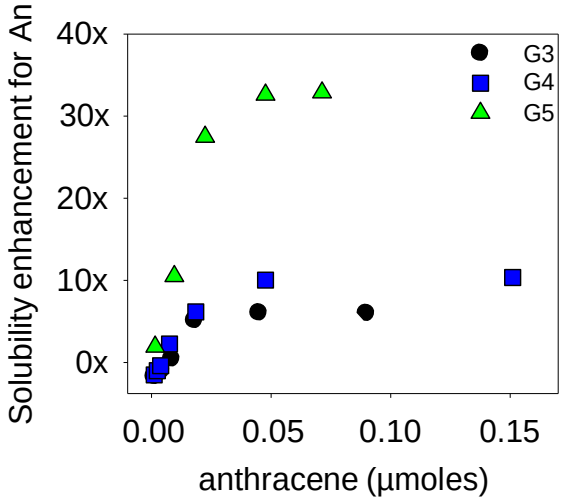

Figure 4.4. Comparing profiles obtained from the dissolution of increasing amounts of anthracene (as a thin film) in the presence of a constant concentration of G3-G5 dendrimer polyelectrolytes (see equation 3).

4.2.4 Cation-Mediated Interactions are Crucial for Binding

We propose that specific interactions between the cationic ammonium ions at the surface of the dendrimer and the aromatic cloud of these hydrocarbons are responsible for the solubilization behavior. This hypothesis is supported by our previously reported observation that an aromatic trianion binds to these dendrimers more strongly than a similar aliphatic species carrying the same charge,[85] thanks to interactions of the dendrimer with the π system of the guest mediated by the presence of the surface ammonium ions of the polyelectrolyte. According to this hypothesis, the surface decoration and charge of the polyelectrolyte would play a crucial role in binding to neutral hydrocarbons.

We confirmed our hypotheses by comparing PAMAM G3.5 and G4 dendrimers as solubilizers for anthracene. G3.5 is an anionic version of the G4 dendrimer that is terminated by

carboxylate groups, instead of the ammonium moieties present in G4. The two dendrimers are otherwise very similar in structure, size and mass (64 surface groups; 14.2 kDa and 12.9 kDa ave. for G4 and G3.5, respectively). The results, summarized in Figure 4.5, show a marked difference in behavior between the positively and negatively charged polyelectrolytes. The cationic G4 PAMAM enhances the solubility of anthracene as expected; on the other hand, anthracene is *less soluble* in a solution containing the G3.5 anionic dendrimer than it is in buffer alone.

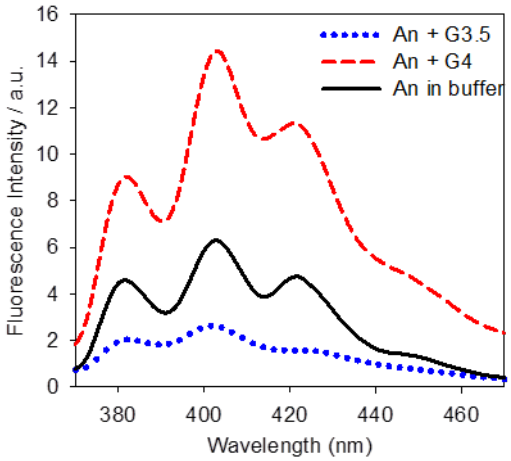

Figure 4.5. Solubilization experiments comparing the effectiveness of positively and negatively charged dendrimers as solubilizing agents for anthracene in buffer. The emission from a saturated solution of anthracene in buffer in the absence of polyelectrolytes is also included as a reference. (AJf-128)

This behavior can be explained by the fact that increasing electrolyte concentration is known to decrease the solubility of polycyclic aromatic hydrocarbons in water.[93] On the one hand, since the G3.5 dendrimers do not establish any specific interactions with anthracene, its presence in solution only has the deleterious effect of increasing the ionic strength of the medium, thus decreasing the solubility of anthracene. On the other hand, in the case of the cationic G4 PAMAM, the same negative effect is more than offset by specific favorable binding interactions between the polyelectrolyte and the anthracene, resulting in a net increase in

solubility. In our opinion, this result unequivocally indicates that cation-mediated interactions between the dendrimer and the aromatic region of these hydrocarbons are the main driving force for the binding process associated with the observed solubility enhancement.

4.3 AFFORDABLE ALTERNATIVES TO PAMAM SOLUBILIZING AGENTS

We have shown that cationic PAMAM dendrimers can significantly increase the solubility of hydrophobic compounds in neutral water solution. However, their relatively high cost is a limitation to more widespread application, so we considered less expensive alternatives to these polyelectrolytes. In particular, randomly hyperbranched poly(ethyleneimine) (PEI) and linear poly(allylamine) (PA) are commercially available cationic polyelectrolytes that are much cheaper than PAMAM dendrimers. They have also drawn attention in recent years for applications such as water and refinery waste treatment, and for cell encapsulation.[63,95] Interaction points in the linear structure of PA or in the hyperbranched structure of PEI (e.g. protonated amines) also resemble those of the cationic PAMAM dendrimers. We therefore carried out dissolution studies with anthracene, randomly hyperbranched PEI (PEI, 750 kDa avg.) and linear PA (PA, 51.5 kDa avg.) using the improved dissolution testing method described.

The results of these experiments with PEI and PA are summarized in Figure 4.6, respectively. Both polyelectrolytes were found to increase the amount of anthracene dissolved in a neutral aqueous solution. These two polyelectrolytes exhibit significantly different loading capacities. In particular, PEI (750 kDa avg.) exhibits a loading capacity that is roughly twice that of PA (51.5 kDa avg.); however, the much smaller PA is more efficient when loading capacity *per functional group* is considered. We tentatively attribute this advantage to the fact that all amine groups in PA are primary, so a larger fraction is protonated and available for interaction

with the hydrocarbon; on the other hand, a significant fraction of the amine groups in the branched polymer is secondary or tertiary, so it is less likely to be protonated, and also possibly less available for interaction because it is buried within the structure of this polymer and less accessible.

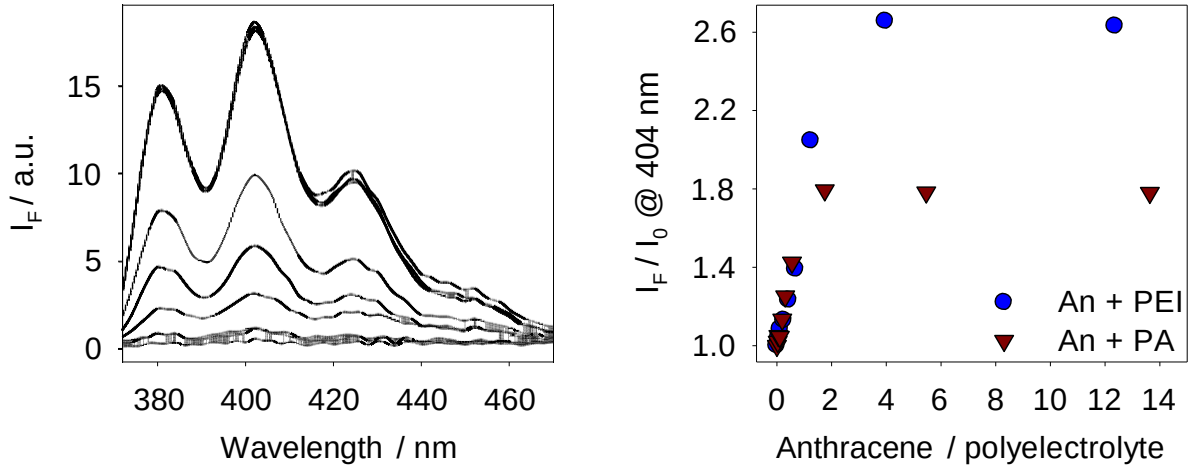

Figure 4.6. Representative fluorescence emission spectra and profiles of solutions containing a constant amount of poly(allylamine) (PA) or poly(ethyleneimine) (PEI), in the presence of increasing amounts of solid anthracene as a thin film. [PA] = 1.03 x 10^{-4} M, [PEI] = 4.54 x 10^{-5} M, anthracene = 0 to 2.81 x 10^{-7} moles. (AJk-138 and AJk-136)

4.4 INTERACTIONS WITH DRUG-LIKE GUEST MOLECULES

We have also explored the possibility of using PAMAM dendrimers to improve the solubility of molecules with more drug-like properties than anthracene and pyrene. To this end, we set up a dissolution experiment using naproxen (2-(6-methoxynaphthalen-2-yl)propanoic acid), a common non-steroidal anti-inflammatory drug (NSAID) (**Scheme 4.3**).

An experiment was set up as described at the start of this chapter: a very large excess of naproxen was deposited on a series of cuvettes, then these samples were exposed to aliquots of solution containing increasing concentrations of G4 PAMAM dendrimer. We had to revert to the original method requiring a large excess of the solid guest because naproxen is *much* more soluble in water than the hydrocarbons studied above, so thin films containing a small amount of

naproxen would spontaneously dissolve in water with or without the presence of the polyelectrolyte. Additionally, naproxen is not as fluorescent as anthracene or pyrene, so dissolution experiments were found to be much less sensitive. These considerations notwithstanding, we were able to carry out dissolution experiments but, as shown in Figure 4.7, solubilizing effects were much smaller in comparison to those induced by the dendrimers on polycyclic hydrocarbons.

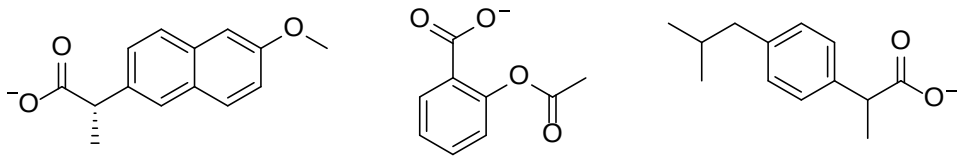

naproxen acetylsalicylate ibuprofen

Scheme 4.3. Structures and protonation states of the non-steroidal anti-inflammatory drugs from left to right; naproxen, acetylsalicylate, and ibuprofen when in dilute aqueous solution buffered to pH 7.4.

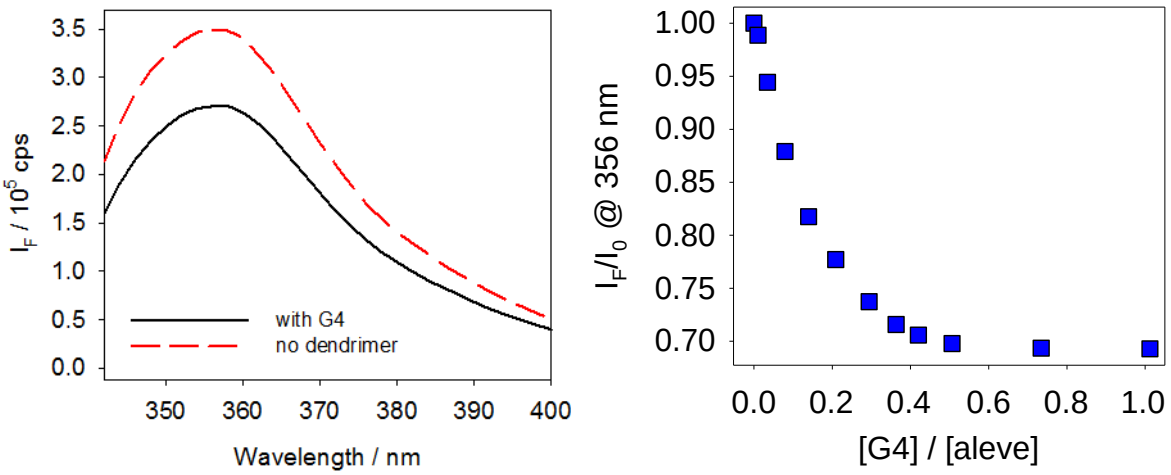

Figure 4.7 Dissolution experiment carried out on naproxen in the presence of G4 cationic dendrimer, in buffered H_2O (pH 7.4). [naproxen] = 5.65×10^{-6} M, [G4] = 0 to 5.72×10^{-4} M

One trend was maintained across those experiments, i.e. the fact that the fluorescence emission of the encapsulated molecule was quenched upon binding (Figure 4.7). This is quite a general behavior of the PAMAM dendrimers that we have had occasion to report multiple times

in the past with a wide array of fluorescent molecules.[34,76] This similarity in behavior with other fluorophores led us to hypothesize that naproxen was at least partially bound to the dendrimer and its solubility was improved thereby, albeit to a smaller extent.

This was a very promising result, so we expanded the panel of drug-like molecules under study to include acetylsalicylate and ibuprofen, two other common non-steroidal anti-inflammatory drugs (Scheme 4.3). However, we quickly realized that the dissolution method was less effective in the case of these water soluble drugs. We therefore set up an indicator displacement procedure[78] to monitor the binding of the spectroscopically silent drugs of interest in homogeneous solution. Fluorescein, a common anionic organic dye, was first bound to G5 cationic dendrimer to form a sensing complex in solution.[34,76] Aliquots of the pharmaceutical of interest were then added to a solution of this complex, while monitoring the fluorescein's emission. Binding of the analyte causes displacement of the dye from its complex with the dendrimer, causing a macroscopic change in the optical properties of the solution that can be translated to report on the binding of the otherwise silent guest. These binding studies were conducted in the same conditions used for dissolution testing, i.e. in aqueous solutions buffered at pH 7.4 using 50 mM 4-(2-hydroxyethyl)-1-piperazineethanesulfonic acid (HEPES), maintained at a constant temperature of 25°C.

Figure 4.8 shows a comparison of the binding profiles obtained with naproxen, acetylsalicylate, and ibuprofen. All three guest molecules carry one negative charge at pH 7.4, so any difference in binding affinity does not stem from electrostatic interactions, but can be ascribed to interactions occurring between the displacers and the dendrimer scaffold. As expected on the basis of its extended π system, naproxen displays a high binding affinity, confirming the results obtained through the dissolution experiment reported above.

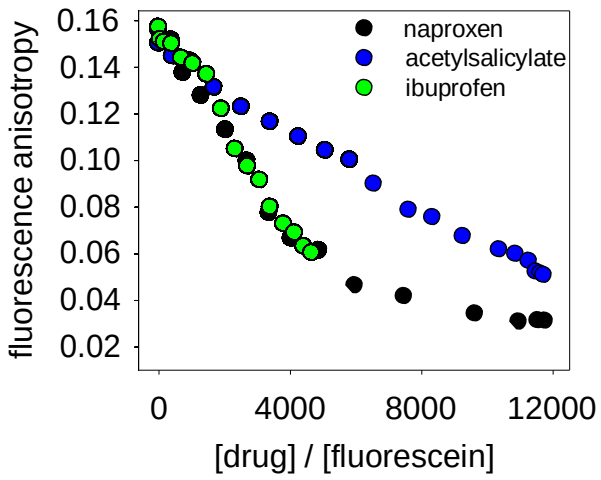

Figure 4.8. Fluorescence anisotropy binding isotherms for a series of three drug-like molecules, naproxen, acetylsalicylate, and ibuprofen, upon binding to a cationic G5 PAMAM dendrimer in neutral water. The binding profiles were obtained by displacement of fluorescein from its pre-formed complex with the G5 dendrimer. (AJk-87)

4.5 CONCLUSIONS

We conducted optical spectroscopy studies demonstrating the significant potential of cationic PAMAM dendrimers of generations G3 through G5 as solubilizing agents for highly hydrophobic molecules. The study of pyrene excimers allowed us to establish that a positive binding interaction is responsible for the solubilization. By comparing the properties of dendrimers with equivalent structure but opposite charge we then established that hydrophobic effects do not play a major role in determining this behavior: we suggested instead that the solubilisation behavior is induced by intermolecular interactions specific to the aromatic hydrocarbons and mediated by the ammonium cations on the surface of these dendrimers.

Results obtained with the costly PAMAM dendrimers were also reproduced with commodity polymers such as poly(ethyleneimine) and poly(allylamine), paving the way for much more significant large-scale applications of this class of cationic ammonium polyelectrolytes.

We proposed an improved experimental setup allowing us access to a second interaction

regime, in which the aromatic hydrocarbon is present in defect with respect to the dendrimer. This alternative method provided direct estimates of the relative loading capacities of these structures for the same hydrocarbon. Additionally, a different approach based on an indicator displacement assay was proposed for the study of more soluble substrates such as drug-like molecules, for which the dissolution experiments are too insensitive. Using this approach, we show that the dendrimers have promising properties for the encapsulation of pharmaceuticals, with promising prospects for influencing their water solubility and pharmacokinetics. In conclusion, our results suggest that these dendrimers present interesting binding properties in solution that can be exploited for a multitude of applications; we look forward to reporting on further studies on the application of these polymers in the field of separation science (e.g. microanalytical separation techniques) and drug delivery.

4.6 EXPERIMENTAL SECTION

Materials. Poly(amidoamine) (PAMAM) dendrimers with ethylenediamine core and primary amine termination were used in these studies. The dendrimers were manufactured by Dendritech, Inc. and purchased from their distributor (Sigma-Aldrich) as MeOH solutions of varying concentrations depending on the dendrimer generation. Dendrimer solutions were stored refrigerated at 4°C. All experiments on dendrimer generations G3 were carried out using the same dendrimer lot, whereas G4 and G5 experiments were conducted from two lots of dendrimer. In the latter case, we confirmed lot-to-lot consistency by successfully replicating on both lots a number of fluorophore interaction experiments that are well established in our lab. The G5 stock solutions in MeOH received from Sigma and used throughout this work contained ~5% w/w dendrimer. After dilution with buffer to obtain the desired working concentration of polymer, the final solutions used for titrations contained a negligible amount of MeOH (<0.2%).

Fluorescent probes, anthracene and pyrene, and active pharmaceuticals were purchased from Sigma-Aldrich or TCI America and used as received.

Instrumentation. Instrumental parameters used for benchtop instruments (HP 8452A diode array spectrophotometer, ISS PC1 spectrofluorimeter) are described in detail in Chapter 2. The sample holder temperature (25°C) was controlled by an external circulating water bath in both instruments.

Instrumental parameters for fluorescence experiments

Anthracene:

- Excitation wavelength: 350 nm
- Emission spectra: 370-470 nm
- Slit, excitation: 8 nm spectral resolution
- Slit, emission: 4 nm spectral resolution
- Iris: open
- Polarizers: None

Pyrene:

- Excitation wavelength: 338 nm
- Emission spectra: 360-600 nm
- Slit, excitation: 4 nm spectral resolution
- Slit, emission: 4 nm spectral resolution
- Iris: open
- Polarizers: None

Naproxen:

- Excitation wavelength: 332 nm
- Emission spectra: 340-430 nm
- Slit, excitation: 2 nm spectral resolution
- Slit, emission: 2 nm spectral resolution
- Iris: open
- Polarizers: None

Thin film studies Solubilization experiments: All experiments were carried out in a buffered aqueous solution prepared in large batches to be used in multiple titrations. The pH of the buffer

was adjusted by addition of NaOH or HCl solutions as needed. Combined glass electrodes were used to measure the pH of all solutions.

We prepared multiple stock solutions of the hydrocarbons that were used as starting points for multiple experiments. For example, an anthracene stock solution was made by adding 5.00 mg of anthracene solid to 10 mL of hexanes, giving a concentration of 2.81×10^{-3} M.

To prepare the solute/water solutions, aliquots of the solute (dye) stock solution in hexanes were transferred into an untreated polystyrene cuvette and hexanes was carefully evaporated off under a stream of nitrogen. Care was taken so that the deposition of dye only happened below the position of the impinging optical beam of the spectrophotometer and spectrofluotimeter, in order to avoid interference from the fluorescence of the solid sample. Aliquots of water buffered with 4-(2-hydroxyethyl)-1-piperazineethanesulfonic acid (HEPES, 50 mM) to pH 7.4 were added, the cuvettes sealed with parafilm, and heated to 50^{o}C in a water bath overnight to effect complete equilibration. The samples were then brought back to 25^{o}C before measurements were taken. These measurements were made in the temperature controlled (25^{o}C) cuvette holder of the instrument.

Constant volume of polyelectrolyte. The solute/polyelectrolyte/water solutions were prepared in a similar manner. Aliquots of the solute (dye) stock solution in hexanes were transferred into a polystyrene cuvette and hexanes was evaporated off under nitrogen. A constant volume of a solution of the polyelectrolyte under study in HEPES buffer was then added. These cuvettes were sealed and placed overnight in a water bath at 50^{o}C and then brought back to room temperature before measurements were taken.

Constant volume of solute (dye). The solute/polyelectrolyte/water solutions were prepared in a similar manner. A constant volume of the solute (dye) stock solution in hexanes ($1.12 \times 10^{-}$

^{4} moles anthracene and 1.07 x 10^{-6} moles pyrene) was transferred into a polystyrene cuvette and hexanes was evaporated off under nitrogen. Aliquots of a solution of the polyelectrolyte under study in HEPES buffer were then added. These cuvettes were sealed and placed overnight in a water bath at 50^{o}C and then brought back to room temperature before measurements were taken.

Drug studies solubilization experiments: We prepared multiple stock solutions of the fluorescein (**F**) dye that were used as starting points for multiple titrations. For example, a fluorescein stock solution was made by adding 2.94 mg of fluorescein solid to 50 mL of 50 mM HEPES buffer giving a concentration of 1.77 x 10^{-4} M.

All solutions used in displacement experiments were made by dilution of aliquots of stock solutions of dyes or polymers. Displacement experiments were carried out using two separate solutions, a "titrant" and a "cuvette" solution. "Titrant" and "cuvette" solutions were made fresh for each experiment.

A "**cuvette**" solution contained the [dendrimer] / [fluorophore] ratio used as our bound solution in buffer at its final working concentration; it was made by dilution of an aliquot of dye stock and of an aliquot of polymer stock into buffer. The final working concentration in these solutions of [PAMAM G5] / [**F**] was [1.3 x 10^{-5} M] / [2.0 x 10^{-6} M] throughout.

A "**titrant**" solution contained the PAMAM G5 and **F** at the same concentrations mentioned above and the displacer anion under study as well. The [**D•CF**$_n$] complex concentration in this solution was always kept rigorously the same as the one in the corresponding "cuvette" solution, so that addition of the "titrant" to the "cuvette" solution would not change the overall concentration of the dye or of the dendrimer. "Titrant" solutions were made by dilution of an aliquot of dye stock, of an aliquot of polymer stock and an aliquot of drug stock; the solution was then brought up to the final volume with buffer.

The pH of these solutions was checked with a calibrated glass electrode after their preparation and corrected to 7.4 by addition of NaOH or HCl if necessary.

The displacement experiment was carried out by addition of aliquots of the “titrant” solution to the “cuvette” solution. The resulting mixture was then left to equilibrate briefly, then a measurement was taken. Serial additions of “titrant” solutions were made to the same “cuvette” solution in a Starna Spectrosil quartz cuvette held in the temperature controlled cuvette holder of the instrument.

Data treatment. Fluorescence emission raw readings were blanked by subtracting the corresponding reading for the buffer. The resulting data was plotted as a function of the [drug] / [fluorophore] ratio to produce binding isotherms.

CHAPTER 5

TOWARDS THE DYNAMICALLY TEMPLATED SYNTHESIS OF POLYAMINE MACROCYCLES

5.1 INTRODUCTION

Macrocycles have attracted significant attention for their symmetrical architecture and high count of functional sites. They show promise in applications such as the construction of chemical sensors, nano-reactors and as building blocks for functional organic materials among others.[96,97] These large, cyclic molecules are widespread in nature and include porphyrins (e.g. heme as a part of hemoglobin, vitamin B12) and cyclic peptides (e.g. antibiotics capreomycin, vancomycin). In recent years, considerable effort has been devoted to the development of synthetic molecular networks of these cyclic molecules that can function as container-like systems.

A key feature of molecular networks is that they are formed by reversible and fragile non-covalent interactions, allowing the geometry of the cavities in these networks to be adjusted according to the shape and size of the guest molecule. A variety of non-covalent interactions are involved, such as H-bonding, metal–ligand, cation-π, and hydrophobic interactions. These reversible systems are capable of error correction: even if less stable products are formed first, such products can be broken down so that the more stable ones can then be accessed.[98]

Macrocycles such as cryptands and crown ethers were some of the first to be extensively studied for their ability to form inclusion complexes and selectively recognize and immobilize guest molecules in their cavities.[99,100] In fact, Jean-Marie Lehn, along with Donald Cram and

Charles Pedersen, received the Nobel Prize in Chemistry in 1987 for their work on the first artificial chemicals whose cavities mimic the selective behavior of biological molecules. Jean-Marie Lehn and coworkers[101] designed the octaaza macrobicycle receptor **5.1** that was found to coordinate to a fluoride anion through hydrogen bonding mediated by the six ammonium sites as shown in **5.2** (Figure 5.1). The crystal structure of this complex was also determined (shown in the same figure as **5.3**).

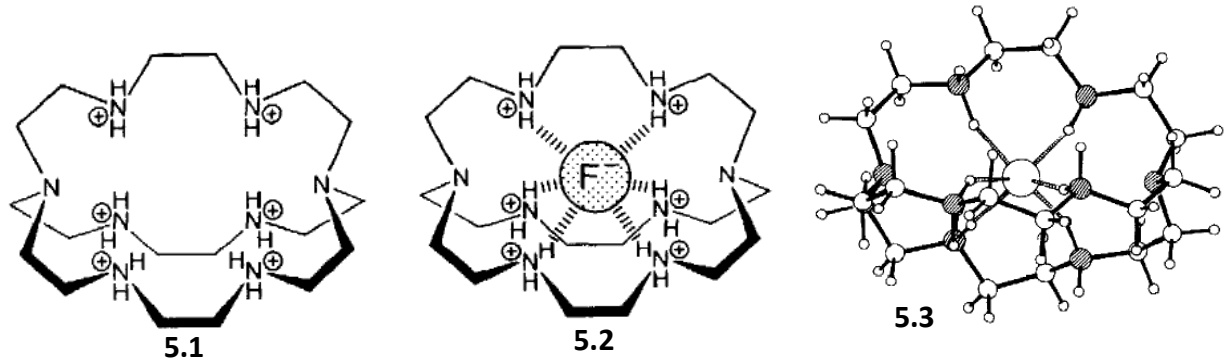

Figure 5.1. The octaaza macrobicycle **5.1** is shown to the left. It has been shown to form a complex with fluoride by forming six hydrogen bonds with the anion **5.2**. The crystal structure of the complex is shown in 5.3.[101]

Fluorescent dyes have been found particularly useful to monitor the formation of discrete host/guest complexes with macrocyclic structures. The inclusion of the dye into the macrocycles's cavity is accompanied by a change in its microenvironment, which has often been used in supramolecular chemistry to determine the binding of competitors by indicator displacement assays. Employing a fluorescent dye allows the use of spectroscopic techniques and the ability to follow the UV-vis absorption and fluorescence properties upon their complex formation of the dye to the macrocyclic hosts.

Fabbrizzi and coworkers[102] used 6-carboxy-tetramethylrhodamine (6-TAMRA) as a fluorescent indicator to develop a dicopper(II) macrocyclic cage that is a selective receptor for L-glutamate, shown in Figure 5.2. The rhodamine dye's two carboxylate groups bridge the two Cu^{II} centers of the dimetallic cage, and when bound to the cage the dye's fluorescence emission

is completely quenched. When this solution was titrated with aliquots of L-glutamic acid, the fluorescence was progressively restored (shown to the right of Figure 5.2). This system was developed into a convenient OFF-ON chemosensor capable of sensing L-glutamate, an important neurotransmitter, in neutral water solution at sub-micromolar concentrations.

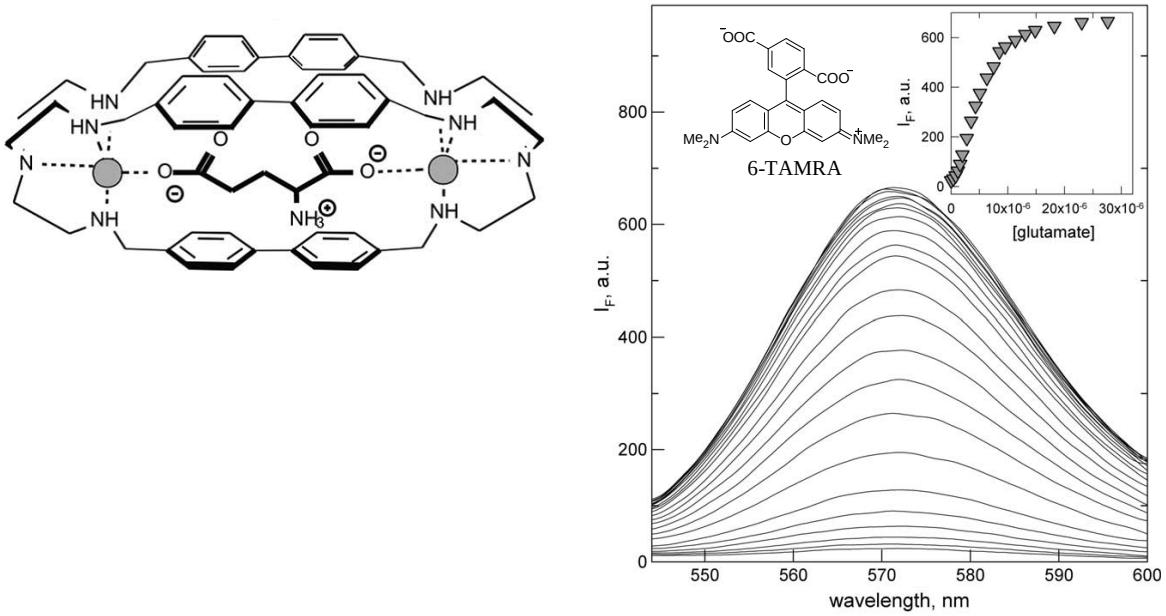

Figure 5.2. Left: Dicopper(II) macrocyclic cage complex with diphenyl spacers with the inclusion of glutamate. Right: emission spectra from titration with glutamic acid to a solution containing the cage complex and the rhodamine dye. Inset: structure of 6-carboxy-tetramethylrhodamine (6-TAMRA) (left) and titration profile (right).[102]

5.2 TEMPLATE DIRECTED SYNTHESIS OF MACROCYCLES

We propose here the design of a set of versatile building blocks for the templated dynamic synthesis of large cyclic structures. The remainder of this chapter will focus on discussing the first steps towards the implementation of this method. Figure 5.3 presents the actual and cartoon structures of one of the macrocycles we intend to prepare. The template will organize the building blocks around itself by forming coordination bonds with transition metal ions, a family of dynamic, “breakable” bonds.

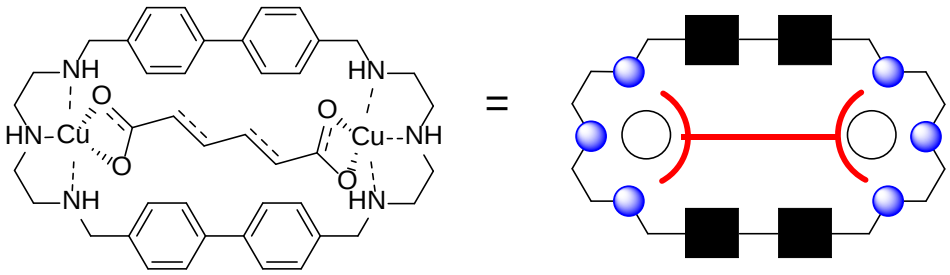

Figure 5.3. A templated macrocycle structure (left) and its cartoon representation (right).

We chose to use imines as dynamic covalent linkages. However, the ruggedness of non-reversible structures is still attractive: therefore, once a product has been prepared, it is desirable to be able to lock it in the final product. The imine linkage will prove handy in this respect, since it can be chemically transformed into a non-dynamic amine moiety in a variety of minimally invasive ways.[103-105] This would turn the reversible linkage into a permanent one and lock the desired product in a fixed, non-reversible form that is easy to handle for further use. Several shapes and functional group attachments were chosen as building blocks (Figure 5.4).

We are interested in studying the inclusion properties of each macrocycle to determine how shape and/or the addition of functional groups inside the cavities of these molecular networks influence the selection towards the anions. In fact, the properties of the spacer defines the shape and size of the cavity and, overall, the selectivity towards the anion that it will encapsulate. Many synthetic receptors for anions are expected to provide a cavity of suitable shape and size, containing positively charged groups (e.g., ammonium, guanidinium, or pyridinium groups).[106-108] However, the electrostatic interactions which are established between the receptor and the substrate are rarely strong enough to compensate for the endothermic dehydration terms, and recognition studies are often restricted to non-aqueous media. The metal-ligand interactions, chosen for this study, are usually stronger and allow the occurrence of selective interactions with anions displaying coordinating tendencies in pure water.

We are particularly interested in the inclusion of ambidentate dicarboxylate anions. Dicarboxylate anions are attractive targets for molecular recognition because several carboxylate functional groups are present in a variety of biomolecules such as amino acids and other metabolites (e.g. members of the citric acid cycle). We will study the inclusion of anions by the incorporation of a fluorescent dye whose interaction with the macrocycle will cause a change in its fluorescence signal. The desired substrates can then be added, displacing the indicator from the cavity, thus allowing us to follow changes in the system's fluorescence signal, which can be translated into binding information.

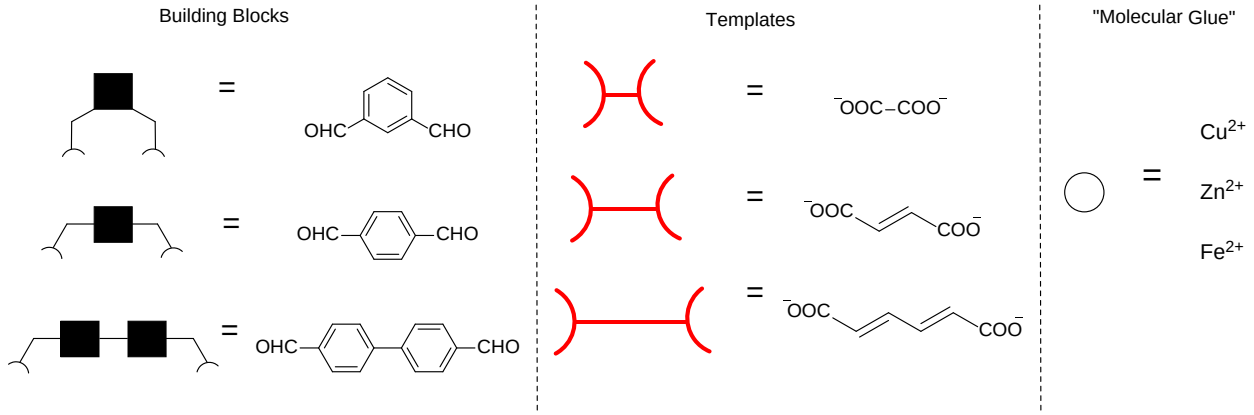

Figure 5.4. Structures and cartoon representations of building blocks proposed for the dynamic combinatorial library.

5.3 SYNTHESIS OF BUILDING BLOCKS AND MACROCYCLES

The aim to starting this project was to establish a proof of feasibility. In collaboration with another group member, we have successfully synthesized and characterized several of the building blocks and macrocycles for this project. Figure 5.5 shows the synthetic pathway we used in order to obtain each macrocycle. The first step was to synthesize the building blocks so that they could be used to put the pieces of the macrocycle together. The dialdehyde building blocks (**1**) were synthesized by using a Suzuki cross-coupling reaction. Following this procedure, a Schiff reaction was performed to obtain the tetraimine macrocycles shown as **2** and **2b**.

However, due to the use of dynamic covalent bonds the most stable and least hindered product should form, so we think that the more symmetrical tetraimine macrocycle **2** will form preferentially. The tetraimine macrocycles could then be reduced using sodium borohydride to obtain the final amine macrocycles (**3**).

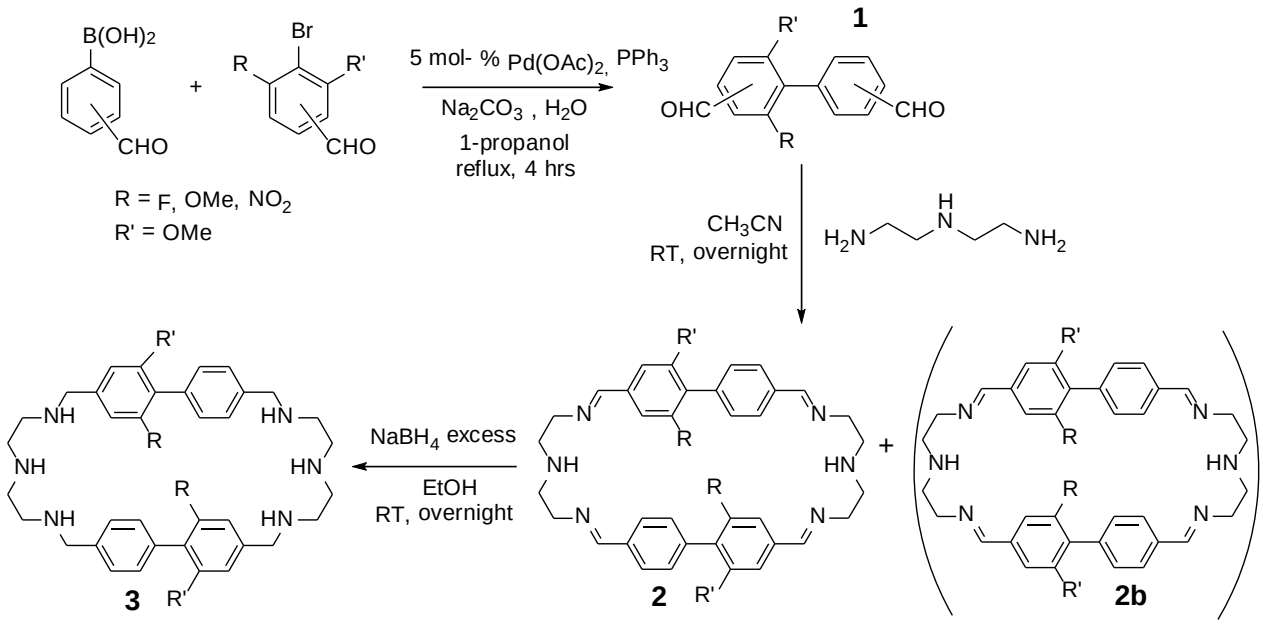

Figure 5.5. Mechanism for the synthesis of amine macrocycles.

Figure 5.6 and Figure 5.7 display the dialdehyde molecules and the macrocycles that have been synthesized thus far with their respective yields. These macrocycles were synthesized so that their cavities are suitable for the inclusion of anions. The size and shape of the cavities of each macrocycle in Figure 5.7 will determine the selectivity toward the anion it will be able to encapsulate.

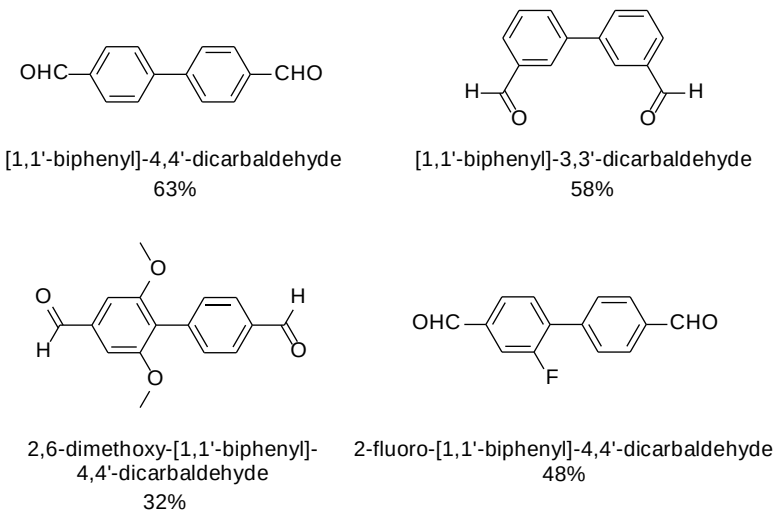

Figure 5.6. Building blocks synthesized by a Suzuki cross coupling reaction and their respective yields.

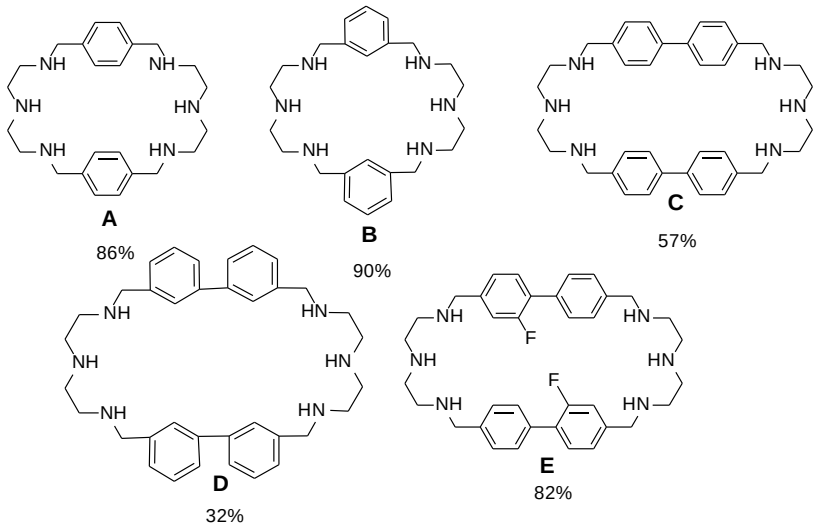

Figure 5.7. Synthesized macrocycles **A-E** and their respective yields.

5.4 Cu(II) TITRATIONS

Before an exhaustive collection of the macrocycles was synthesized, it was important to be certain that these structures would bind copper(II), and to determine the stoichiometry of that process. We expected the stoichiometry to be 1:2, where one copper forms a square-planar complex with the three amine groups present on each end of the macrocycle (shown in Figure

5.8). We conducted titrations of Cu(II) triflate with macrocycle **C** in aqueous HEPES buffer at pH 7.4.

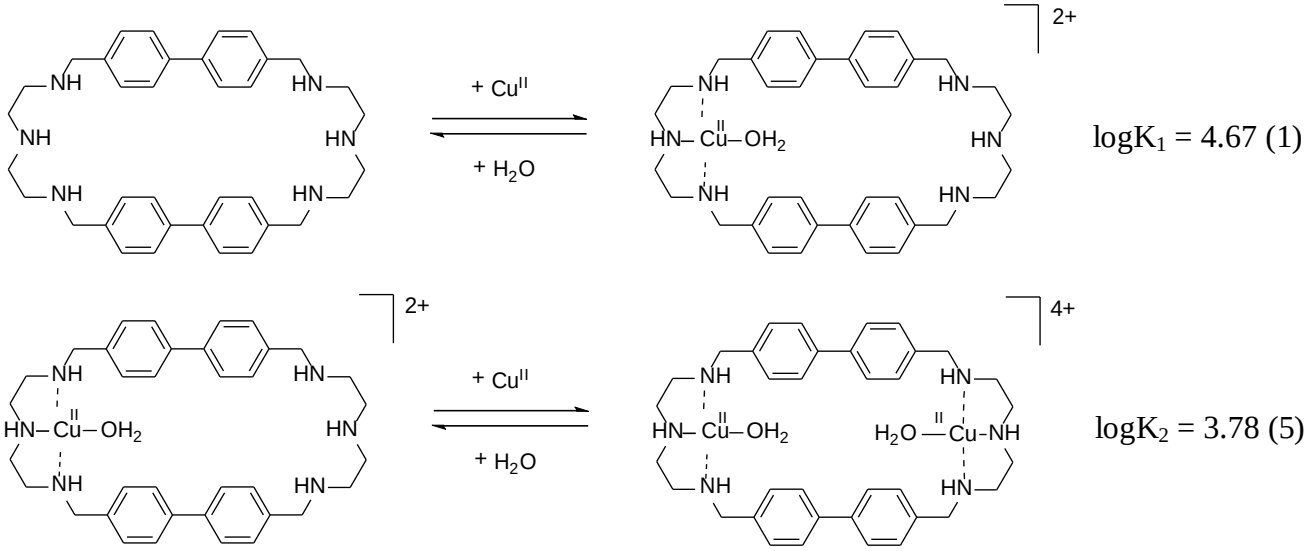

Figure 5.8. The placement of two copper(II) ions inside of the cage. Each amine compartment is expected to coordinate a metal center.

We performed the titration in two ways. First, we kept the concentration of copper(II) triflate constant. However, the absorbance of the macrocycle titrant, which was being added in aliquots, interfered with the determination of the binding profile (shown in circles on the left of Figure 5.9): the linear increase in absorbance shown after 0.5 equivalence of macrocycle was added can be attributed to the intrinsic absorbance of the free macrocycle. In order to remove the linear component in our titration profile, we accounted for the increasing concentration of the macrocycle in the titration vessel and subtracted this contribution from the experimental profile. The results are shown to the left of Figure 5.9 (squares).

We thought that by performing the titration the opposite way, keeping the concentration of the macrocycle constant and adding increasing amounts of copper(II), we could bypass the issue of the changing absorbance of the macrocycle ligand. Regardless of which way the experiment was performed, we measured comparable binding parameters (right, Figure 5.9). In

fact, both methods indicate that the stoichiometry of interaction is the anticipated 2:1 (Cu:Ligand). Furthermore, binding constants were determined from both titration methods (Figure 5.10) and their values were in agreement within the experimental error.

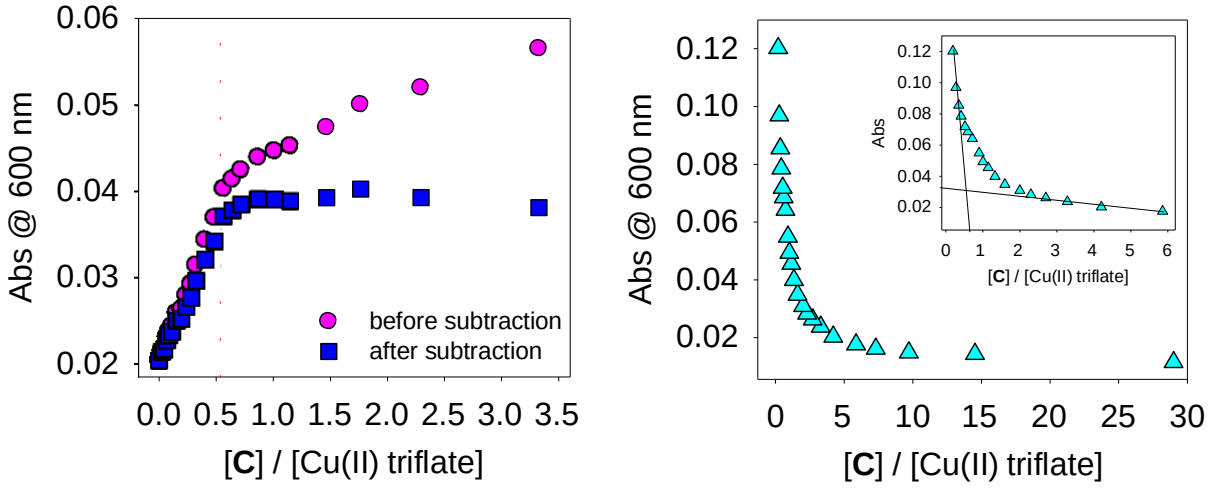

Figure 5.9. Left: titration profiles of a constant concentration of Cu(II) triflate (4.0×10^{-4} M) with increasing aliquots of **C** before and after subtraction from the contribution of the macrocyle. Right: titration profile of a constant concentration of **C** (4.0×10^{-4} M) with increasing aliquots of Cu(II) triflate, Inset: enhanced portion of same graph. (AJj-100)

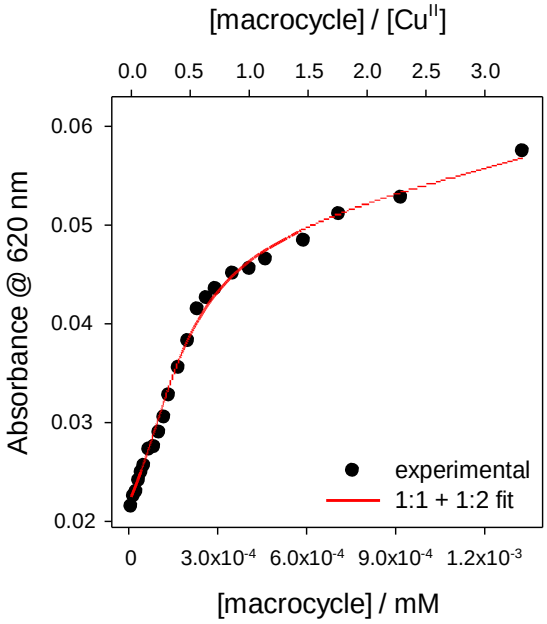

Figure 5.10. A 2:1 (Cu:Ligand) binding constant determined from the titration profiles of a constant concentration of Cu(II) triflate (4.0×10^{-4} M) with increasing aliquots of **C.**

5.5 CONCLUSIONS

In conclusion, the work presented thus far has demonstrated that we can prepare a variety of macrocycles that can be used for studying carboxylate recognition in aqueous solvents. The binding constants determined from the titrations of copper(II) triflate with macrocycle **C** show that two copper molecules bind to the macrocycles and will provide a strong metal-ligand interaction between the anion and the cage.

In the future, other group members will be able to pick up where we left off. We were able to provide a proof of principle for the binding of Cu(II) to these macrocycles. Other macrocycles will have to be studied similarly. Once those interactions have been clarified, an indicator displacement assay will be set up, determining the binding of fluorescent dyes carrying carboxylate groups to the $Cu_2(L)^{4+}$ receptor. The developed receptor-dye complexes will them be used in displacement experiments for the detection of carboxylates in water solution. We are particularly interested in the sub-micromolar determination of dicarboxylates of biological relevance in neutral aqueous solution. The first targets will be the dicarboxylates that participate in the citric acid cycle depicted in Figure 5.11.

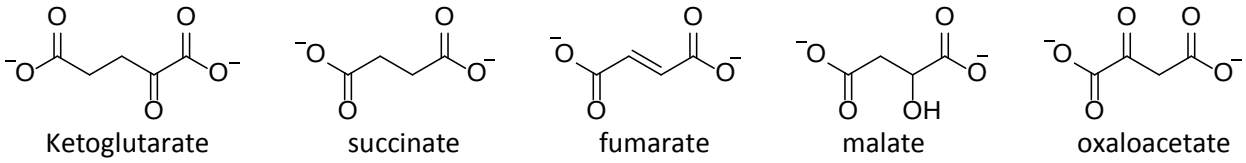

Figure 5.11. Structures and names of the dicarboxylate molecules that participate in the citric acid cycle.

5.6 EXPERIMENTAL SECTION

Materials. All reagents were used as received.

General method for the Suzuki cross-coupling reactions.

An oven-dried 3-neck round bottom flask was cooled under nitrogen flow. Bromobenzaldehyde (1 equivalent) and phenylboronic acid (1.3 equivalent) were dissolved in 1-propanol to give a 0.3 M solution. Then 5 mg $Pd(OAc)_2$ and 10 mg PPh_3 were added. The solution was stirred with gentle heat until all solids dissolved. Under a N_2 purge, 50 equivalents of Na_2CO_3 were added as a 1.25 M solution in DI H_2O with a syringe. The solution was then heated to reflux under N_2 for 4 hours. Heat was then removed and DI water was added to the solution. The reaction was opened to the atmosphere and left stirring for 2.5 hours. After stirring, ethyl acetate was added to the mixture and the water layer was washed twice with ethyl acetate. All organic layers were collected. The combined organic layers were washed twice with 2% $NaHCO_3$ and saturated brine, and dried over anhydrous magnesium sulfate and a spoonful of activated charcoal. The suspension was suction-filtered through a 1-cm Celite bed to obtain a clear liquid and then evaporated to obtain a precipitate.

[1,1'-Biphenyl]-4,4'-dicarboxaldehyde. First, 5.8 g (31 mmol) of 4-bromobenzaldehyde and 5 g (33 mmol) of 4-formylphenylboronic acid were dissolved into 70 mL of 1-propanol. Then 5 mg $Pd(OAc)_2$ and 10 mg PPh_3 was added. After heat was removed 51 mL of DI water were added to the solution. A white precipitate was obtained. Yield 4.09 g (63%). ^{1}H NMR ($CDCl_3$, 360 MHz), δ(ppm): 7.78 (d, 2H), 7.97 (d, 2H), 10.07 (s, 1H,CHO). ^{13}C NMR ($CDCl_3$, 500 MHz), δ(ppm): 128.51, 130.83, 136.51, 146.04, 192.12. MS (ESI) *m/z* 211.0 $(MH)^+$. (AJi-23)

[1,1'-Biphenyl]-3,3'-dicarbaldehyde. First, 293 µl (2.5 mmol) of 3-bromobenzaldehyde and 0.49 g (3.25 mmol) of 3-formylphenylboronic acid were dissolved into 8 mL of 1-propanol. After heat was removed 20 mL of DI water were added to the solution. A light yellow precipitate

was obtained. Yield 0.31 g (58%). ^{1}H NMR (DMSO, 360 MHz), δ(ppm): 7.75 (t, J = 7.7 Hz, 1H), 7.96 (dt, J = 7.6, 1.4 Hz, 1H), 8.12 (ddd, J = 7.8, 2.0, 1.1 Hz, 1H), 8.30 (t, J = 1.7 Hz, 1H), 10.13 (s, 1H,CHO). ^{13}C NMR (DMSO, 500 MHz), δ(ppm): 128.61, 129.09, 130.50, 133.22, 137.45, 140.19, 193.60. MS (ESI) *m/z* 211.0 $(MH)^{+}$. (AJj-48)

2-Fluoro-[1,1'-biphenyl]-4,4'-dicarbaldehyde. First, 0.41 g (2.0 mmol) of 4-bromo-3-fluorobenzaldehyde and 0.39 g (2.6 mmol) of 4-formylphenylboronic acid were dissolved into 7 mL of 1-propanol. After heat was removed 8 mL of DI water were added to the solution. A white precipitate was obtained. Yield 0.22 g (48%). ^{1}H NMR ($CDCl_3$, 500 MHz), δ(ppm): 7.64 (t, J = 7.5 Hz, 1H), 7.70 (dd, J = 10.2, 1.5 Hz, 1H), 7.75 (dd, J = 8.3, 1.7 Hz, 2H), 7.77 (dd, J = 7.9, 1.5 Hz, 1H), 7.97 (d, 2H), 10.02 (d, J = 1.7 Hz, 1H), 10.07 (s, 1H,CHO). ^{13}C NMR ($CDCl_3$, 500 MHz), δ(ppm): 116.80, 126.30, 129.99, 130.13, 131.70, 133.95, 136.40, 138.16, 140.65, 159.26 and 161.27 (F coupling, J = 255 Hz), 190.51, 191.83. MS (ESI) *m/z* 227.1 $(MH)^{-}$. (AJi-94)

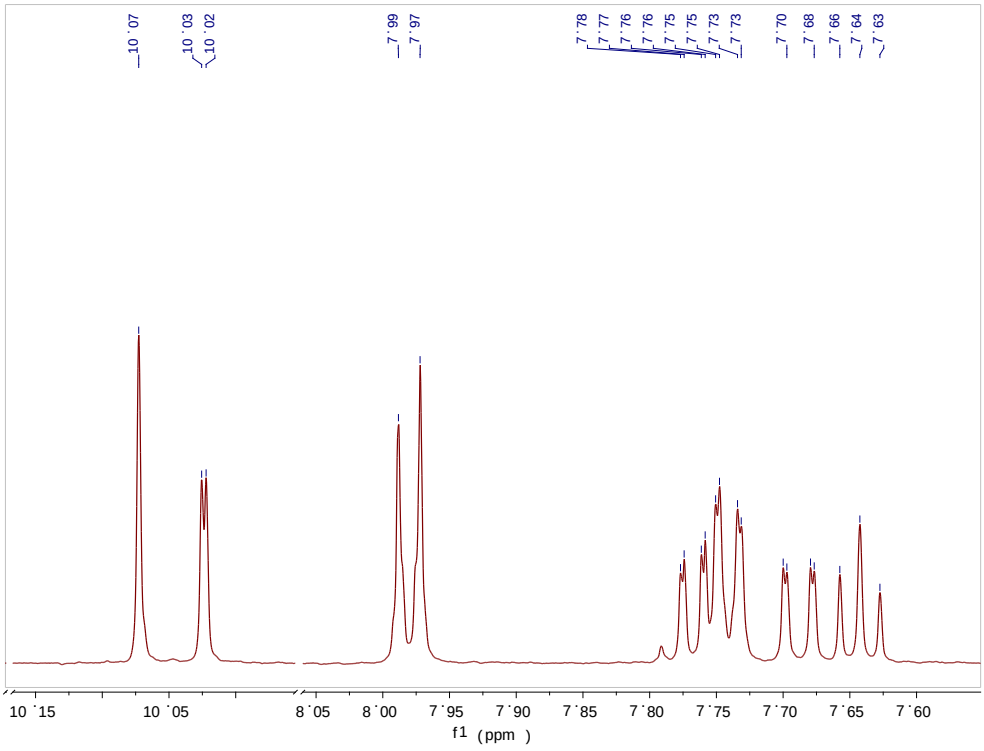

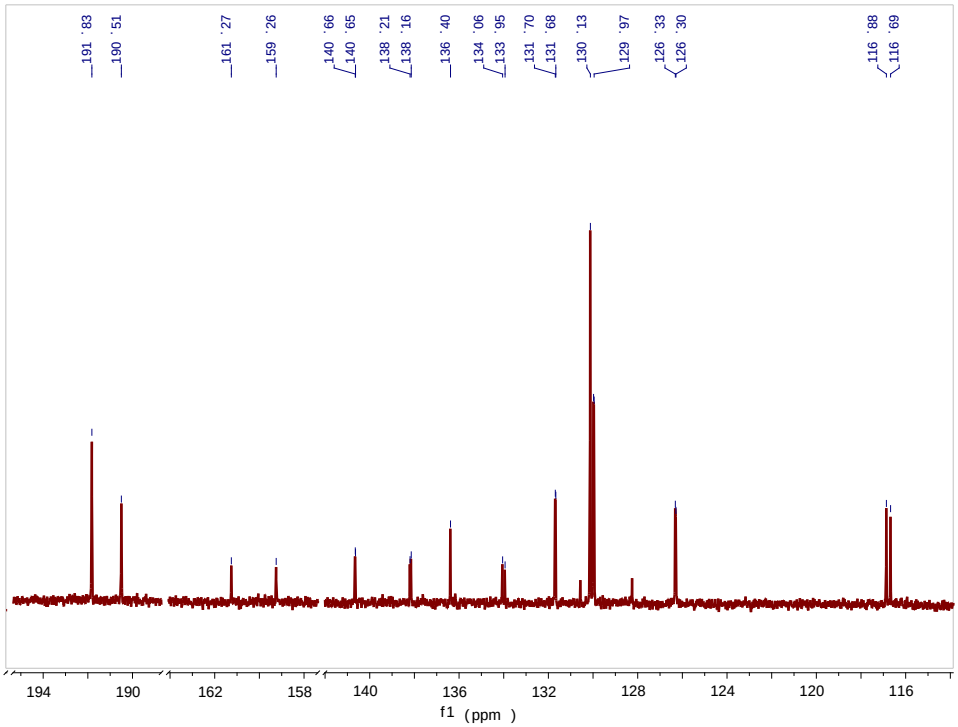

Figure 5.12. ^{1}H and ^{13}C NMR for 2-Fluoro-[1,1'-biphenyl]-4,4'-dicarbaldehyde.

2,6-Dimethoxy-[1,1'-biphenyl]-4,4'-dicarbaldehyde. First, 0.37 g (1.5 mmol) of 4-bromo-3,5-dimethoxybenzaldehyde and 0.29 g (2.0 mmol) of 4-formylphenylboronic acid were dissolved into 5 mL of 1-propanol. After heat was removed 7 mL of DI water was added to the solution. A white precipitate was obtained. Yield 0.13 g (32%). ^{1}H NMR (DMSO, 360 MHz), δ(ppm): 3.78 (s, 6H), 7.34 (s, 2H), 7.49 (d, 2H), 7.93 (d, 2H), 10.026 (s, 1H, CHO), 10.033 (s, 1H, CHO) . ^{13}C NMR (DMSO, 500 MHz), δ(ppm): 58.46, 107.75, 125.69, 131.21, 133.61, 137.41, 139.78, 159.87, 194.89, 195.13. MS (ESI) *m/z* 271.0 $(MH)^{+}$. (AJi-140)

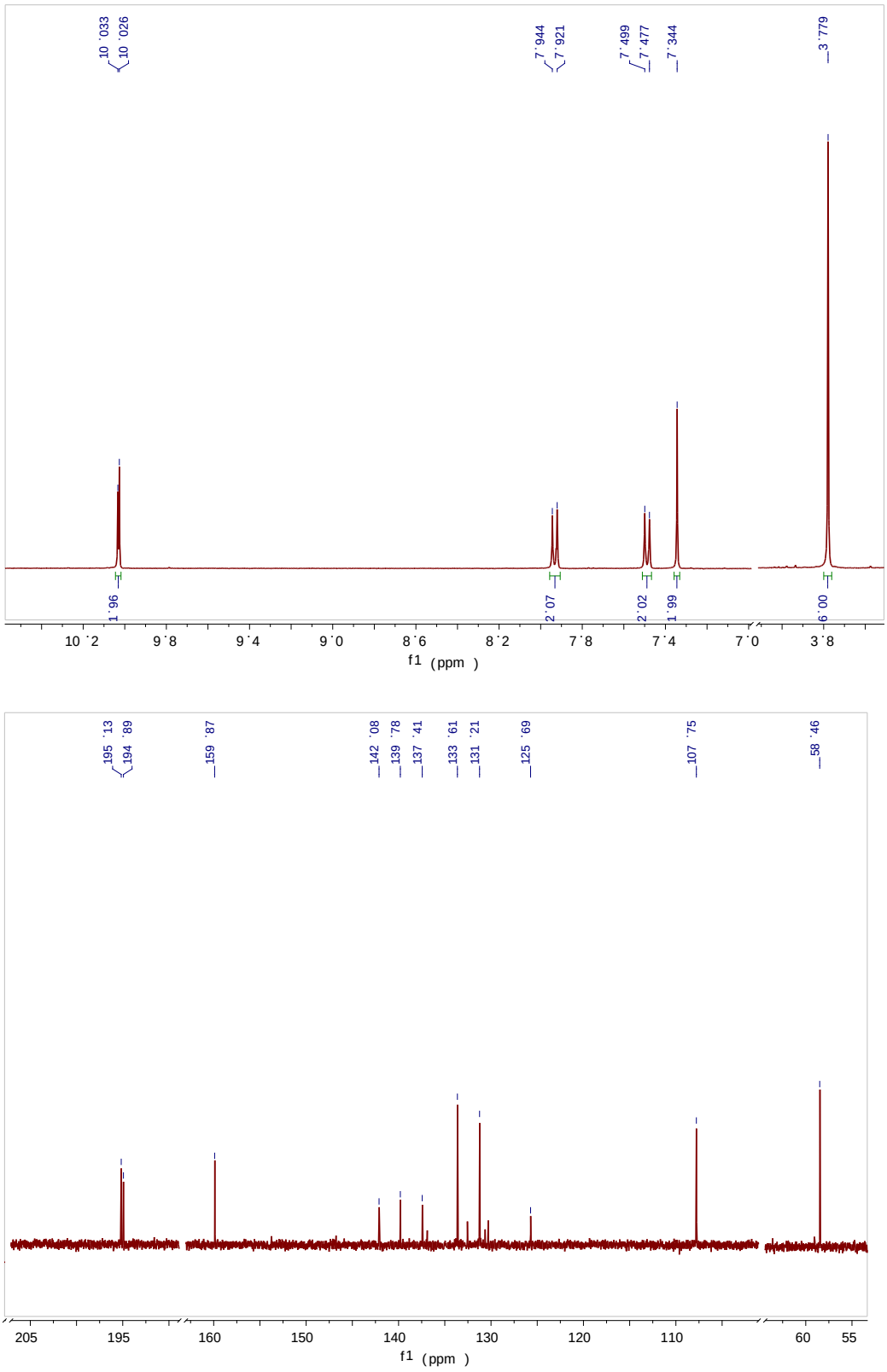

Figure 5.13. ^{1}H and ^{13}C NMR for 2,6-Dimethoxy-[1,1'-biphenyl]-4,4'-dicarbaldehyde.

General method for the formation of the Schiff bases.

In a single-necked, round-bottom flask equipped with a magnetic stirring bar, the specific dialdehyde was dissolved in CH_3CN. To this, a 1:1 equivalent solution of diethylenetriamine in CH_3CN was added dropwise over 1 hr with a syringe. The mixture was left stirring. Overnight a precipitate formed which was separated by filtration, washed with acetonitrile on the filter, and dried in a vacuum. No purification was necessary. The product was used as obtained for reduction with $NaBH_4$.

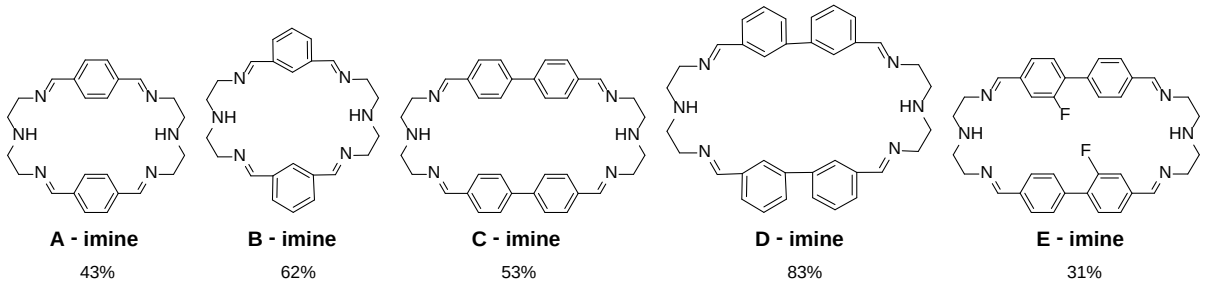

Figure 5.14. Structure of Schiff base products.

3,6,9,16,19,22-Hexaazatricyclo[22.2.2.2^{11,14}]triaconta-2,9,11,13,15,22,24,26,27,29-decaene (A - imine). A solution of terephthaldehyde was made by dissolving 2.0 g (15.0 mmol) in 200 mL of CH_3CN. A solution of 1620 µl (15.0 mmol) diethylenetriamine in 200 mL of CH_3CN was slowly added to the above solution. A light yellow precipitate was obtained. Yield 2.6 g (43%). (AJk-23)

3,6,9,17,20,23-Hexaazatricyclo[23.3.1.1^{11,15}]triaconta-1(29),2,9,11,13,15(30),16,23,25,27-decaene (B - imine). A solution of isophthalaldehyde was made by dissolving 2.0 g (15.0 mmol) in 200 mL of CH_3CN. A solution of 1620 µl (15.0 mmol) diethylenetriamine in 200 mL of CH_3CN was slowly added to the above solution. A light yellow precipitate was obtained. Yield 3.7 g (62%). (AJk-27)

(C - imine). A solution of [1,1'-Biphenyl]-4,4'-dicarboxaldehyde was made by dissolving 1.5 g

(7.2 mmol) in 100 mL of CH_3CN. A solution of 773 µl (7.2 mmol) diethylenetriamine in 100 mL of CH_3CN was slowly added to the above solution. A light yellow precipitate was obtained. Yield 2.1 g (53%). (AJj-102)

(D - imine). A solution of [1,1'-biphenyl]-3,3'-dicarbaldehyde was made by dissolving 0.1 g (0.5 mmol) in 10 mL of CH_3CN. A solution of 54 µl (0.5 mmol) diethylenetriamine in 10 mL of CH_3CN was slowly added to the above solution. A light yellow precipitate was obtained. Yield 2.8 g (83%). (AJj-59)

(E - imine). A solution of 2-fluoro-[1,1'-biphenyl]-4,4'-dicarbaldehyde was made by dissolving 0.05 g (0.2 mmol) in 5 mL of CH_3CN. A solution of 24 µl (0.2 mmol) diethylenetriamine in 5 mL of CH_3CN was slowly added to the above solution. A yellow precipitate was obtained. Yield 0.04 g (31%). (AJi-122)

General method for the reduction of Schiff base product with $NaBH_4$.

To a vigorously stirred suspension of the Schiff base product in EtOH, 16 equivalents of solid $NaBH_4$ were slowly added. After the addition was completed, the mixture was left stirring for two or more hours, until it clarified. The solution was evaporated under vacuum to dryness, yielding a copious white precipitate: to the flask containing this solid CH_2Cl_2 was added to give a suspension, which clarified readily on addition of DI water. The mixture was transferred to an extraction funnel, thoroughly mixed and the organic layer recovered. The water layer was then washed with CH_2Cl_2. The organic portions were collected in an Erlenmeyer flask and dried over Na_2SO_4, then evaporated to dryness. The solid was dissolved in MeOH and a solution of a 1:1 ratio of HCl and MeOH was added slowly producing a white solid. The solid was filtered and washed with MeOH, yielding the product.

A. 2.0 g (5 mmol) of the corresponding Schiff base product and 3.0 g (80 mmol) of $NaBH_4$ was added to 50 mL EtOH. Yield 1.77 g (86%). ^1H NMR (D_2O, 360 MHz), δ(ppm): 3.34 (t, 4H),

3.44 (t, 4H), 4.39 (s, 4H), 7.59 (s, 4H). ^{13}C NMR (D_2O, 500 MHz), δ(ppm): 41.9, 43.7, 50.8, 131.2, 131.3. MS (ESI) *m/z* 411.3 $(MH)^+$. (AJk-24)

B. 2.0 g (5 mmol) of the corresponding Schiff base product and 3.0 g (80 mmol) of $NaBH_4$ was added to 50 mL EtOH. Yield 1.92 g (94%). ^{1}H NMR (D_2O, 500 MHz), δ(ppm): 3.48 (t, 4H), 3.55 (t, 4H), 4.41 (s, 4H), 7.62 (s, 3H), 7.67 (s, 1H). ^{13}C NMR (D_2O, 500 MHz), δ(ppm): 42.38, 43.98, 51.06, 130.64, 130.76, 131.79, 131.83. MS (ESI) *m/z* 411.3 $(MH)^+$. (AJi-115 & Ajk-28)

C. 1.5 g (2.7 mmol) of the corresponding Schiff base product and 1.6 g (43.2 mmol) of $NaBH_4$ was added to 50 mL EtOH. Yield 1.50 g (99%). ^{1}H NMR (D_2O, 500 MHz), δ(ppm): 3.38 (t, 2H), 3.43 (t, 2H), 4.32 (s, 2H), 4.37 (s, 2H), 7.58 (d, 2H), 7.79 (d, 2H). ^{13}C NMR (D_2O, 360 MHz), δ(ppm): 41.98, 43.37, 50.80, 127.81, 129.34, 130.86, 140.93. MS (ESI) *m/z* 563.4 $(MH)^+$. (AJj-103)

D. 0.080 g (0.14 mmol) of the corresponding Schiff base product and 0.083 g (2.2 mmol) of $NaBH_4$ was added to 25 mL EtOH. Yield 0.025 g (32%). ^{1}H NMR (D_2O, 500 MHz), δ(ppm): 3.50 (t, 4H), 4.39 (s, 2H), 7.51 (d, 1H), 7.58 (t, 1H), 7.78 (s, 2H). ^{13}C NMR (D_2O, 500 MHz), δ(ppm): 41.92, 43.71, 50.75, 127.52, 128.25, 131.20, 131.32, 132.20 139.54. MS (ESI) *m/z* 563.4 $(MH)^+$. (AJj-61)

E. 0.035 g (0.6 mmol) of the corresponding Schiff base product and 0.036 g (1.0 mmol) of $NaBH_4$ was added to 5 mL EtOH. Yield 0.019 g (53%). MS (ESI) *m/z* 599.4 $(MH)^+$. (AJi-123)

CHAPTER 6

SUMMARY AND PERSPECTIVE

6.1 SUMMARY

I successfully defined and used binding and displacement assays based on optical spectroscopy to study the relative binding affinities of small organic molecules to cationic polyelectrolytes of differing architectures. The following variables have been kept strictly constant in my work: solvent composition, pH, ionic strength, and the counterion to the dendrimer. On the basis of these results, we were able to highlight the relative importance of the contribution from various intermolecular interaction modes to the binding. The structural features of the guest that influence the binding process most significantly were shown to be electrostatics, the presence of hydrogen bond donor groups, and the presence of an aromatic core.

The latter result was unexpected and novel, and sparked our interest in using these polyelectrolytes as solubilizing agents for hydrophobic molecules possessing aromatic cores. Extensive dissolution studies were conducted using aromatic hydrocarbon probes to demonstrate that select cationic polyelectrolytes and dendrimers are able to increase the solubility of these molecules in neutral water. We hope that these insights may encourage more widespread use of such powerful soft materials in the many fields of chemistry in which non-covalent encapsulation of small organic molecules is of interest.

6.2 FUTURE WORK

Further studies currently underway in our lab will attempt to obtain quantitative measurements of the loading capacity for these hosts, which is another parameter of key importance to their application. Isothermal calorimetry (ITC) will be used to help us obtain a complete picture for the thermodynamics of polyelectrolyte complexations, and to probe the effect of the solvent and counterion on these interactions. A more complete understanding of similar interactions in other linear and hyperbranched cationic polyelectrolytes of more strictly comparable mass is also required, and work in this direction is underway in our group.

REFERENCES

1. Crooks, R. M.; Ricco, A. J. New Organic Materials Suitable for Use in Chemical Sensor Arrays. *Acc. Chem. Res.* **1998**, *31*, 219-227.

2. Willerich, I.; Li, Y.; Gröhn, F. Influencing Particle Size and Stability of Ionic Dendrimer-Dye Assemblies. *J. Phys. Chem. B* **2010**, *114*, 15466-15476.

3. Svenson, S.; Tomalia, D. A. Dendrimers in Biomedical Applications - Reflections on the Field. *Adv. Drug Deliver. Rev.* **2005**, *57*, 2106-2129.

4. Boas, U.; Heegaard, P. M. H. Dendrimers in Drug Research. *Chem. Soc. Rev.* **2004**, *33*, 43-63.

5. Tomalia, D. A.; Fréchet, J. M. J. Discovery of Dendrimers and Dendritic Polymers: A Brief Historical Perspective. *J. Polym. Sci. Part A: Polym. Chem.* **2002**, *40*, 2719-2728.

6. Wolf, K. L.; Frahm, H.; Harms, H. The State of Arrangement of Molecules in Liquids. *Z. physik. Chem.* **1937**, *B36*, 237-87.

7. Lehn, J. Chemistry - From the Lock and Key to Molecular Recognition and Instructed Chemistry. *Pharm. Acta Helv.* **1995**, *69*, 205-211.

8. Anslyn, Eric V., Dougherty, Dennis A., *Modern Physical Organic Chemistry;* University Science: Sausalito, CA, 2006.

9. Lehn, J. M. Perspectives in Supramolecular Chemistry: From Molecular Recognition Towards Self-Organization. *Pure & Appl. Chem.* **1994**, *66*, 1961-1966.

10. Behr, J.; Editor. *The Lock and Key Principle: The State of the Art 100 Years On. In: Perspect. Supramol. Chem., 1994; 1];* Wiley: 1994; pp 325 pp.

11. Chang, S. K.; Engen, D. V.; Fan, E.; Hamilton, A. D. Hydrogen Bonding and Molecular Recognition: Synthetic, Complexation, and Structural Studies on Barbiturate Binding to an Artificial Receptor. *J. Am. Chem. Soc.* **1991**, *113*, 7640-7645.

12. Ma, J. C.; Dougherty, D. A. The Cation-π Interaction. *Chem. Rev.* **1997**, *97*, 1303-1324.

13. Meot-Ner, M.; Deakyne, C. A. Unconventional Ionic Hydrogen Bonds. 1. CH-X Complexes of Quaternary Ions With n- and pi-donors. *J. Am. Chem. Soc.* **1985**, *107*, 469-474.

14. Diederich, F.; Griebel, D. Proton NMR Investigations of Host-Guest Complexation Between a Macrocyclic Host of the Cyclophane Type and Aromatic Guests in Aqueous Solution. *J. Am. Chem. Soc.* **1984**, *106*, 8037-46.

15. Shepodd, T. J.; Petti, M. A.; Dougherty, D. A. Molecular Recognition in Aqueous Media: Donor-Acceptor and Ion-Dipole Interactions Produce Tight Binding for Highly Soluble Guests. *J. Am. Chem. Soc.* **1988**, *6*, 1983-1985.

16. Dougherty, D. A. The Cation-π Interaction. *Acc. Chem. Res.* **2013**, *46*, 885-893.

17. Stauffer, D. A.; Barrans, R. E. J.; Dougherty, D. A. Concerning the Thermodynamics of Molecular Recognition in Aqueous and Organic Media. Evidence for Significant Heat Capacity Effects. *J. Org. Chem.* **1990**, *55*, 2762-2767.

18. Steed, J. W.; Turner, D. R.; Wallace, K. *Core Concepts in Supramolecular Chemistry and Nanochemistry;* John Wiley & Sons, Inc.: 2007.

19. Anslyn, E. V. Supramolecular Analytical Chemistry. *J. Org. Chem.* **2007**, *72*, 687-699.

20. Lakowicz, J. R. *Principles of Fluorescence Spectroscopy;* Springer: New York, NY, 2006.

21. Parsons, M.; Vojnovic, B.; Ameer-Beg, S. Imaging Protein–Protein Interactions in Cell Motility Using Fluorescence Resonance Energy Transfer (FRET). *Biochem. Soc. Trans.* **2004**, *32*, 431-433.

22. Willard, D. M.; Carillo, L. L.; Jung, J.; Van Orden, A. CdSe-ZnS Quantum Dots as Resonance Energy Transfer Donors in a Model Protein-Protein Binding Assay. *Nano Lett.* **2001**, *1*, 469-474.

23. de Silva, A. P.; Fox, D. B.; Huxley, A. J. M.; Moody, T. S. Combining Luminescence, Coordination and Eelectron Transfer for Signaling Purposes. *Coord. Chem. Rev.* **2000**, *205*, 41-57.

24. Bolto, B.; Gregory, J. Organic Polyelectrolytes in Water Treatment. *Water Res.* **2007**, *41*, 2301-2324.

25. Dam, H. H.; Caruso, F. Formation and Degradation of Layer-by-Layer-Assembled Polyelectrolyte Polyrotaxane Capsules. *Langmuir* **2013**, *29*, 7203-7208.

26. Zhou, Z.; Shen, Y.; Tang, J.; Jin, E.; Ma, X.; Sun, Q.; Zhang, B.; Van Kirk, E. A.; Murdoch, W. J. Linear polyethyleneimine-based charge-reversal nanoparticles for nuclear-targeted drug delivery. *J. Mater. Chem.* **2011**, *21*, 19114-19123.

27. Farinato, R. S. Applications of Polyelectrolytes in Aqueous Media. *ACS Symp. Ser.* **2006**, *937*, 153-168.

28. Fuoss, R. M.; Katchalsky, A.; Lifson, S. The Potential of an Infinite Rod-Like Molecule and the Distribution of the Counter Ions. *Proc. Natl. Acad. Sci. U. S. A.* **1951**, *37*, 579-589.

29. Manning, G. S. Limiting Laws and Counterion Condensation in Polyelectrolyte Solutions I. Colligative Properties. *J. Chem. Phys.* **1969**, *51*, 924-933.

30. Buhleier, E.; Wehner, W.; Vögtle, F. "Cascade"- and "Nonskid-Chain-like" Syntheses of Molecular Cavity Topologies. *Synthesis* **1978**, *2*, 155-158.

31. Hawker, C. J.; Wooley, K. L.; Fréchet, J. M. J. Unimolecular Micelles and Globular Amphiphiles: Dendritic Macromolecules as Novel Recyclable Solubilization Agents. *J. Chem. Soc. , Perkin Trans. 1* **1993**, *12*, 1287-1297.

32. Šebestík, J.; Reiniš, M.; Ježek, J. In *Synthesis of Dendrimers: Convergent and Divergent Approaches;* Springer Vienna: 2012; pp 55-81.

33. Tomalia, D. A.; Baker, H.; Dewald, J.; Hall, M.; Kallos, G.; Martin, S.; Roeck, J.; Ryder, J.; Smith, P. A New Class of Polymers: Starburst-Dendritic Macromolecules. *Polym. J.* **1985**, *17*, 117-132.

34. Bonizzoni, M.; Long, S. R.; Rainwater, C.; Anslyn, E. V. PAMAM Dendrimer-Induced Aggregation of 5(6)-Carboxyfluorescein. *J. Org. Chem.* **2012**, *77*, 1258-1266.

35. Klajnert, B.; Pastucha, A.; Shcharbin, D.; Bryszewska, M. Binding Properties of Polyamidoamine Dendrimers. *J. Appl. Polym. Sci.* **2007**, *103*, 2036-2040.

36. Richter-Egger, D. L.; Li, H.; Tucker, S. A. Spectroscopic investigations of polyamido amine starburst dendrimers with Reichard's ET-30 dye. *Appl Spectrosc* **2000**, *54*, 1151-1156.

37. Tang, M. X.; Redemann, C. T.; Szoka, F. C. In Vitro Gene Delivery by Degraded Polyamidoamine Dendrimers. *Bioconjugate Chem.* **1996**, *7*, 703-714.

38. Cakara, D.; Kleimann, J.; Borkovec, M. Microscopic Protonation Equilibria of Poly(amidoamine) Dendrimers from Macroscopic Titrations. *Macromolecules* **2003**, *36*, 4201-4207.

39. James, T. D.; Shinmori, H.; Takeuchi, M.; Shinkai, S. A Saccharide 'sponge'. Synthesis and Properties of a Dendritic Boronic Acid. *Chem. Commun.* **1996**, 705-706.

40. Willerich, I.; Gröhn, F. Thermodynamics of Photoresponsive Polyelectrolyte-Dye Assemblies with Irradiation Wavelength Triggered Particle Size. *Macromolecules* **2011**, *44*, 4452-4461.

41. Willerich, I.; Schindler, T.; Gröhn, F. Effect of Polyelectrolyte Architecture and Size on Macroion-Dye Assemblies. *J. Phys. Chem. B* **2011**, *115*, 9710-9.

42. Wu, C.; Gao, J. A Simple Scaling for the Core-Shell Nanostructure Formed by Self-Assembly of Block Copolymers in a Selective Solvent. *Macromolecules* **2000**, *33*, 645-646.

43. Hawe, A.; Sutter, M.; Jiskoot, W. Extrinsic Fluorescent Dyes as Tools for Protein Characterization. *Pharm. Res.* **2008**, *25*, 1487-1499.

44. Nagatani, H.; Sakamoto, T.; Torikai, T.; Sagara, T. Encapsulation of Anilinonaphthalenesulfonates in Carboxylate-Terminated PAMAM Dendrimer at the Polarized Water|1,2-Dichloroethane Interface. *Langmuir* **2010**, *26*, 17686-17694.

45. Caminati, G.; Turro, N. J.; Tomalia, D. A. Photophysical Investigation of Starburst Dendrimers and Their Interactions With Anionic and Cationic Surfactants. *J. Am. Chem. Soc.* **1990**, *112*, 8515-8522.

46. Duncan, R. The Dawning Era of Polymer Therapeutics. *Nat. Rev. Drug Discov.* **2003**, *2*, 347-360.

47. Willerich, I.; Groehn, F. Molecular Structure Encodes Nanoscale Assemblies: Understanding Driving Forces in Electrostatic Self-Assembly. *J. Am. Chem. Soc.* **2011**, *133*, 20341-20356.

48. Stojanovic, N.; Murphy, L. D.; Wagner, B. D. Fluorescence-Based Comparative Binding Studies of the Supramolecular Host Properties of PAMAM Dendrimers Using Anilinonaphthalene Sulfonates: Unusual Host-Dependent Fluorescence Titration Behavior. *Sensors* **2010**, *10*, 4053-4070.

49. Coelho, F.; Eberlin, M. N. The Bridge Connecting Gas-Phase and Solution Chemistries. *Angew. Chem. Int. Ed.* **2011**, *50*, 5261-5263.

50. Wang, D.; Imae, T.; Miki, M. Fluorescence Emission From PAMAM and PPI Dendrimers. *J. Colloid Interface Sci.* **2007**, *306*, 222-227.

51. Erat, M. C.; Coles, J.; Finazzo, C.; Knobloch, B.; Sigel, R. K. O. Accurate analysis of MG2+ binding to RNA: From classical methods to a novel iterative calculation procedure. *Coord. Chem. Rev.* **2012**, *256*, 279-288.

52. Correia, J. J.; Chaires, J. B. Analysis of drug-DNA binding isotherms: A Monte Carlo approach. *Methods Enzymol.* **1994**, *240*, 593-614.

53. Aschi, M.; D'Archivio, A. A.; Fontana, A.; Formiglio, A. Physiochemical Properites of Fluorescenct Probes: Experimental and Computational Determination of the Overlapping pKa Values of Carboxyfluorescein. *J. Org. Chem.* **2008**, *73*, 3411-3417.

54. Harianawala, A. I.; Bogner, R. H. Correction for the dielectric constant of pH values in heterogenous solutions obtained from fluorescein fluorescence. *J. Lumin.* **1998**, *79*, 215-224.

55. Underberg, W. J. M.; Schulman, S. G. Fluorimetric determination of acidity constants of naphthoic and anthroic acids. *Anal. Chim. Acta* **1979**, *105*, 311-317.

56. Prosa, T. J.; Bauer, B. J.; Amis, E. J. From Stars to Spheres: A SAXS Analysis of Dilute Dendrimer Solutions. *Macromolecules* **2001**, *34*, 4897-4906.

57. The M_w, diameter, and number of surface NH_2 groups were taken from literature on the manufacturer's website. (accessed 04/08, 2014).

58. Petsalakis, I. D.; Lathiotakis, N. N.; Theodorakopoulos, G. Theoretical study on tertiary amine-fluorophore photoinduced electron transfer (PET) systems. *J. Mol. Struct. - Theochem.* **2008**, *867*, 64-70.

59. Mecozzi, S.; West, A. P., Jr.; Dougherty, D. A. Cation-π Interactions in Simple Aromatics: Electrostatics Provide a Predictive Tool. *J. Am. Chem. Soc.* **1996**, *118*, 2307-2308.

60. Stewart, J. P. Optimization of Parameters for Semiempirical Methods V: Modification of NDDO Approximations and Application to 70 Elements. *J. Mol. Model.* **2007**, *13*, 1173-1213.

61. Frisch, M. J.; Trucks, G. W.; Schlegel, H. B.; Scuseria, G. E.; Robb, M. A.; Cheeseman, J. R.; Scalmani, G.; Barone, V.; Mennucci, B.; Petersson, G. A.; Nakatsuji, H.; Caricato, M.; Li, X.; Hratchian, H. P.; Izmaylov, A. F.; Bloino, J.; Zheng, G.; Sonnenberg, J. L.; Hada, M.; Ehara, M.; Toyota, K.; Fukuda, R.; Hasegawa, J.; Ishida, M.; Nakajima, T.; Honda, Y.; Kitao, O.; Nakai, H.; Vreven, T.; Montgomery, J. A., Jr.; Peralta, J. E.; Ogliaro, F.; Bearpark, M.; Heyd, J. J.; Brothers, E.; Kudin, K. N.; Staroverov, V. N.; Kobayashi, R.; Normand, J.; Raghavachari, K.; Rendell, A.; Burant, J. C.; Iyengar, S. S.; Tomasi, J.; Cossi, M.; Rega, N.; Millam, N. J.; Klene, M.; Knox, J. E.; Cross, J. B.; Bakken, V.; Adamo, C.; Jaramillo, J.; Gomperts, R.; Stratmann, R. E.; Yazyev, O.; Austin, A. J.; Cammi, R.; Pomelli, C.; Ochterski, J. W.; Martin, R. L.; Morokuma, K.; Zakrzewski, V. G.; Voth, G. A.; Salvador, P.; Dannenberg, J. J.; Dapprich, S.; Daniels, A. D.; Farkas, Ö.; Foresman, J. B.; Ortiz, J. V.; Cioslowski, J.; Fox, D. J.; Gaussian-09 Revision A.02 ed.; Gaussian Inc.: Wallingford, CT, 2009.

62. HyperChem Professional; 8.0.3 ed.; Hypercube Inc.: Gainesville, FL.

63. Bolto, B.; Gregory, J. Organic Polyelectrolytes in Water Treatment. *Water Res.* **2007**, *41*, 2301-2324.

64. Krol, S.; Gliozzi, A.; Diaspro, A. Polyelectrolyte Nanocapsules-Promising Progress in Development of New Drugs and Therapies. *Front. Drug Des. Discovery* **2006**, *2*, 333-348.

65. Mchedlov-Petrossyan, N.; Bryleva, E. Y.; Vodolazkaya, N. A.; Dissanayake, A. A.; Ford, W. T. Nature of Cationic Poly(propylenimine) Dendrimers in Aqueous Solutions as Studied Using Versatile Indicator Dyes. *Langmuir* **2008**, *24*, 5689-5699.

66. Greaney, M. J.; Nguyen, M. A.; Chang, C.; Good, A.; Margerum, L. D. Indicator Displacement Assays for Amino Acids Using Ni-NTA Tethered to PAMAM Dendrimers on Controlled Pore Glass. *Chem. Commun.* **2010**, *46*, 5337-5339.

67. Mallet, A. M.; Liu, Y.; Bonizzoni, M. An Off-the-Shelf Sensing System for Physiological Phosphates. *Chem. Commun.* **2014**, *50*, 5003-5006.

68. Duering, J.; Hoelzer, A.; Kolb, U.; Branscheid, R.; Gröhn, F. Supramolecular Organic-Inorganic Hybrid Assemblies with Tunable Particle Size: Interplay of Three Non-Covalent Interactions. *Angew. Chem. Int. Ed.* **2013**, *52*, 8742-8745.

69. By Li, T.; Shao, N.; Liu, Y.; Hu, J.; Wang, Y.; Zhang, L.; Wang, H.; Chen, D.; Cheng, Y. Poly(amidoamine) and Poly(propyleneimine) Dendrimers Show Distinct Binding Behaviors with Sodium Dodecyl Sulfate: Insights from SAXS and NMR Analysis. *J. Phys. Chem. B* **2014**, *118*, 3074-3084.

70. Willerich, I.; Ritter, H.; Gröhn, F. Structure and Thermodynamics of Ionic Dendrimer-Dye Assemblies. *J. Phys. Chem. B* **2009**, *113*, 3339-3354.

71. Stojanovic, N.; Murphy, L. D.; Wagner, B. D. Fluorescence-Based Comparative Binding Studies of the Supramolecular Host Properties of PAMAM Dendrimers Using Anilinonaphthalene Sulfonates: Unusual Host-Dependent Fluorescence Titration Behavior. *Sensors* **2010**, *10*, 4053-4070.

72. Mcdonnell, P. F.; Lambert, R. J.; Kelly, R. A.; Tierney, F. W. United States of America Patent US20060094833A1, 2006.

73. Braude, E. A.; Nachod, F. C.; Phillips, W. D., Eds.; In *Determination of Organic Structures by Physical Methods;* Academic Press: New York, 1955; Vol. 1.

74. Kemp, D. S.; Petrakis, K. S. Synthesis and Conformational Analysis of Cis, Cis-1,3,5-trimethylcyclohexane-1,3,5-Tricarboxylic Acid. *J. Org. Chem.* **1981**, *46*, 5140-5143.

75. Dawson, R. M. C., Ed.; In *Data for Biochemical Research;* Oxford: Clarendon Press, 1959.

76. Jolly, A. M.; Bonizzoni, M. PAMAM Dendrimers as Supramolecular Hosts Through Non-Covalent Interactions. *Supramol. Chem.* **2014**, *27*, 151-160.

77. Long, S. R.; Bonizzoni, M.; Ray, B. M.; Anslyn, E. V. Differentiation of Functional Groups and Biologically Relevant Anions Using AT-PAMAM Dendrimers. *Supramol. Chem.* **2013**, *25*, 641-649.

78. Wiskur, S. L.; Ait-Haddou, H.; Lavigne, J. J.; Anslyn, E. V. Teaching Old Indicators New Tricks. *Acc. Chem. Res.* **2001**, *34*, 963-972.

79. Nguyen, B. T.; Anslyn, E. V. Indicator–Displacement Assays. *Coord. Chem. Rev.* **2006**, *250*, 3118-3127.

80. Damitio, J.; Smith, G.; Meany, J. E.; Pocker, Y. A Comparative Study of the Enolization of Pyruvate and the Reversible Dehydration of Pyruvate Hydrate. *J. Am. Chem. Soc.* **1992**, *114*, 3081-3087.

81. Caceres-Alonso, M.; Costas, M.; Andreoli-Ball, L.; Patterson, D. Steric Effects on the Self-Association of Branched and Cyclic Alcohols in Inert Solvents. Apparent Heat Capacities of Secondary and Tertiary Alcohols in Hydrocarbons. *Can. J. Chem.* **1988**, *4*, 989-998.

82. Bae, Y.; Kataoka, K. Intelligent Polymeric Micelles from Functional Poly(ethylene glycol)-Poly(amino acid) Block Copolymers. *Adv. Drug Deliv. Rev.* **2009**, *61*, 768-784.

83. Chandra, S.; Dietrich, S.; Lang, H.; Bahadur, D. Dendrimer–Doxorubicin Conjugate for Enhanced Therapeutic Effects for Cancer. *J. Mater. Chem.* **2011**, *21*, 5729-5737.

84. Huang, X.; Wu, Z.; Gao, W.; Yu, B. Polyamidoamine Dendrimers as Potential Drug Carriers for Enhanced Aqueous Solubility and Oral Bioavailability of Silybin. *Drug Dev. Ind. Pharm.* **2011**, *37*, 419-427.

85. Jolly, A. M.; Bonizzoni, M. Intermolecular Forces Driving Encapsulation of Small Molecules by PAMAM Dendrimers in Water. *Macromolecules* **2014**, *47*, 6281-6288.

86. Savla, S.; Surjusee, A.; Rokade, V.; Sawant, S.; Kadu, P. Approaches to Improve Solubility of Poorly Water Soluble Drugs. *World J. Pharm. Pharm. Sci.* **2015**, *4*, 610-626.

87. Kakran, M.; Li, L.; Muller, R. H. Overcoming the Challenge of Poor Drug Solubility. *Pharm. Engg.* **2012**, *32*, 1-7.

88. Watanabe, S.; Iwamura, M. Dendritic caged compounds. *J. Photochem. Photobiol. A–Chem.* **2003**, *155*, 57-62.

89. Gowthamarajan, K.,; Singh, S. K. Dissolution Testing for Poorly Soluble Drugs: A Continuing Perspective. *Dissolut. Technol.* **2010**, *17*, 24-32.

90. Duhamel, J. New Insights in the Study of Pyrene Excimer Fluorescence to Characterize Macromolecules and their Supramolecular Assemblies in Solution. *Langmuir* **2012**, *28*, 6527-6538.

91. Goncalves, M. S. T. In *Optimized UV/Visible Fluorescent Markers;* Demchenko, A. P., Ed.; Springer Berlin Heidelberg: 2010; Vol. 8, pp 27-64.

92. Fernandez, L.; Gonzalez, M.; Cerecetto, H.; Santo, M.; Silber, J. J. Solubilization and Release Properties of Dendrimers. Evaluation as Prospective Drug Delivery Systems. *Supramol. Chem.* **2006**, *18*, 633-643.

93. Arias-Gonzalez, I.; Reza, J.; Trejo, A. Temperature and Sodium Chloride Effects on the Solubility of Anthracene in Water. *J. Chem. Thermodynamics* **2010**, *42*, 1386-1392.

94. Oliveira, M. B.; Oliveira, V. L.; Coutinho, J. A. P.; Queimada, A. J. Thermodynamic Modeling of the Aqueous Solubility of PAHs. *Ind. Eng. Chem. Res.* **2009**, *48*, 5530-5536.

95. Krol, S.; Gliozzi, A.; Diaspro, A. Polyelectrolyte Nanocapsules-Promising Progress in Development of New Drugs and Therapies. *Front. Drug Des. Discovery* **2006**, *2*, 333-348.

96. Taylor, R. W.; Coulston, R. J.; Biedermann, F.; Mahajan, S.; Baumberg, J. J.; Scherman, O. A. In Situ SERS Monitoring of Photochemistry within a Nanojunction Reactor. *Nano Lett.* **2013**, *13*, 5985-5990.

97. Yang, C.; Spinelli, N.; Perrier, S.; Defrancq, E.; Peyrin, E. Macrocyclic Host-Dye Reporter for Sensitive Sandwich-Type Fluorescent Aptamer Sensor. *Anal. Chem.* **2015**, *87*, 3139-3143.

98. Liu, Y.; Li, Z. T. A Dynamic Route to Structure and Function: Recent Advances in Imine-Based Organic Nanostructured Materials. *Aust. J. Chem.* **2013**, *66*, 9-22.

99. Lehn, J. M. Cryptates: The Chemistry of Macropolycyclic Inclusion Complexes. *Acc. Chem. Res.* **1978**, *11*, 49-57.

100. Pedersen, C. J. Cyclic Polyethers and Their Complexes with Metal Salt**s**. *J. Am. Chem. Soc.* **1967**, *89*, 7017-7036.

101. Dietrich, B.; Lehn, J. M.; Guilhem, J.; Pascard, C. Anion Receptor Molecules : Synthesis of an Octaaza-cryptand and Structure of its Fluoride Cryptate. *Tetrahedron Lett.* **1989**, *30*, 4125-1428.

102. Bonizzoni, M.; Fabbrizzi, L.; Piovani, G.; Taglietti, A. Fluorescent Detection of Glutamate With a Dicopper(II) Polyamine Cage. *Tetrahedron* **2004**, *60*, 11159-11162.

103. Chase, P. A.; Jurca, T.; Stephan, D. W. Lewis acid-catalyzed hydrogenation: $B(C_6F_5)3$-mediated reduction of imines and nitriles with H_2. *Chem. Commun.* **2008**, 1701-1703.

104. Kumar, K. A.; Sreelekha, T. S.; Shivakumara, K. N.; Prakasha, K. C.; Gowda, D. C. Zinc-Catalyzed Reduction of Imines by Triethylsilane. *Synth. Commun.* **2009**, *39*, 1332-1341.

105. Kong, D.; Mcbee, J.; Holliness, L. Structures of aza-macrocyclic ligands with polyphosphonated dangling groups. *Tetrahedron Lett.* **2008**, *49*, 3512-3515.

106. Beer, P. D.; Gale, P. A. Anion Recognition and Sensing: The State of the Art and Future Perspectives. *Angew. Chem. Int. Ed.* **2001**, *40*, 486-516.

107. Boiocchi, M.; Bonizzoni, M.; Fabbrizzi, L.; Piovani, G.; Taglietti, A. A Dimetallic cage With a Long Ellipsoidal Cavity for the Fluorescent Detection of Dicarboxylate Anions in Water. *Angew. Chem. Int. Ed.* **2004**, *43*, 3847-3852.

108. Bowman-James, K. Alfred Werner Revisited: The Coordination Chemistry of Anions. *Acc. Chem. Res.* **2005**, *38*, 671-678.